

University of Alberta

**A Comparative Study of Flowback Rate and Pressure Transient Behaviour
in Multifractured Horizontal Wells**

by

Majid Ali Abbasi

A thesis submitted to the Faculty of Graduate Studies and Research
in partial fulfillment of the requirements for the degree of

**Master of Science
in
Petroleum Engineering**

Department of Civil and Environmental Engineering

©Majid Ali Abbasi
Fall 2013
Edmonton, Alberta

Permission is hereby granted to the University of Alberta Libraries to reproduce single copies of this thesis and to lend or sell such copies for private, scholarly or scientific research purposes only. Where the thesis is converted to, or otherwise made available in digital form, the University of Alberta will advise potential users of the thesis of these terms.

The author reserves all other publication and other rights in association with the copyright in the thesis and, except as herein before provided, neither the thesis nor any substantial portion thereof may be printed or otherwise reproduced in any material form whatsoever without the author's prior written permission.

Dedicated to my parents, brothers, sisters and all family members.

ABSTRACT

Tight reservoirs stimulated by multistage hydraulic fracturing are commonly characterized by analyzing the hydrocarbon production data. However, analyzing the hydrocarbon production data can best be applied to estimate the effective fracture-matrix interface, and is not enough for a full fracture characterization. Before flowback, the induced fractures are filled with the compressed water. Therefore, analyzing the early-time rate and pressure of fracturing water and gas/oil should in principle be able to partly characterize the induced fractures, and complement the conventional production data analysis.

We develop an analytical model to compare the pressure/rate transient behaviour of multifractured horizontal wells (MFHW) completed in one tight oil and two tight gas wells. We also construct a series of diagnostic plots to study the flowback behaviour of 18 MFHW completed in the Horn River basin. We observe unique signatures that suggest initial free gas in the fracture network before starting the flowback operation.

ACKNOWLEDGEMENTS

Foremost, I want to thank to Almighty Allah for granting me His blessings and give me the strength to successfully complete this research.

I would like to express my deepest gratitude to my supervisor, Dr. Hassan Dehghanpour for providing me an opportunity to work under his supervision. He equipped me with technical knowledge and lots of brilliant ideas that will be helpful in future. I am greatly benefited under his supervision. I would also like to appreciate his encouragement and support during the difficult moments.

I would also like to thank Dr. Ergun Kuru and Dr. Mustafa Gul for serving on my advisory committee.

I would like to thank FMC Technologies, Trican Well Services and Natural Sciences and Engineering Research Council of Canada (NSERC) for their financial assistance. I would also like to thank Nexen and Lightstream Energy Resources for measurement and provision of the field data.

I want to acknowledge the endless support of my parents and my family. I would like to thanks to my dearest friends Ankit, Umair, Asmar, Danish, Jibran, Yasir, Shahab, Obinna, Ebrahim, Jaskaran, Imran and Kai for their useful discussions and constant help.

In the last but not least, I would like to express my gratitude to the Petroleum Engineering Department faculty and staff for keeping me on track and making my time a unique experience at the University of Alberta.

TABLE OF CONTENTS

CHAPTER	PAGE
I INTRODUCTION.....	1
1.1. Overview.....	1
1.2. Objective.....	3
1.3. Thesis Outline.....	4
II LITERATURE REVIEW.....	5
2.1. Flowback Management.....	6
2.2. Qualitative and Quantitative Flowback Analysis.....	7
2.3. Chemical Analysis.....	8
III DEVELOPMENT OF ANALYSIS EQUATION.....	10
3.1. Flowback Rate and Pressure History.....	10
3.1.1. Well 1.....	10
3.1.1.1. Flowback History.....	11
3.1.2. Well 2.....	14
3.1.2.1. Flowback History.....	14
3.1.3. Well 3.....	17
3.1.3.1. Flowback History.....	17
3.1.4. Comparative Interpretation.....	21
3.1.5. Approximate Volume and Interface of Fractures Depleted after Flowback.....	23
3.2. Comparing the Pressure Transient Behaviour.....	25
3.2.1. Conceptual Model.....	25
3.2.2. Material Balance Equation for Early Time Flowback.....	26
3.2.3. Combining Material Balance and Diffusivity Equations...	28
3.2.4. Radial Transient Model.....	29

3.2.5.	Linear Transient Model.....	31
3.2.6.	Relationship between RNP and MBT.....	31
3.3.	Model Application.....	33
3.3.1.	Analysis Procedure.....	33
3.3.2.	Example Applications.....	33
3.3.3.	Discussion of Results.....	36
3.4.	Data Acquisition.....	38
IV	DIAGNOSTIC PLOTS.....	40
4.1.	Introduction.....	40
4.2.	Well Pad Description.....	40
4.2.1.	Muskwa Formation.....	43
4.2.2.	Otter Park Formation.....	44
4.2.3.	Evie Formation.....	45
4.3.	Cumulative Production Plots.....	46
4.3.1.	Interpretation of Cumulative Production Plots.....	53
4.4.	Flowback Rate History	54
4.4.1.	Interpretation of Rate Plots.....	63
4.5.	Gas Water Flow Rate Ratio Plots.....	64
4.5.1.	Interpretation of Gas Water Flow Rate Ratio Plots.....	70
4.6.	Flowback Pressure History.....	73
4.7.	Water Normalized Productivity Index Plots.....	78
4.7.1.	Interpretation of Water Normalized Productivity Index Plots.....	83
4.8.	Unique Feature of the Horn River Wells.....	84
4.9.	Comparative Interpretation of Cumulative Production, Flow Rate, GWR and WNPI Plots	88
4.10.	Flowback Analysis of Shale Gas Wells.....	92

V	CONCLUSIONS AND RECOMMENDATIONS.....	93
5.1.	Conclusions.....	93
5.1.1.	Volumetric Analysis.....	93
5.1.2.	Transient Analysis.....	94
5.1.3.	Diagnostic Analysis.....	95
5.2.	Recommendations and Future Work.....	95
	REFERENCES.....	97
	APPENDIX A.....	106
	APPENDIX B.....	110

LIST OF TABLES

TABLE	PAGE
3.1. Completion data and fluid properties of the three wells considered in this study.....	11
3.2. Comparison of relative volumes of water recovered during the flowback of Well 1, Well 2 and Well 3.....	21
3.3. Approximate fracture volume and matrix-fracture cross-sectional area created per stage at the end of the flowback operation of the three wells.....	24
3.4. Calculated values for the total storage coefficient the dimensionless radial fracture parameter and the dimensionless linear fracture parameter.....	36
4.1. Completion design summary of a well pad of eighteen wells.....	43
4.2. Observed behaviour (Region 1) of the four plot types in the Horn River basin.....	91
4.3. Observed behaviour (Region 2) of the four plot types in the Horn River basin.....	91

LIST OF FIGURES

FIGURE	PAGE
3.1. Pressure and flow rate history measured hourly during the flowback operation of Well 1. Three different regions are identified. In Region 1, water production dominates. In Region 2, water production decreases and gas production increases. In Region 3, gas production dominates.....	13
3.2. Comparison between cumulative water and gas production curves and wellbore volume of Well 1	13
3.3. Gas water flow rate ratio (GWR) versus cumulative gas production (GP) of Well 1.....	14
3.4. Pressure and flow rate history measured hourly during the flowback operation of Well 2. Three different regions are identified. In Region 1, water production dominates. In Region 2, water production decreases and gas production increases. In Region 3, gas production dominates.....	16
3.5. Comparison between cumulative water and gas production curves and wellbore volume of Well 2.....	16
3.6. Gas water flow rate ratio (GWR) versus cumulative gas production (GP) of Well 2.....	17
3.7. Pressure and flow rate history measured hourly during the flowback operation of Well 3. Three different regions are identified. In Region 1, water production dominates. In Region 2, water production decreases and oil production increases. In Region 3, oil production dominates.....	19
3.8. Comparison between cumulative water and oil production curves and wellbore volume of Well 3.....	20

3.9.	Oil water flow rate ratio (OWR) versus cumulative oil production (N_p) of Well 3.....	20
3.10.	Average matrix-fracture interface created per stage versus fracture aperture at the end of the flowback operation for the three wells.....	25
3.11.	3D view of a fractured horizontal well considered for developing the material balance equation. Dashed arrows show fluid flow direction, which is sequentially from matrix to fractures, fractures to wellbore, and finally from wellbore to surface.....	28
3.12.	3D view of a fracture with a horizontal well in the center considered for solving the diffusivity equation. Bold arrows show (a) radial and (b) linear water flow towards the horizontal well.	30
3.13.	RNP versus MBT of Region 1 and the best linear fit for well 1.....	34
3.14.	RNP versus MBT of Region 1 and the best linear fit for well 2.....	35
3.15.	RNP versus MBT of Region 1 and the best linear fit for well 3.....	35
4.1.	Stratigraphic section of Devonian-Mississippian (Gal & Jones, 2003)....	41
4.2.	Layout of a well pad drilled and completed in the Horn River basin. Total of eighteen wells were drilled, nine wells on the right side of the pad and nine wells on the left side of the pad.....	42
4.3.	3D view of multilateral horizontal wells completed in the Muskwa formation. Total of six wells were drilled. Three wells on the right side of the pad and three wells on the left side of the pad.....	44
4.4.	3D view of multilateral horizontal wells completed in the Otter Park formation. Total of six wells were drilled. Three wells on the right side of the pad and three wells on the left side of the pad.....	45

4.5.	3D view of multilateral horizontal wells completed in the Evie formation. Total of six wells were drilled. Three wells on the right side of the pad and three wells on the left side of the pad.....	46
4.6.	Comparison of cumulative water and gas production (WP and GP) versus cumulative time of the six wells drilled in the Muskwa formation. Total injected volume (TIV) for the six wells is given in each graph.....	48
4.7.	Comparison of cumulative water and gas production (WP and GP) versus cumulative time of the six wells drilled in the Otter Park formation. Total injected volume (TIV) for six wells is mentioned in each graph.....	50
4.8.	Comparison of cumulative water and gas production (WP and GP) versus cumulative time of the six wells drilled in the Evie formation. Total injected volume (TIV) for the six wells is given in each graph.....	52
4.9.	Water and gas flow rate history measured during the flowback operation of six wells in the Muskwa formation.....	56-57
4.10.	Water and gas flow rate history measured during the flowback operation of six wells in the Otter Park formation.....	59-60
4.11.	Water and gas flow rate history measured during the flowback operation of six wells in the Evie formation.	61-62
4.12.	Gas water flow rate ratio (GWR) versus cumulative gas production (Gp) of the six wells drilled in the Muskwa formation. The dotted arrow shows the transition time in fractures.....	65-66
4.13.	Gas water flow rate ratio (GWR) versus cumulative gas production (Gp) of the six wells drilled in the Otter Park formation. The dotted arrow shows the transition time in fractures	67-68

4.14.	Gas water flow rate ratio (GWR) versus cumulative gas production (G_p) of the six wells drilled in the Evie formation. The dotted arrow shows the transition time in fractures	69-70
4.15.	Casing Pressure measured at surface during the flowback of the six wells in the Muskwa formation.....	74
4.16.	Casing Pressure measured at surface during the flowback of the six wells in the Otterpark formation.....	75-76
4.17.	Casing Pressure measured at surface during the flowback of the six wells in the Evie formation.....	77-78
4.18.	Water normalized productivity index (WNPI) versus cumulative water production (W_p) of the six wells drilled in the Muskwa formation.....	79-80
4.19.	Water normalized productivity index (WNPI) versus cumulative water production (W_p) of the six wells drilled in the Otter park formation.....	81
4.20.	Water normalized productivity index (WNPI) versus cumulative water production (W_p) of the six wells drilled in the Evie formation.....	82-83
4.21.	Gas water flow rate ratio (GWR) versus cumulative gas production (G_p) of Well 1 in a tight gas reservoir.....	86
4.22.	Gas water flow rate ratio (GWR) versus cumulative gas production (G_p) of Well 2 in a tight gas reservoir.....	86
4.23.	Oil water flow rate ratio (OWR) versus cumulative oil production (N_p) of Well 3 in a tight oil reservoir.....	87
4.24.	Gas water flow rate ratio (GWR) versus cumulative gas production (G_p) of Well EV_{R3} in the Horn River basin.....	87

4.25.	Cumulative water and gas production plot of well MU _{L3} with most pronounced Regions 1 and 2 used for the comparison study.....	89
4.26.	Water and gas flow rate plot of well MU _{L3} with most pronounced Regions 1 and 2 used for the comparison study.....	89
4.27.	Gas water flow rate ratio versus cumulative gas production of well MU _{L3} with most pronounced Regions 1 and 2 used for the comparison study...	90
4.28.	Water normalized productivity index versus cumulative water production plot of well MU _{L1} with most pronounced Regions 1 and 2 used for the comparison study.....	90

NOMENCLATURE

A	=	drainage area of fracture, ft ²
A_{cm}	=	matrix-fracture cross-sectional area, ft ²
B	=	formation volume factor, ft ³ /std ft ³
B_m	=	matrix formation volume factor, ft ³ /std ft ³
B_s	=	surface formation volume factor, ft ³ /std ft ³
C_A	=	Dietz shape factor
C_f	=	compressibility of fracturing fluid, psi ⁻¹
C_{st}	=	total storage coefficient, ft ³ /psi
C_g	=	gas compressibility, psi ⁻¹
C_o	=	oil compressibility, psi ⁻¹
C_w	=	water compressibility, psi ⁻¹
C_m	=	matrix compressibility, psi ⁻¹
C_t	=	total compressibility, psi ⁻¹
C_{wb}	=	compressibility of fluid in wellbore, psi ⁻¹
dV	=	change in volume, ft ³
dP	=	change in pressure, psi
G_p	=	cumulative gas production, m ³

h_f	=	fracture height, ft
K_g	=	gas permeability, ft ²
K_o	=	permeability of oil, ft ²
K_w	=	permeability of water, ft ²
K_f	=	fracture bulk permeability, ft ²
N_p	=	cumulative oil production, m ³
N_f	=	number of fracture stages
P_f	=	pressure of fluid in fractures, psi
P_i	=	initial reservoir pressure, psi
P_{wb}	=	pressure of fluid in wellbore, psi
P_{wf}	=	flowing bottom hole pressure, psi
\bar{P}	=	average reservoir pressure, psi
q_s	=	flow rate at surface, m ³ /h
q_m	=	flow rate in matrix, m ³ /h
r_e	=	drainage radius, ft
r_w	=	wellbore radius, ft
S_w	=	water saturation, %
S_o	=	oil saturation, %
S_g	=	gas saturation, %

V	=	volume, m ³
V_f	=	volume of fluid in fractures, ft ³
V_{wb}	=	wellbore volume, ft ³
W_f	=	fracture aperture, ft
X_e	=	horizontal well length, ft
Y_e	=	fracture half length, ft
$\frac{N_P}{q_w}$	=	material balance time, hr

Symbols

ρ_f	=	density of fluid in fractures, kg/m ³
ρ_m	=	density of fluid in matrix, kg/m ³
ρ_s	=	density of fluid at surface, kg/m ³
ρ_{wb}	=	density of fluid in wellbore, kg/m ³
μ	=	viscosity of produced fluid, cp
Υ	=	Euler's Constant
ϕ_f	=	fractures bulk porosity, fraction

Subscripts

f	=	fracture
s	=	surface

m = matrix

wb = wellbore volume

w = water

o = oil

t = total

g = gas

Chapter I

Introduction

1.1. Overview

The amount of hydrocarbon stored in previously inaccessible shale and tight reservoirs is significantly higher than that stored in conventional reservoirs (Zahid et al., 2007, Abdelaziz et al., 2011). Recent advances in horizontal drilling and multi-stage hydraulic fracturing have unlocked these challenging hydrocarbon plays. Characterizing the induced fracture network is important for evaluating the fracturing operation, and predicting the reservoir performance. Various mathematical models have been proposed for analyzing the hydrocarbon production data for the purpose of characterizing the fractured horizontal wells. The fracture-matrix interface and fracture half-length are usually determined by analyzing the hydrocarbon production data. The dual porosity model has been extended for analyzing the fractured horizontal wells (Bello, 2009; El-Banbi, 1998; Medeiros et al., 2008; Ozkan et al., 2010; Medeiros et al., 2010). The available hydrocarbon production data mainly match the late linear transient part of the type curves, which relates to the fluid transfer from the matrix into the fracture. This match can be interpreted to determine the effective fracture half-length. However, a full characterization of the fracture network by only analyzing the hydrocarbon data is challenging because:

- The early-time oil or gas production data is usually unavailable or of low quality for history matching.
- The induced fracture network is initially filled with compressed fracturing fluid not hydrocarbon. Therefore, analyzing the hydrocarbon data for determining the fracture storage capacity can be misleading.
- Production data analysis does not account for the fractures, which are filled with water and do not contribute to the hydrocarbon flow.

Conventional rate transient methods have been applied for analyzing the flowback data. For example, the reciprocal productivity index method has been applied on the early time flowback data to evaluate the stimulated vertical gas wells (Crafton, 1996; Crafton, 1997; Crafton, 1998). However, application of this approach for analyzing the flowback data of fractured horizontal wells needs further modifications. Ilk et al., (2010) introduced a workflow for a qualitative interpretation of early time flowback data by developing various diagnostic plots to observe wellbore unloading and fracture clean-up/depletion trends. Clarkson (2012) presented a quantitative analysis of two-phase flowback data using a two-phase tank model simulator to estimate fracture permeability and total fracture half length. Later, Clarkson's model was improved by applying Monte Carlo simulation for stochastic history matching of two-phase flowback data measured after multi-stage hydraulic fracturing (Williams-Kovacs and Clarkson, 2013). Recently, Ghanbari et al. (2013) studied the flowback data of several multi-fractured horizontal wells, completed in the Horn River basin. His study

demonstrates that shale gas and tight gas (oil) wells behave differently. Ezulike et al. (2013) compared the relative permeability versus time and relative permeability versus cumulative gas/oil production plots of the similar well groups. Consistently, they observed different relative permeability profiles for tight oil/gas and shale gas wells. In addition to rate transient models, compositional simulators have been developed to history-matching flowback salt concentration change (Gdanski et al. 2007).

1.2. Objective

The objectives of this thesis are: 1) Qualitative and careful analysis of multi-phase flowback data for understanding water displacement patterns, and 2) Development of a simple analytical tool for analyzing early-time rate and pressure data. The first objective is achieved by developing various diagnostic plots to qualitatively interpret the flowback water displacement mechanisms in the fracture system by using multiphase flowback data. Various plot types were proposed to analyze the qualitative behavior of flowback water (Ilk et al., 2010). The second objective is achieved by extending the existing models of fracture testing. Various flow and shut-in tests have been proposed for recording the fracture response transferred by the fracturing fluid. Examples include the injection/fall off test (Craig, 2006), the fracture-calibration test (Mayerhofer et al., 1995) and the slug test (Peres et al., 1993). The mathematical models for such tests are developed by solving the material balance equation for fluid transport in the reservoir, fracture, and wellbore. The solutions have been reported in the form

of type curves (Craig, 2006). The main outputs of the fracture tests are fracture conductivity and storativity.

1.3. Thesis Outline

This thesis is divided into five chapters and organized as follows: This chapter provides the overview and objective of this research.

Chapter II provides the literature review of the early time flowback rate and pressure data analysis and interpretation. Chapter II also discusses the flowback management strategies, qualitative and quantitative analysis of the early time flowback data and compositional analysis of flowback water.

Chapter III qualitatively interprets the rate, pressure and cumulative production of water and oil/gas recorded during three different flowback operations. Based on the rate, pressure and cumulative production interpretation we develop a simple analytical model to compare the pressure/rate transient behavior of the three flowback cases. Finally we apply the proposed model to the field data and discuss the results.

In chapter IV, we construct a series of diagnostic plots by using the flowback data of eighteen multifractured horizontal wells drilled and completed in the Horn River basin. The purpose of this chapter is to diagnose the displacement behavior of flowback water in shale gas reservoirs.

Chapter V presents the conclusions and recommendations and for the future work.

Chapter II

Literature Review

Multistage hydraulic fracturing has been proved to be the best technology to enhance the productivity of low permeability tight reservoirs (King, 2010). During a hydraulic fracturing operation, water, sand and few chemicals are injected under high pressure into the tight reservoir to create fractures. The injection of fracturing fluid is always followed by a flowback operation, where the injected fluid is flowed back to the surface. The flow rate, pressure and chemical composition of fracturing fluid are measured at the surface. These measurements can provide meaningful information about the stimulated reservoir.

The concept of flowback is as old as the advent of hydraulic fracturing. But historically, very limited work has been practiced and documented for quantitative and qualitative analysis of flowback data. This chapter discusses the previous studies on the post stimulation flowback operation that involves the flowback management strategies, rate/pressure data interpretation and chemical analysis of flowback water in multistage hydraulically fractured (MSHF) horizontal wells. This literature review focuses on the following main topics:

- Flowback Management
- Qualitative and Quantitative Flowback Analysis
- Chemical Analysis

2.1. Flowback Management

This section briefly summarizes the careful management strategies needed for a successful flowback operation and for determining the fracture properties using the post stimulation flowback data.

Careful and accurate measurement of flowback rate, pressure and chemical data is important for better management of flowback process. Unfortunately, the flowback rate and pressure data are not measured accurately and frequently for a comprehensive flowback analysis. Crafton and Gunderson (2006) discussed the importance of high frequency rate and pressure data collection. The rate and pressure data measured during the flowback operation, usually contain meaningful information about the fracture half-length, fracture closure pressure, fracture permeability and the reservoir transmissibility.

Later, Crafton and Gunderson (2007) conducted a simulation study on flowback data using a multiphase transient reservoir/fracture simulator. Their simulation study shows that delay in the start of flowback, and shut-ins during flowback operation can impact future performance of the well. They also investigated that excessively higher flowback rates can cause proppant flowback or fracture collapse. This ultimately results in fracture underperformance. Therefore, they concluded that careful management of the flowback operation and proper rate/pressure data measurement can significantly improve the well's long term performance.

Crafton (2008) performed physical experiments and numerical simulations to investigate the effect of various parameters (flowback rate, shut-ins, surfactants, increasing reservoir/fracture contrast ratio, near wellbore/fracture complexity and lateral orientation) on early time flowback data. He found that these parameters have a strong effect on reservoir performance and gas recovery. Therefore, careful management of early time flowback data is very important to improve the long term well performance.

Crafton (1998) applied the reciprocal productivity index method to observe the effect of shut-ins, excessive drawdown and the duration of flowback on well clean-up. He also showed that there is a minimum rate below which fracture clean-up is inefficient.

2.2. Qualitative and Quantitative Flowback Analysis

The first attempt to perform the qualitative and quantitative analysis of the flowback data was done by Crafton. Crafton (1998) performed quantitative analysis of flowback rate and pressure data in the form of a reciprocal productivity index method. RPI method provides a good estimate of the effective permeability-thickness, the apparent fracture half length, the effective wellbore radius and unusual reservoir pressure conditions. But his work was limited to: 1) single phase flow, and 2) vertical wells.

Crafton (2010) conducted a numerical simulation study and investigated the effects of flow rate and pressure drawdown in two different multistage fracture systems.

Ilk et al. (2010) introduced a workflow for qualitative interpretation of early time flowback data by developing various diagnostic plots to observe water unloading effect, clean up trend/fracture depletion trend and early dominance of the water production.

Clarkson (2012) presented a quantitative analysis of two-phase flowback data using a two-phase tank model simulator to estimate fracture permeability and the total fracture half length.

Williams-Kovacs and Clarkson (2013) improved Clarkson's previous model, by applying Monte Carlo simulation for stochastic history matching of two-phase flowback data of multifractured horizontal wells.

2.3. Chemical Analysis

This section discusses the compositional analysis of the recovered water to model fracturing fluid flowback. Analyzing the ionic composition of water can be interpreted to estimate the true load recovery after the fracturing operation.

In addition to the flow rate and pressure, the chemical composition of fracturing water is another tool to evaluate the stimulated reservoir. The flowback chemical analysis has been used for evaluating acidizing (Hayatdavoudi, 1996) and fracturing operations (Asadi et al., 2008; Gdanski et al., 2007). Asadi et al. (2002) presented a technique, where tracing of fracturing fluid was implemented in a multistage hydraulic fracturing job by using chemical tracers.

Hurtado et al. (2005) presented a field case where four chemical tracers were injected and a low recovery of fracturing fluid was observed. To improve the

fracturing fluid recovery a shut-in was done. Upon re-opening, the flowback efficiency was increased by 50%. Their study showed that chemical tracers are useful tools to evaluate the effectiveness of flowback operation and the clean-up process.

Gdanski et al. (2007) developed a compositional numerical simulator to history match the chemical component concentrations measured during flowback. In this simulator, the flowback rate and ion concentration are used to determine the reservoir properties. The subsequent papers (Gdanski et. al., 2012; Gdanski et. al., 2010; Gdanski et. al., 2011) show the applications of this model in reservoir/fracture characterization. Gdanski et al. (2010) demonstrated that the characterization of both the reservoir properties and fracture structure can be improved by history matching well-return compositions with a fracture clean up model.

Chapter III

Development of Analysis Equation

This chapter develops a simple analytical model to compare the rate and pressure transient behavior in tight reservoirs. The chapter is organized as follows: Section I qualitatively interprets the rate, pressure, and cumulative production of water and oil/gas recorded during the three different flowback operations. Section II develops a simple analytical model to compare the pressure/rate transient behavior of the three flowback cases. Section III applies the proposed model to the field data and discusses the results.

3.1. Flowback Rate and Pressure History

In this section, we interpret flowback rate and pressure history of three multifractured horizontal wells completed in one tight oil and two tight gas reservoirs. Table 3.1 shows the completion data and fluid properties of the three wells.

3.1.1. Well 1

This well is completed in a tight gas reservoir. Initially, the well was flowed back with variable choke sizes for 14 hours. Then, two different choke sizes of 19.05 mm and 38.10 mm were used for almost 24 hours and 48 hours, respectively.

Table 3.1. Completion data and fluid properties of the three wells considered in this study.

Given Parameters	Well 1	Well 2	Well 3
Hydrocarbon Type	Gas	Gas	Oil
Fracturing Fluid	Water	Water	Water
Distance b/w fracture stages (L_f), ft	242.78	91.86	236.22
Horizontal Well Length (X_e), ft	4593.17	1312.3	4265
Number of Fracture Stages (N_f)	20	15	20
Total Compressibility (c_t), psi^{-1}	$2.85e^{-4}$	$2.87e^{-4}$	$2.90e^{-4}$
Water Compressibility (c_w), psi^{-1}	$3.33e^{-6}$	$3.33e^{-6}$	$3.33e^{-6}$
Viscosity of Fracturing Fluid(μ_w),cp	0.331	0.331	0.331
Water Formation Volume Factor (B_w)	1.0311	1.0290	1.0003
Wellbore Radius (r_w), ft	0.2916	0.2998	0.2874
True Vertical Depth (TVD), ft	7575.4	7946.1	9875.3

3.1.1.1. Flowback History

Figure 3.1 shows the flow rate and pressure measured at the surface during the flowback of well 1. Casing pressure is initially high and quickly drops with time. The rate plot is divided into three regions. In the first region, $q_g=0$ and only water flows with a rate specified by the choke size. In the second region, gas production starts and q_w gradually decreases. In the third region, $q_w \approx 0$ and mainly gas is produced.

Figure 3.2 compares the cumulative water production and gas production versus cumulative time. Cumulative water production curve in Figure 3.2 shows two distinct regions. The first region is denoted by a black dashed line which shows a steep increase in water production for about 25 hours and is named Early Water Production (EWP) region. The second region shows the gradual increase in

water production until the end of flowback operation and is named Late Water Production (LWP) region. During EWP, water flow rate (determined by the curve slope) remains relatively high. During LWP, water flow rate decreases gradually. Faster initial water production rate can be explained by two reasons: 1) Water saturation and in turn, water relative permeability in fractures is initially high and drops with time as gas is introduced from the matrix into the fractures, 2) Initially conductive primary fractures contribute to water production, followed by secondary fractures with a relatively less conductivity. The gas production curve, in Figure 3.2, shows that gas breaks through almost 5 hours after opening the well, and cumulative production gradually increases. This indicates gradual gas saturation increase or water saturation drop that was discussed above.

Figure 3.3 shows the log-log plot of gas water flow rate ratio (GWR) versus cumulative gas production (G_P) of Well 1. In general, GWR plot shows an increase in GWR with time. Increase in GWR means that the ratio between gas and water saturations and that between gas and water relative permeabilities in fractures increases with time.

Table 3.2 lists the relative volumes of water recovered during the flowback of this well. The total injected volume (TIV) is 1501 m^3 . After 86 hours of flowback, the total load recovery (TLR) is 329.64 m^3 , which is only 21.96 % of TIV. During EWP, 261 m^3 of water is produced which is about 79.17 % of TLR and the remaining 20.83 % is recovered during LWP. The wellbore volume (WV) is 92.042 m^3 , which is initially filled with water and contributes to 27.92 % of the TLR.

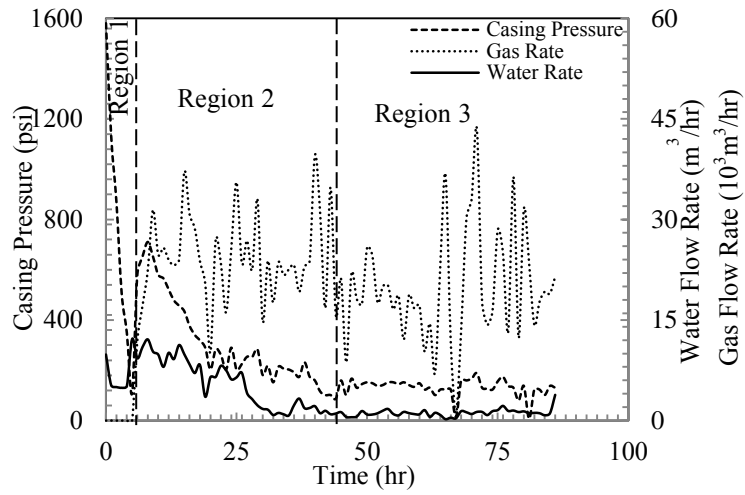


Fig. 3.1. Pressure and flow rate history measured hourly during the flowback operation of Well 1. Three different regions are identified. In Region 1, water production dominates. In Region 2, water production decreases and gas production increases. In Region 3, gas production dominates.

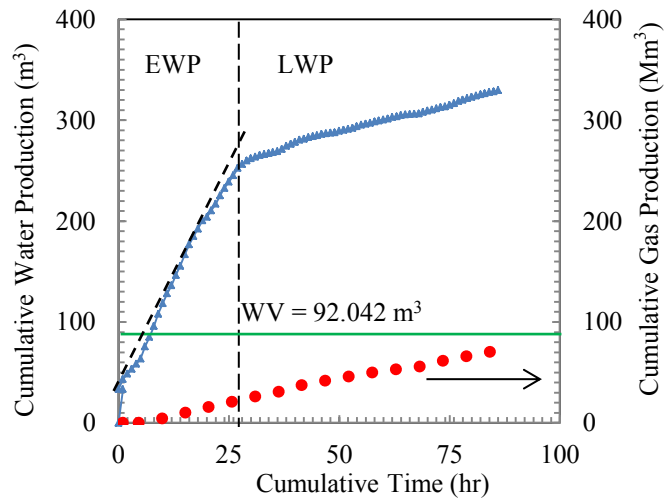


Fig. 3.2. Comparison between cumulative water and gas production curves and wellbore volume of Well 1.

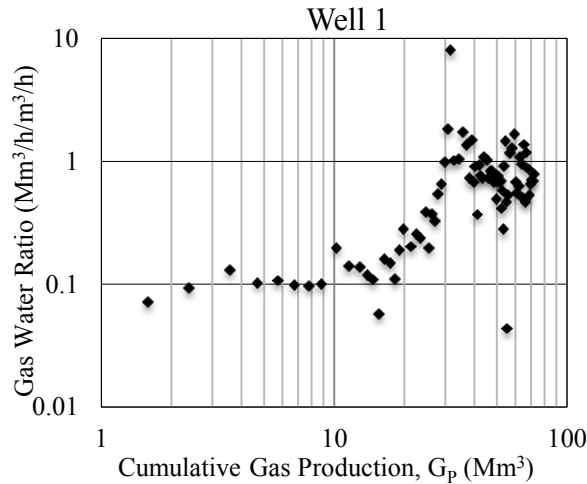


Fig. 3.3. Gas water flow rate ratio (GWR) versus cumulative gas production (G_p) of Well 1.

3.1.2. Well 2

This well is completed in a tight gas reservoir. Initially, the well was flowed back with five choke sizes for 16 hours. Then a choke size of 19.05 mm was used for 100 hours.

3.1.2.1. Flowback History

Figure 3.4 shows the flow rate and pressure measured at the surface during the flowback of Well 2. Tubing pressure is initially high and quickly drops with time. Several peaks followed by decline behaviors are observed in the pressure plot, which indicate that this well has been shut-in several times after starting the flowback operation. The rate and pressure plot is divided into three regions. In the first region, q_g is relatively low and water production dominates with a rate specified by the choke size. In the second region, gas flow rate ramps up and q_w

gradually decreases in different steps, which are specified by the choke size. In the third region, q_w is relatively low and gas production dominates.

Figure 3.5 compares the cumulative water and gas production versus time. Similar to well 1, the cumulative water production curve here shows two distinct regions. The first region (EWP) is denoted by a black dashed line which shows a steep increase in water production for about 24 hours. The second region (LWP) shows a gradual increase in water production until the end of flowback operation. The relatively high water flow rate during EWP, and its gradual decrease during LWP can be explained by relative permeability effect as was done for Well 1. The other curve in Figure 3.5 shows the gradual increase in gas production after the breakthrough that occurs almost 6 hours after opening the well.

Figure 3.6 shows the log-log plot of gas water flow rate ratio (GWR) versus cumulative gas production (G_P) of Well 2. In general, GWR plot shows an increase in GWR with time. Increase in GWR can be explained in the similar manner as was done for Well 1.

Table 3.2 shows that TIV for well 2 is 6443.38 m^3 . After 116 hours of flowback, 1521.16 m^3 of water (TLR) is recovered that is only 23.60 % of TIV. During EWP, 760 m^3 of water is produced which is about 49.96 % of TLR, and the remaining is recovered during LWP. The wellbore volume is 74.089 m^3 , which is initially filled with water and contributes to 4.87 % of the TLR.

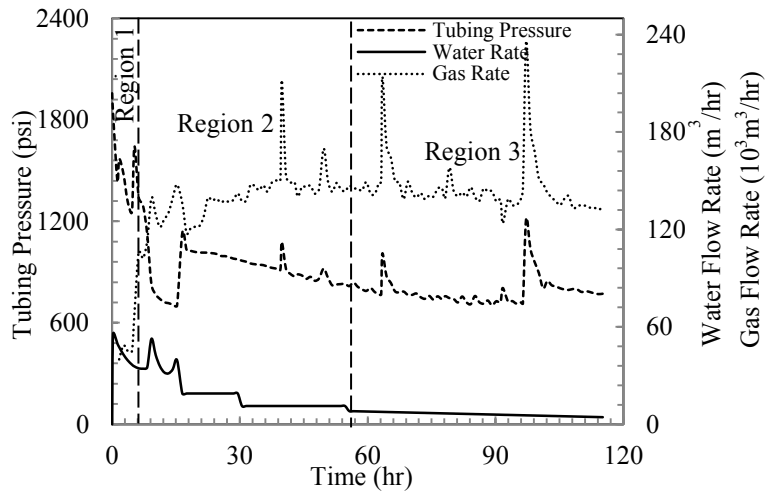


Fig. 3.4. Pressure and flow rate history measured hourly during the flowback operation of Well 2. Three different regions are identified. In Region 1, water production dominates. In Region 2, water production decreases and gas production increases. In Region 3, gas production dominates.

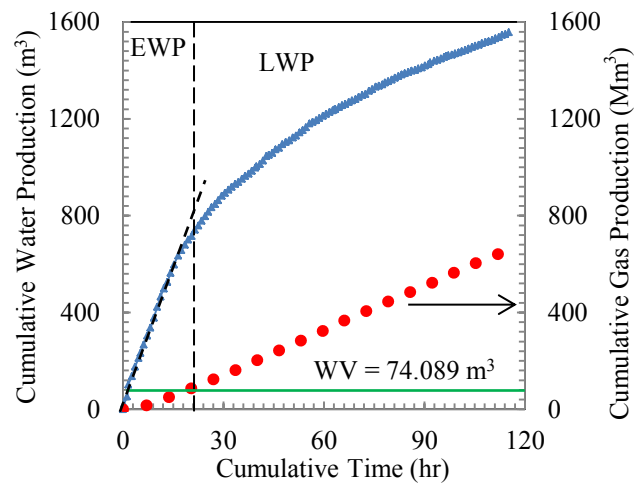


Fig. 3.5. Comparison between cumulative water and gas production curves and wellbore volume of Well 2.

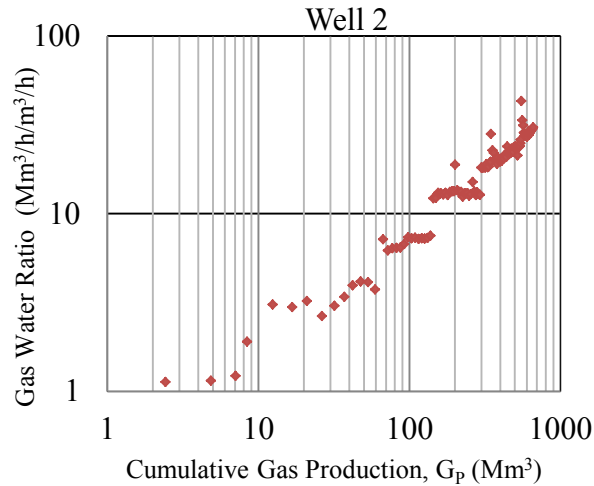


Fig. 3.6. Gas water flow rate ratio (GWR) versus cumulative gas production (G_p) of Well 2.

3.1.3. Well 3

This well is completed in a tight oil reservoir. Initially, the well was flowed back with seven choke sizes for about 38 hours. Then a choke size of 38.10 mm was used for about 37 hours.

3.1.3.1. *Flowback History*

Figure 3.7 shows the flow rate and pressure measured at the surface during the flowback of Well 3. Casing pressure is initially high and quickly drops with time. Similarly, the rate and pressure plot is divided into three regions. In the first region, q_o is zero and water production dominates with a rate specified by the choke size. In the second region, oil flow rate ramps up and q_w gradually decreases. In the third region, q_w is relatively low and oil production dominates.

Figure 3.8 compares the cumulative water and oil production versus time. Again the cumulative water curve shows two distinct regions. The first region (EWP) is denoted by a black dashed line which shows a steep increase in water production for about 38 hours. During the second region (LWP), water production slowly increases and reaches to a constant value at the end of flowback operation. Interestingly, this plateau observed here was not observed in the previous two gas cases. Furthermore, the oil breakthrough occurs at a much later time compared with gas breakthrough in the previous cases. Similarly, the fast water production during EWP can be explained by the relative permeability effect. The other curve shows that 38 hours after opening the well, oil breaks through and its production gradually increases. One should note that water recovery curve shown in Figure 3.8 is analogous to oil recovery curve in water flood projects. After oil breakthrough, water cumulative curve deviates from the linear behavior, and water rate gradually decreases to very low values.

Figure 3.9 shows the log-log plot of oil water flow rate ratio (OWR) versus cumulative oil production (N_p) of Well 3. In general, OWR plot shows an increase in OWR with time. Increase in OWR means that the ratio between oil and water saturations and that between oil and water relative permeabilities in fractures increases with time.

Table 3.2 shows that TIV in Well 3 is 2783.2 m³, and 1346.51 m³ of that is recovered after 75 hours of flowback operation. This means that flowback efficiency (TLR/TIV) is 48.37 % that is more than two times of flowback efficiency for the previous two gas cases. This can be partly explained by lower

mobility of oil compared with gas that leads to a more efficient water displacement in fractures. This argument is backed with later breakthrough of oil compared with that of gas observed in the first two field cases. The wellbore volume (WV) here is 103.922 m^3 , which is initially filled with water and contributes to 7.71 % of the TLR. During EWP, 1200 m^3 of water is produced which is about 89.11 % of TLR and the remaining recovered water is produced during LWP.

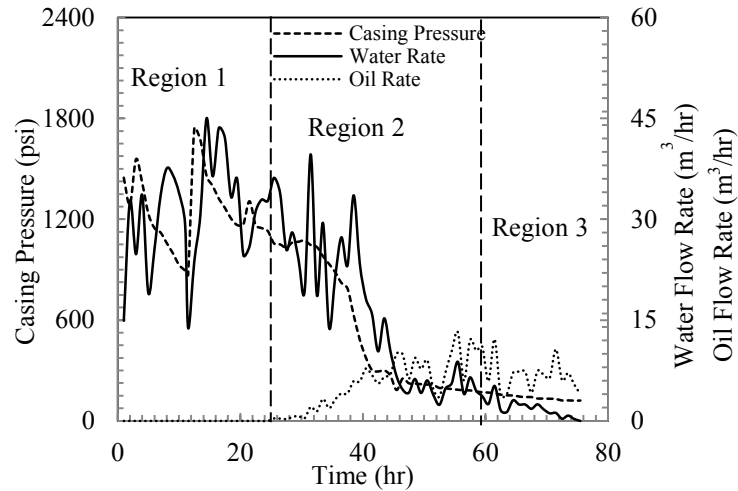


Fig. 3.7. Pressure and flow rate history measured hourly during the flowback operation of Well 3. Three different regions are identified. In Region 1, water production dominates. In Region 2, water production decreases and oil production increases. In Region 3, oil production dominates.

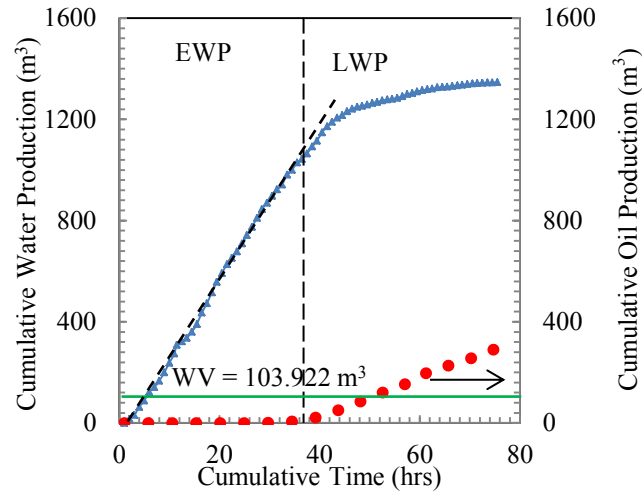


Fig. 3.8. Comparison between cumulative water and oil production curves and wellbore volume of Well 3.

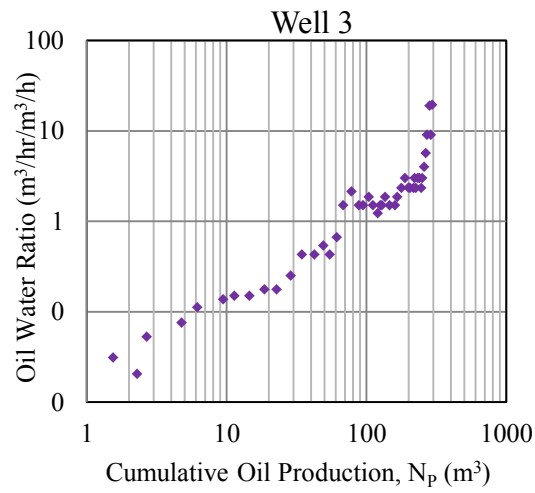


Fig. 3.9. Oil water flow rate ratio (OWR) versus cumulative oil production (N_p) of Well 3.

Table 3.2. Comparison of relative volumes of water recovered during the flowback of Well 1, Well 2 and Well 3.

Relative Water Volume	Well 1	Well 2	Well 3
Total Injected Volume (TIV), m ³	1501	6443.38	2783.2
Breakthrough Time, hrs	5	6	38
Total Flowback Time, hrs	86	116	75
Total Load Recovery (TLR), m ³	329.64	1521.16	1346.5
Wellbore Volume (WV), m ³	92.042	74.089	103.92
Ratio of TLR to TIV, %	21.96	23.60	48.37
Ratio of WV to TLR, %	27.92	4.87	7.71
Ratio of LR @ EWP to TLR, %	79.17	49.96	89.11

3.1.4. Comparative Interpretation

The rate plots of the three field cases consistently show three regions:

- Region 1, where water production dominates.
- Region 2, where water production drops and hydrocarbon production increases.
- Region 3, where hydrocarbon production dominates.

Region 1 is very short for the gas wells while it lasts much longer for the oil well. Furthermore, this region is influenced by wellbore storage. The data presented in Table 3.2, and Figures 3.2, 3.5, and 3.8 indicate that the volume of water recovered during region 1 is comparable to the volume of wellbore. This is more pronounced for well 1 as is indicated in Figure 3.2. After oil or gas breakthrough (region 2 and region 3) the phase saturation (S_w , S_o or S_g) in fractures change with time, and the system variables include

- Phase saturation (S_w, S_o or S_g)
- Phase mobility ($\frac{k_w}{\mu_w}, \frac{k_o}{\mu_o}$ or $\frac{k_g}{\mu_g}$)
- Total compressibility ($C_t = C_g S_g + C_o S_o + C_w S_w + C_m$)

We further classify the flowback history based on the water and gas/oil production curves into two major periods of EWP and LWP. Table 3.2 compares the relative volumes of water recovered during the flowback of the three wells. The low flowback efficiency of wells 1 and 2 compared with well 3 is consistent with early gas breakthrough compared with relatively late oil breakthrough due to its lower mobility. Gas can easily channel through water especially in vertical fractures below the horizontal well, that leads to poor sweep efficiency (Parmar et al., 2012; Parmar et al., 2013). This partly explains why the ratio of TLR to TIV is only 21.96 % and 23.60 % for wells 1 and 2 respectively, while it is 48.37 % for well 3. Furthermore, in contrast to wells 1 and 2, the water recovery curve of well 3 reaches to a plateau that can be explained by a similar argument.

We also observe that the fraction of TLR produced during EWP (early linear part of water production curve) for well 2 (49.96 %) is much lower than that for wells 1 and 3 (79.17 % and 89.11 %, respectively). This can be explained by the fact that well 2 has a shorter horizontal length and a lower number of fracture stages compared with the other two wells.

3.1.5. Approximate Volume and Interface of Fractures Depleted after Flowback

We can also estimate the depleted fracture volume by using the cumulative water recovery and a simple material balance. Assuming negligible water influx from the matrix, the recovered water volume is given by

$$V_{Rec} = V_f \phi_f (1 - S_w)$$

Here, V_{Rec} , ϕ_f and S_w , represent total water volume recovered, fracture porosity and water saturation left in the hydraulic fractures at that point in time, respectively. Therefore, depleted fracture volume V_f is given by

$$V_f = \frac{V_{Rec}}{\phi_f(1-S_w)}$$

This equation is only valid if we assume that the water produced during the flowback comes from the induced fractures, and matrix water influx is negligible. One should note that this assumption does not mean that there is no water imbibition or leak off. Instead, it means that the imbibed or leaked-off water can hardly be produced back due to the capillarity and relative permeability effects. Dilution of fracture water with formation water or leak-off water can be investigated by flowback chemical analysis (Asadi et al., 2008), that is beyond the scope of this work. Table 3.3 shows the approximate fracture volume for the three flowback cases. ϕ_f and S_w are uncertain parameters, and are assumed to be 48% and 30%, respectively.

We can also estimate the fracture interface created per stage by using the depleted fracture volume and assuming an average fracture aperture

$$A_{cm} = \frac{V_f}{(W_f \cdot N_f)}$$

Here, A_{cm} , W_f and N_f represent the matrix-fracture cross-sectional area, fracture aperture and number of fracture stages, respectively. Table 3.3 and Figure 3.10 present the matrix-fracture cross-sectional area created per stage for different values of fracture aperture. We assume four sets of fracture aperture varying from 0.5 mm to 0.5 cm to estimate the matrix-fracture cross-sectional area created per stage.

Table 3.3. Approximate fracture volume and matrix-fracture cross-sectional area created per stage at the end of the flowback operation of the three wells.

		Well 1	Well 2	Well 3
V_f, (ft³)		34646	159930	141520
w_f, (m)	w_f, (ft)	A_{cm}, (ft²)		
0.005	0.0164	105601	650000	431000
0.003	0.0098	176001.7	1080000	719000
0.001	0.0033	528005	3250000	2160000
0.0005	0.0016	1056010	6500000	4310000

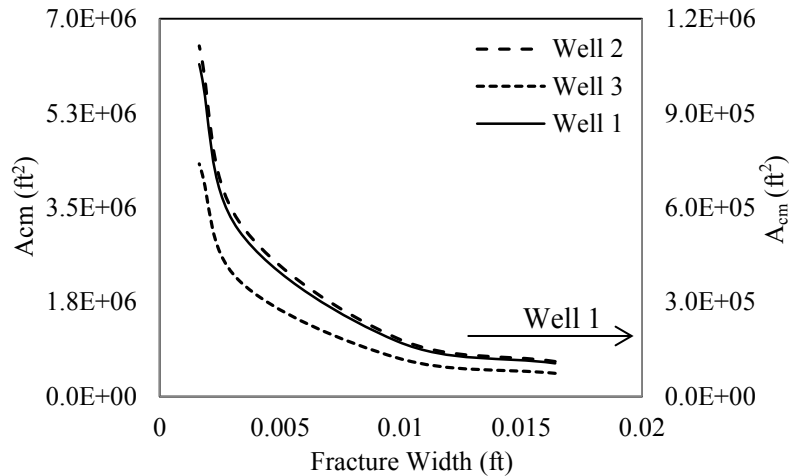


Fig. 3.10. Average matrix-fracture interface created per stage versus fracture aperture at the end of the flowback operation for the three wells.

3.2. Comparing the Pressure Transient Behaviour

This section develops an analytical model to compare the pressure transient behavior of the three wells. First, we describe the conceptual model assumed for developing the governing equations. Then we combine the solutions of continuity and diffusivity equations to present an analytical solution for the average fracture pressure. Finally, we develop a linear relationship between rate normalized pressure (RNP) and material balance time (MBT) by assuming negligible matrix influx at the early time scales.

3.2.1. Conceptual Model

The conceptual model used in this study is similar to that proposed by Fan et al., (2010) and Clarkson (2012). Figure 3.11 shows a multifracted horizontal well with multiple perforation clusters per stage. A stimulated tight reservoir consists of 1) the wellbore (*wb*) consisting of the horizontal and vertical sections,

2) the fractures (f), which are mainly vertical if the minimum stress is in the horizontal direction, and 3) the rock matrix (m). The vertical hydraulic fractures are connected to the horizontal well with the length of X_e . The formation thickness and fractures half-length are denoted by h and y_e , respectively.

3.2.2. Material Balance Equation for Early Time Flowback

We use the mass conservation law to develop a relationship between the water production rate and average system pressure drop with respect to time. Figure 3.11 shows the control volume, which includes the hydraulic fractures and wellbore including both horizontal and vertical sections. The material balance equation is given by

$$\text{Mass in} - \text{Mass out} = \text{Accumulation}, \quad (3.1)$$

$$q_m \rho_m B_m - q_s \rho_s B_s = \frac{d}{dt} (\rho_f V_f + \rho_{wb} V_{wb}). \quad (3.2)$$

Here, subscripts f , s , wb and m denote fracture, surface, wellbore and matrix, respectively. B represents formation volume factor, which is the ratio between the fluid volume in the reservoir to that on the surface conditions.

We assume single phase flow at very early times. Therefore, we assume no matrix influx ($q_m = 0$) for that short time period. Expanding the derivative term on the right-hand side of Eq. (3.2) gives

$$-q_s \rho_s B_s = \rho_f \frac{d}{dt} V_f + V_f \frac{d}{dt} \rho_f + V_{wb} \frac{d}{dt} \rho_{wb}. \quad (3.3)$$

The first term on the right-hand side describes the change in fracture volume with time. This term is negative during the fracture closure, and it is zero

after fracture closure. The second and third terms represent the change in the density of the fluid in fractures and wellbore, respectively. We further simplify the above equation by using the chain rule:

$$-q_s \rho_s B_s = \rho_f \frac{dV_f}{dP_f} \frac{dP_f}{dt} + V_f \rho_f \frac{1}{\rho_f} \frac{d\rho_f}{dP_f} \frac{dP_f}{dt} + V_{wb} \rho_{wb} \frac{1}{\rho_{wb}} \frac{d\rho_{wb}}{dP_{wb}} \frac{dP_{wb}}{dt}. \quad (3.4)$$

By considering the definition of isothermal compressibility for wellbore fluid (C_{wb}) and fracture fluid (C_f), the above equation can be written as

$$-q_s \rho_s B_s = \rho_f \frac{dV_f}{dP_f} \frac{dP_f}{dt} + V_f \rho_f C_f \frac{d\rho_f}{dt} + V_{wb} \rho_{wb} C_{wb} \frac{d\rho_{wb}}{dt}. \quad (3.5)$$

We assume that $\rho_s \approx \rho_{wb} \approx \rho_f$. This assumption means that the average density of fluid recovered at the surface, that of fluid in the wellbore, and in the fractures are almost equal.

We also assume $\frac{dP_{wb}}{dt} \approx \frac{dP_f}{dt} \approx \frac{d\bar{P}}{dt}$, that means the rate of change of pressure with respect to time in the wellbore is almost equal to that in the fracture, and is given by an average pressure drop with respect to time in the control volume $\frac{d\bar{P}}{dt}$.

Now equation Eq. (3.55) becomes

$$-q_s B_s = \left(\frac{dV_f}{dP_f} + V_f C_f + V_{wb} C_{wb} \right) \frac{d\bar{P}}{dt}. \quad (3.6)$$

The total storage coefficient is defined as

$$C_{st} = \frac{dV_f}{dP_f} + V_f C_f + V_{wb} C_{wb}. \quad (3.7)$$

The first term on the right-hand side accounts for fracture closure. The second and third terms represent the fracture and wellbore storage, respectively.

One should note that the cumulative water production plots in Figures 3.2, 3.5, and 3.8 and the estimations given in Table 3.2 indicate that $V_f \gg V_{wb}$. Finally, the material balance equation is given by

$$\frac{d\bar{P}}{dt} = \frac{-q_s B_s}{C_{st}} \quad (3.8)$$

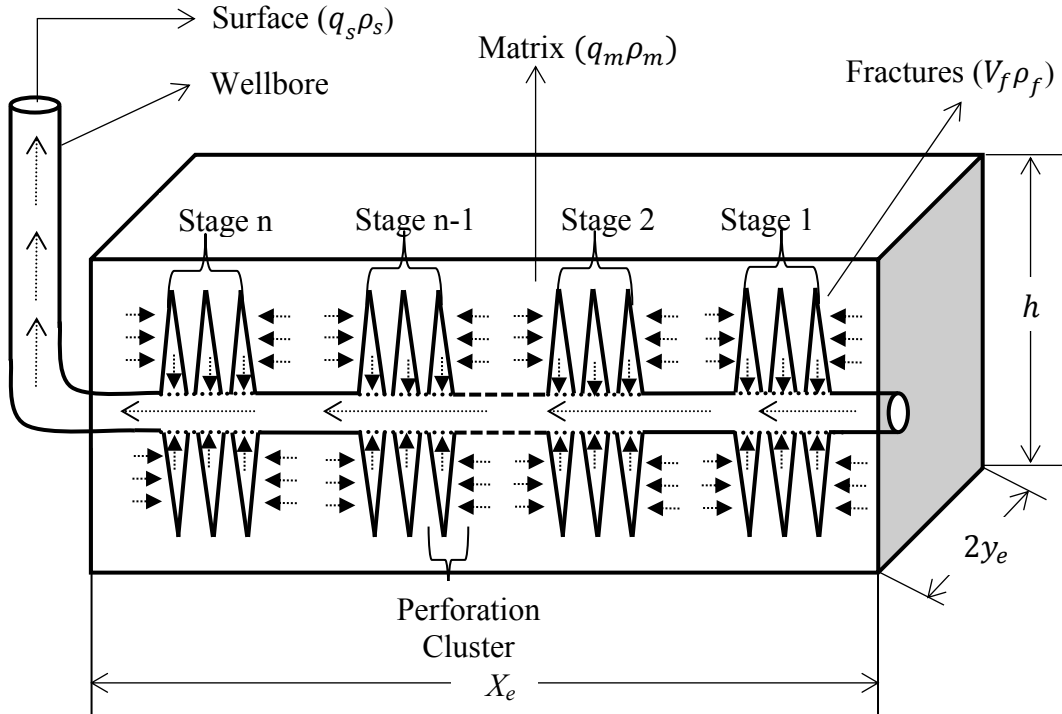


Fig. 3.11. 3D view of a fractured horizontal well considered for developing the material balance equation. Dashed arrows show fluid flow direction, which is sequentially from matrix to fractures, fractures to wellbore, and finally from wellbore to surface.

3.2.3. Combining Material Balance and Diffusivity Equations

We consider radial and linear flow of fracture water towards the horizontal well, as shown in Figure 3.12 (a and b). The fracture height and fracture half-length are denoted by h_f and y_e , respectively.

3.2.4. Radial Transient Model

The radial diffusivity equation for single-phase water flow through the hydraulic fracture towards the horizontal well is given by

$$\frac{1}{r} \frac{\partial}{\partial r} \left(r \frac{\partial P_f}{\partial r} \right) = \frac{\phi_f C_{t\mu}}{K_f} \frac{\partial P_f}{\partial t}. \quad (3.9)$$

The application of Eq. 3.9 also involves the following assumptions:

1. Negligible gravity effect
2. Constant temperature and viscosity
3. Constant porosity, permeability, and total compressibility
4. Negligible fluid influx from matrix into the fractures

Equation (3.9) can be solved under the following boundary conditions:

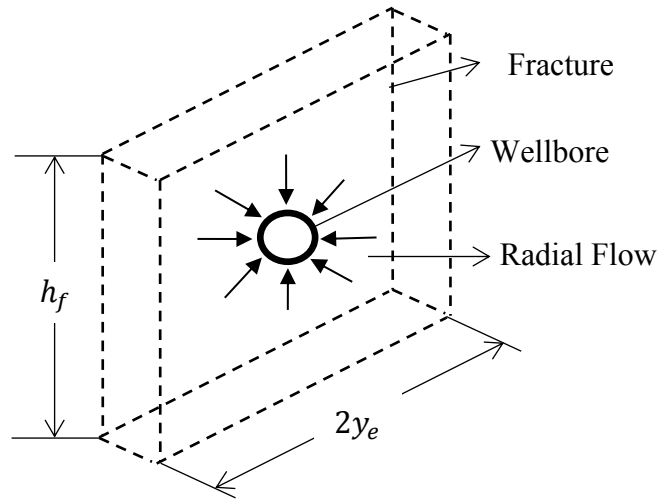
- $\frac{\partial P}{\partial r} = 0$ at $r = r_e$
- $P = P_{wf}$ at $r = r_w$
- $\frac{r_w^2}{r_e^2} \approx 0$

Therefore, the fracture pressure in time and space is given by (see Appendix A).

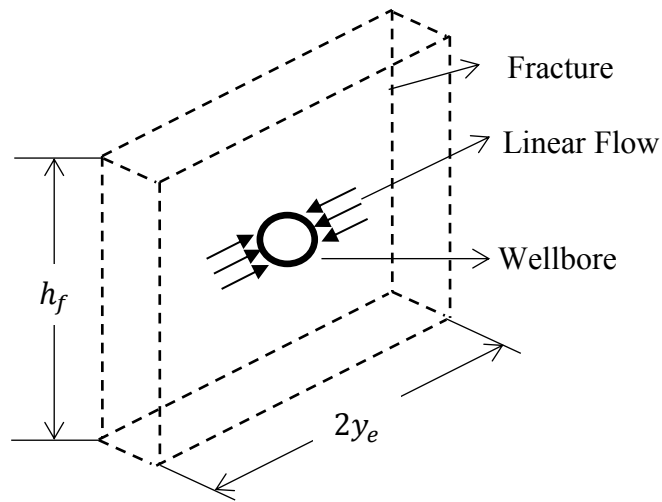
$$P_f(r, t) = P_{wf} - \frac{\phi_f C_{t\mu} q_s B_s}{K_f 2C_{st}} r_e^2 \left[\ln \left(\frac{r_w}{r} \right) + \frac{r^2}{2r_e^2} \right]. \quad (3.10)$$

Where, r_e is an equivalent fracture drainage radius. The average fracture pressure as a function of time is

$$\bar{P}(t) = P_{wf} - \frac{\phi_f C_{t\mu} q_s B_s}{K_f 2C_{st}} r_e^2 \left[\ln \left(\frac{r_w}{r_e} \right) + \frac{3}{4} \right]. \quad (3.11)$$



(a) Radial flow through fracture



(b) Linear flow through fracture

Fig. 3.12. 3D view of a fracture with a horizontal well in the center considered for solving the diffusivity equation. Bold arrows show **(a)** radial and **(b)** linear water flow towards the horizontal well.

In reality, the fracture geometry is not circular. The following generalized solution applies for different fracture geometries (see Appendix A):

$$\bar{P}(t) = P_{wf} + \frac{\phi_f C_{t\mu} q_s B_s}{K_f 2C_{st}} r_e^2 \left[\frac{1}{2} \ln \left(\frac{4A}{C_A \gamma r_w^2} \right) \right]. \quad (3.12)$$

Where, A is the area of a single vertical fracture and C_A is the shape factor, which specifies the fracture geometry.

3.2.5. Linear Transient Model

A similar approach can be followed to solve the system pressure assuming linear flow of fracturing fluid towards the horizontal well (see Figure 3.12 (b)). The derivation details are given in Appendix (B), and the final solution is given by Equation. 3.13 that is analogous to Equation 3.12.

$$\bar{P}(t) = P_{wf} + \frac{\phi_f C_{t\mu} q_s B_s}{K_f 3C_{st}} y_e^2. \quad (3.13)$$

3.2.6. Relationship between RNP and MBT

Fluid expansion and fracture closure are the dominant mechanisms at the early time scales in the absence of matrix influx ($q_m = 0$):

$$N_p B_s = -C_{st}(\bar{P} - P_i). \quad (3.14)$$

Where, N_p is the cumulative fracturing fluid production. Rearranging Eq. (3.14) gives the average fracture pressure:

$$\bar{P}(t) = P_i - \frac{N_p B_s}{C_{st}}. \quad (3.15)$$

Substituting Eq. (3.15) into Eq. (3.12), and dividing both sides by $q_s B_s$ gives

$$\frac{P_i - P_{wf}}{q_s} = \frac{N_P B_s}{q_s C_{st}} + \frac{\phi_f C_t \mu B_s}{2 C_{st} K_f} r_e^2 \left[\frac{1}{2} \ln \left(\frac{4A}{C_A \gamma r_w^2} \right) \right]. \quad (3.16)$$

The terms $\frac{P_i - P_{wf}}{q_s}$ and $\frac{N_P}{q_s}$ are referred to as rate normalized pressure (RNP) and material balance time (MBT):

$$RNP = \frac{B_s}{C_{st}} MBT + \frac{\phi_f C_t \mu B_s}{2 C_{st} K_f} r_e^2 \left[\frac{1}{2} \ln \left(\frac{4A}{C_A \gamma r_w^2} \right) \right]. \quad (3.17)$$

An analogous expression can be derived for linear flow starting from Eq. 3.13:

$$RNP = \frac{B_s}{C_{st}} MBT + \frac{\phi_f C_t \mu B_s}{3 C_{st} K_f} y_e^2. \quad (3.18)$$

Equations (3.17) and (3.18) describe a linear relationship between RNP and MBT. These equations are analogous to the equations proposed by Palacio and Blasingame (1993) for application of material balance time for boundary dominated liquid and gas flow in vertical wells. The proposed equations are also analogous to the flowing material balance equation (FMB), (Agarwal et. al., 1999, Mattar and Anderson, 2003 and Mattar and Anderson, 2005). Clarkson et. al. (2008), demonstrated that FMB could be applied to single phase coal bed methane (CBM) reservoirs. Furthermore, application of MBT and RNP has been recently discussed and applied for production data analysis of shale gas reservoirs (Song et. al., 2011a; and Song et al., 2011b). Equations (3.17) and (3.18) can be used for history matching the production data measured during the early-time flowback with a relatively high frequency and accuracy. The line slope can be interpreted to estimate the total storage coefficient defined by Eq. (3.7). If other parameters are

known, the intercept can be used to characterize the fracture geometry by calculating $(\frac{A}{C_A})$ for the radial case, and fracture half length (y_e) for the linear case. However, successful application of this model requires high frequency and accurate rate and pressure data.

3.3. Model Application

The proposed model can be used to history match single phase water rate and pressure measured at the beginning of flowback operation. Therefore, Region 1 provides the most representative data set for history matching using Eq. (3.17) and Eq. (3.18).

3.3.1. Analysis Procedure

We propose the following analysis procedure:

1. Obtain early-time flowback pressure and rate data.
2. Plot rate normalized pressure (RNP) versus material balance time (MBT).
3. Determine the slope and intercept of the best linear match.
4. Calculate total storage coefficient (C_{st}) by using the line slope.
5. Obtain a relationship for dimensionless radial fracture parameter

$$\frac{\phi_f}{K_f} r_e^2 \left[\frac{1}{2} \ln \left(\frac{4A}{C_A \gamma r_w^2} \right) \right] \text{ and dimensionless linear fracture parameter } \frac{\phi_f}{K_f} y_e^2 \text{ by}$$

using line intercept and C_{st} determined in step 4.

3.3.2. Example Applications

Unfortunately, the pressure and rate data are not measured with sufficient frequency required for an accurate analysis. Furthermore, we observe an early gas

breakthrough for the first two cases (wells 1 and 2) that shortens the duration of Region 1 described by the proposed model. However, we find it useful to demonstrate the application of the proposed model by using Region 1 of the three field data sets. Table 3.1 shows the completion data and fluid properties of the three wells. We first plot rate normalized pressure (RNP) versus material balance time (MBT) for Region 1 of the three wells as shown in Figures 3.13, 3.14 and 3.15. A linear relationship in the form of $RNP = m MBT + b$ is obtained in each case, where m and b can be interpreted as

$$m = \frac{B_s}{C_{st}}$$

$$b = \frac{\phi_f C_t \mu B_s}{2 C_{st} K_f} r_e^2 \left[\frac{1}{2} \ln \left(\frac{4A}{C_A \gamma r_w^2} \right) \right] \quad (\text{for radial fracture depletion})$$

$$b = \frac{\phi_f C_t \mu B_s}{3 C_{st} K_f} y_e^2 \quad (\text{for linear fracture depletion})$$

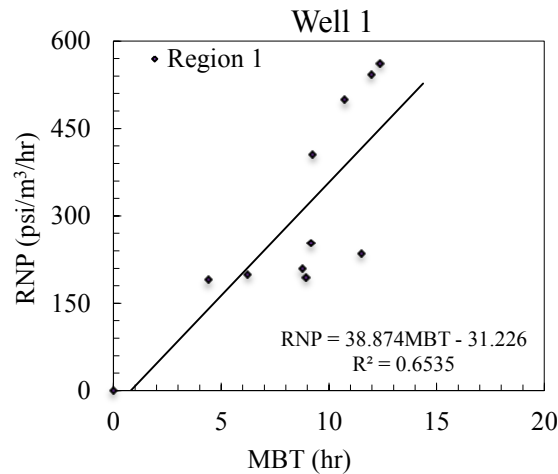


Fig. 3.13. RNP versus MBT of Region 1 and the best linear fit for Well 1.

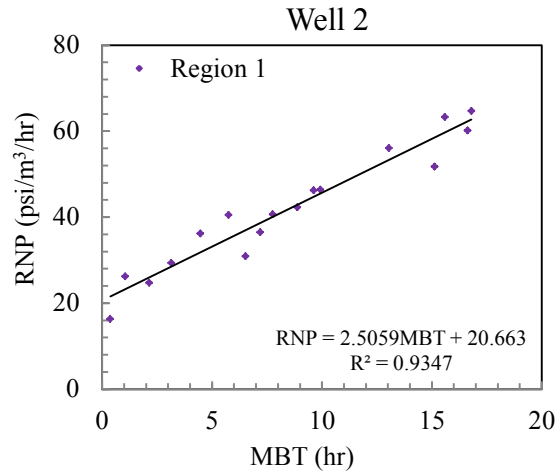


Fig. 3.14. RNP versus MBT of Region 1 and the best linear fit for Well 2.

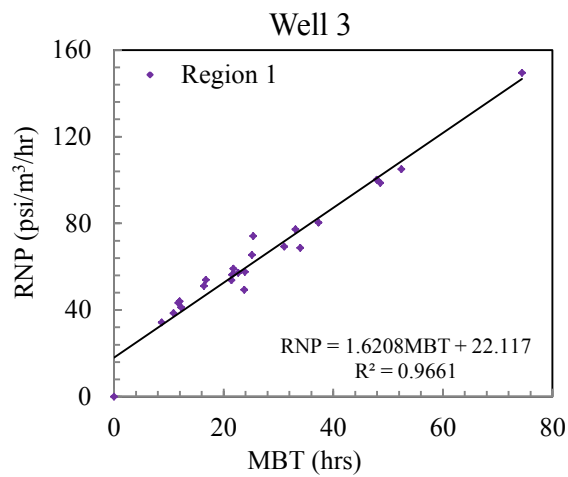


Fig. 3.15. RNP versus MBT of Region 1 and the best linear fit for Well 3.

The line intercept for Well 1 is negative that can't be described by the proposed model. The data points in this case are scattered. Dominance of wellbore volume and early gas breakthrough are among several reasons responsible for the lack of match. A better linear match is observed for the other

two wells. We first use the line slope to calculate the total storage coefficient (C_{st}) for the three multifracted horizontal wells. Next, we use the line intercept and other known parameters to obtain a relationship for the dimensionless fracture parameters; $\frac{\phi_f}{K_f} r_e^2 \left[\frac{1}{2} \ln \left(\frac{4A}{C_A \gamma r_w^2} \right) \right]$ for the radial case, and $\frac{\phi_f}{K_f} y_e^2$ for the linear case. Table 3.4 lists the calculated values of the total storage coefficient and the dimensionless fracture parameters for the three cases.

Table 3.4. Calculated values for the total storage coefficient, the dimensionless radial fracture parameter and the dimensionless linear fracture parameter.

Calculated Parameters	Well 1	Well 2	Well 3
Slope (m)	38.874	2.5059	1.6208
Intercept (b)	- 31.226	20.663	22.117
C_{st} , ft ³ /psi	0.936	14.504	21.800
$\frac{\phi_f}{K_f} r_e^2 \left[\frac{1}{2} \ln \left(\frac{4A}{C_A \gamma r_w^2} \right) \right]$, ft ² /md	N/A	45.759	74.942
$\frac{\phi_f}{K_f} y_e^2$, ft ² /md	N/A	68.638	112.41

3.3.3. Discussion of Results

The transient analysis leads to the following key observations:

1. The negative line intercept for well 1 cannot be described by the proposed model.
2. Total storage coefficient of well 3 is almost 30% higher than that of well 2.
3. The dimensionless fracture parameter of well 3 is higher than that of

well 2 for both radial and linear cases.

Result 1 indicates that the proposed model requires high frequency pressure and rate measurement before gas breakthrough. Furthermore, the wellbore volume should be relatively low enough compared with water volume produced before gas breakthrough.

Result 2 can be explained by comparing the completion and stimulation of wells 2 and 3: (i) The wellbore volume of well 3 is 30% higher than that of well 2. (ii) The number of fracture stages in well 3 is 25% higher than that in well 2. (iii) The water volume injected per stage in well 3 is almost 30 % of that in well 2. In contrast to the first two items, item (iii) is not in agreement with the observed trend. Although a lot more water is injected for treatment of well 2, it does not lead to a higher storage coefficient based on the proposed analysis. This is backed with the observation that flowback efficiency of well 3 is more than two times of that of well 2. Furthermore, a large volume of water injected in well 2 can leak off into the gas saturated matrix, and does not contribute to fracture storage. Furthermore, some of the induced hydraulic fracture may be cut-off from the effective hydraulic fracture network and in turn can not contribute to the flow. Hence the water becomes trapped in the ineffective hydraulic fracture clusters.

Result 3 indicates that the fracture length scale for well 3 is higher than that for well 2. Assuming equal fracture porosity and permeability, the fracture half-length of well 3 is estimated to be 20 % higher than that of well 2. Therefore, it qualitatively complements result 2 that indicates higher induced fracture volume

of well 3 compared with that of well 2. Results 2 and 3 indicate that fracturing operation of well 3 is more successful than that of well 2. However, the amount of water used for treatment of each stage in well 2 is almost three times higher than that in well 3. This can be explained by a stronger water leak-off in well 2 that is a gas well compared with well 3 that is an oil well.

3.4. Data Acquisition

Accurate and frequent measurement of flow rate and pressure during flowback operations is critical for history-matching using the proposed models. Therefore, data collection during flowback operations is the first and most important step for flow-back analysis. However, due to the operational issues, the data become noisy that may lead to discrepancies in the final analysis. Generally, flowback rate and pressure data are measured on hourly basis which is not sufficient for studying the transport phenomena quickly occurring at the early-time scales. In general, the flowing pressure can be measured with a high frequency (points/minute or points/second) (Ilk. et al., 2010), while the flow rate cannot be measured with this frequency due to the limitations of flow rate measurement devices. However, the frequency of flow rate data can be improved by using the pressure data, cumulative production data, and a technique called wavelet analysis which reduces the uncertainty and noise from the data. Athichanagorn et al. (2002), Kikani and He (1998) and Ouyang and Kikani (2002) introduced the wavelet analysis technique for analysis of the data measured by permanent downhole gauges. Furthermore, it is strongly recommended to conduct

a careful flow-regime analysis by constructing various diagnostic plots (Ilk. et al., 2010) before history-matching using the mathematical models.

Chapter 4

Diagnostic Plots

4.1. Introduction

This chapter presents a qualitative analysis and interpretation of the flow rate, pressure and cumulative gas and water production measured during the early time flowback operation of a well pad. This well pad consists of eighteen multifractured horizontal wells which were drilled and completed in the three shale members of the Horn River basin. We developed various diagnostic plots based on the work of Ilk et. al., (2010). Ilk et. al., (2010) introduced a series of diagnostic plots for interpreting the early time flowback data. The diagnostic plots were used to identify the fracture depletion/clean up trend and tubing/casing lift curve.

4.2. Well Pad Description

The flowback rate and pressure data analyzed in this study are obtained from a pad of eighteen wells drilled and stimulated in the Horn River basin. The Horn River basin is located in the northeastern part of the British Columbia and extends northward into the northwest territories of Canada (Reynolds and Munn (2010)). Figure 4.1 shows the stratigraphic section of Horn River formation which belongs to Devonian age of the Western Canada Sedimentary Basin (WCSB). The three shale members of the Horn River basin (from top to bottom) are:

1. The Muskwa Shale (MU)
2. The Otter Park Shale (OP)
3. The Evie Shale (EV)

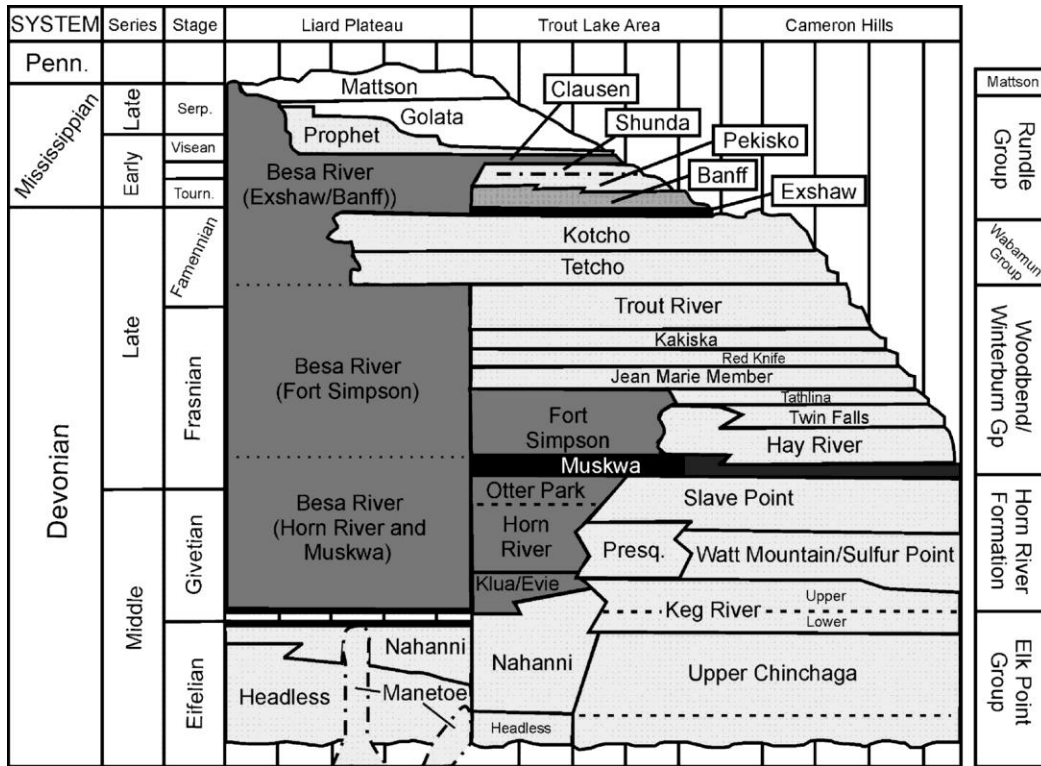


Fig. 4.1. Stratigraphic section of Devonian-Mississippian (Gal and Jones, 2003).

In this section, we present 1) the layout of the well pad, 2) the 3D view of the three shale members of the Horn River basin (each of the shale members consists of six multifractured horizontal wells), and 3) the completion design summary of the eighteen wells.

Figure 4.2 shows the layout of the eighteen wells drilled and completed in the three shale formations. Three wells were placed on the right side of the pad

and three wells on the left side of the pad in each formation. This results in the total of six wells in each formation, and the total of eighteen wells for the pad.

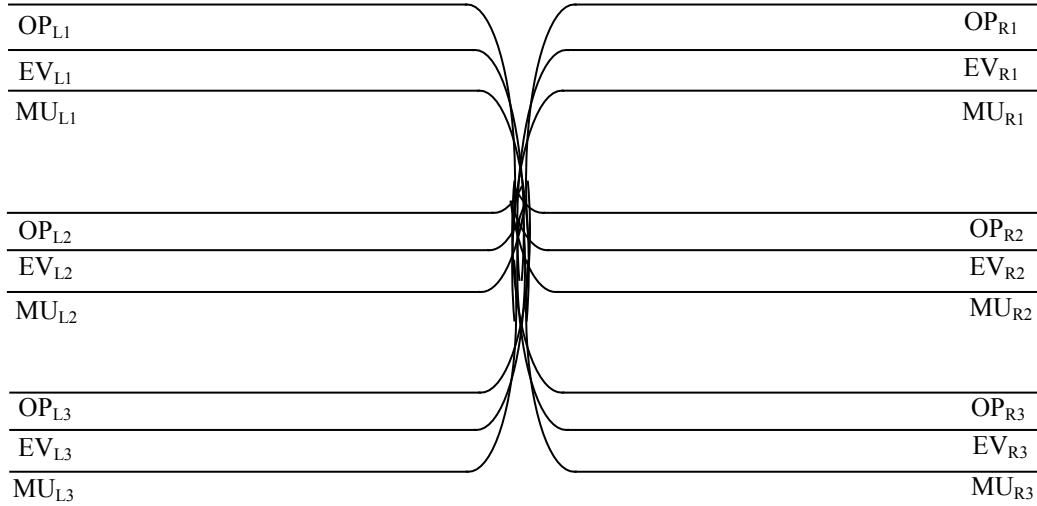


Fig. 4.2. Layout of a well pad drilled and completed in the Horn River basin. Total of eighteen wells were drilled, nine wells on the right side of the pad and nine wells on the left side of the pad.

The completion design summary of the eighteen wells is given in Table 4.1. The nine wells on the left side of the Muskwa, the Otter Park and the Evie formations are MU_{L1} , MU_{L2} , MU_{L3} , OP_{L1} , OP_{L2} , OP_{L3} and EV_{L1} , EV_{L2} , EV_{L3} , respectively. The nine wells on the right side of the Muskwa, the Otter Park and the Evie formations are MU_{R1} , MU_{R2} , MU_{R3} , OP_{R1} , OP_{R2} , OP_{R3} and EV_{R1} , EV_{R2} , EV_{R3} , respectively. Table 4.1 also lists the number of perforation clusters per stage, stage spacing, stimulated horizontal well length, number of fracture stages and the total injected water volume (TIV) for each well. The number of

perforation clusters per stage ranges from 3 to 5 perforation clusters per stage. The number of fracture stages varies from 16 to 21.

Table 4.1. Completion design summary of a well pad of eighteen wells.

Well Name	Formation Name	Perforation Clusters/stage	Stage Spacing (m)	Horizontal Well Length (m)	Fracture Stages	Total Injected Volume (TIV), m ³
MU _{R1}	Muskwa	3	40	2317	18	51523.00
MU _{R2}	Muskwa	5	25	2300	18	54231.60
MU _{R3}	Muskwa	5	25	2296	18	51153.10
MU _{L1}	Muskwa	5	25	2315	16	45392.10
MU _{L2}	Muskwa	5	25	2314	17	49543.00
MU _{L3}	Muskwa	5	25	2310	16	45533.00
OP _{R1}	Otter Park	3	40	2319	18	51753.50
OP _{R2}	Otter Park	3	40	2314	19	55338.90
OP _{R3}	Otter Park	5	25	2297	19	32619.50
OP _{L1}	Otter Park	5	25	2315	17	47516.00
OP _{L2}	Otter Park	5	25	2312	17	48361.00
OP _{L3}	Otter Park	4	25	2312	19	42360.00
EV _{R1}	Evie	3	40	2312	18	60326.10
EV _{R2}	Evie	3	40	2313	19	100000.0
EV _{R3}	Evie	3	40	2305	20	63677.90
EV _{L1}	Evie	4	25	2314	21	53349.50
EV _{L2}	Evie	4	25	2311	20	51417.80
EV _{L3}	Evie	4	25	2307	20	51561.80

4.2.1. Muskwa Formation

The total of six wells were drilled and completed in the Muskwa formation of the Horn River basin. Figure 4.3 shows the 3D view of six multilateral horizontal wells completed in the Muskwa formation. Wells MU_{R1}, MU_{R2} and MU_{R3} were placed on the right side of the formation. Wells MU_{L1}, MU_{L2}, and MU_{L3} were placed on the left side of the formation. All of the wells were

perforated with 5 perforation clusters per stage except MU_{R1} that was perforated with 3 perforation clusters per stage (see Table 4.1). Wells MU_{R1} , MU_{R2} and MU_{R3} were stimulated in 18 stages. Wells MU_{L1} and MU_{L3} were stimulated in 16 stages. Well MU_{L2} was stimulated in 17 stages.

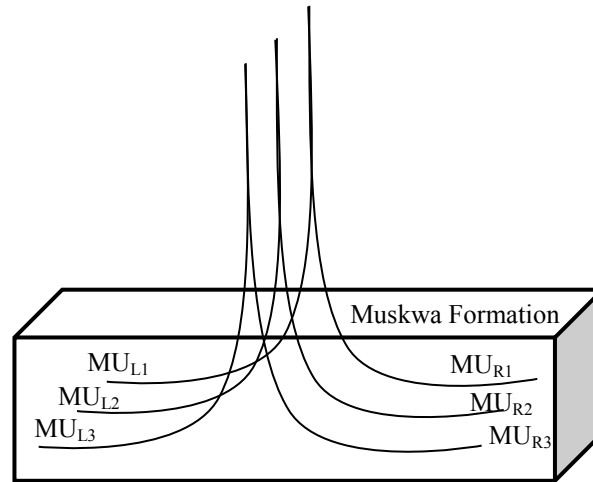


Fig. 4.3. 3D view of multilateral horizontal wells completed in the Muskwa formation. Total of six wells were drilled. Three wells on the right side of the pad and three wells on the left side of the pad.

4.2.2. Otter Park Formation

In Otter Park formation, a total of six wells were drilled and completed. Figure 4.4 shows the 3D view of six multilateral horizontal wells completed in the Otter Park formation. Wells OP_{R1} , OP_{R2} and OP_{R3} were placed on the right side of the formation. Wells OP_{L1} , OP_{L2} and OP_{L3} were placed on the left side of the formation. Out of the six wells, three were perforated with 5 perforation clusters per stage, two with 3 perforation clusters per stage and one with 4 perforation clusters per stage (see Table 4.1). Wells OP_{R2} , OP_{R3} and OP_{L3} were stimulated in

19 stages. Wells OP_{L1} and OP_{L2} were stimulated in 17 stages. Well OP_{R1} was stimulated in 18 stages.

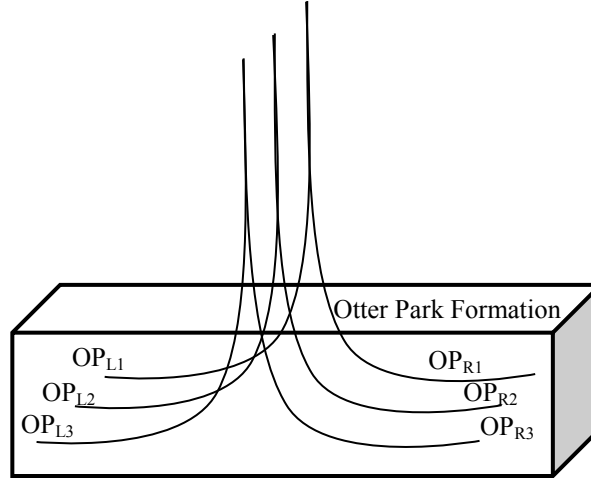


Fig. 4.4. 3D view of multilateral horizontal wells completed in the Otter Park formation. Total of six wells were drilled. Three wells on the right side of the pad and three wells on the left side of the pad.

4.2.3. Evie Formation

Evie formation is the deepest shale member of the Horn River basin. Similar to the Muskwa and the Otter Park, a total of six wells were drilled and completed in the Evie formation. Figure 4.5 shows the 3D view of six multilateral horizontal wells completed in the Evie formation. Wells EV_{R1} , EV_{R2} and EV_{R3} were placed on the right side of the formation. Wells EV_{L1} , EV_{L2} and EV_{L3} were placed on the left side of the formation. Wells EV_{R1} , EV_{R2} and EV_{R3} on right side of the pad were perforated with 3 perforation clusters per stage. Wells EV_{L1} , EV_{L2} and EV_{L3} on the left side of the pad were perforated with 4 perforation clusters per stage

(see Table 4.1). Wells EV_{R3} , EV_{L2} and EV_{L3} were stimulated in 20 stages. Wells EV_{R1} , EV_{R2} and EV_{L1} were stimulated in 18, 19 and 21 stages, respectively.

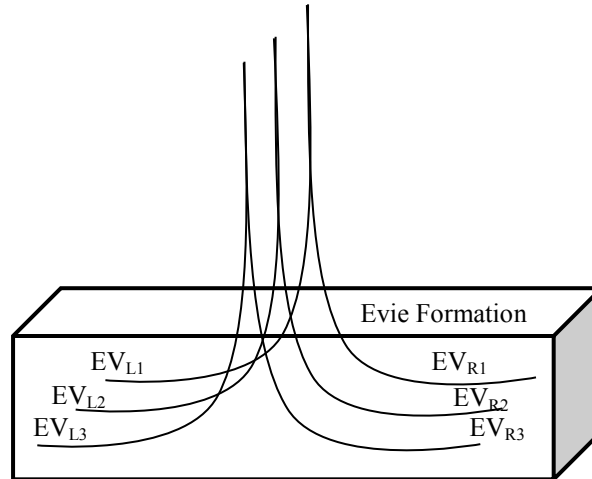


Fig. 4.5. 3D view of multilateral horizontal wells completed in the Evie formation. Total of six wells were drilled. Three wells on the right side of the pad and three wells on the left side of the pad.

4.3. Cumulative Production Plots

In Figure 4.6, we compare the cumulative water and gas production (W_P and G_P) versus cumulative time. Plots (b, d, and f for wells MU_{R1} , MU_{R2} , and MU_{R3} , respectively) on the right hand side of Figure 4.6 show W_P and G_P versus cumulative time of the three wells drilled and completed on the right side of the pad. Plots (a, c, and e for wells MU_{L1} , MU_{L2} , and MU_{L3} , respectively) on the left hand side of Figure 4.6 show W_P and G_P versus cumulative time of the three wells drilled and completed on the left side of the pad in the Muskwa formation. Figure 4.6 also shows the total injected volume (TIV) in each well.

Cumulative gas (G_p) plots of all the six wells show an immediate gas breakthrough at the very early time of the flowback operation. In general, three dominant Regions are observed based on the shape of the cumulative production (W_p) plots:

- Region 1, where W_p plot shows an upward curvature ($\frac{d^2W_p}{dt^2} > 0$).
- Region 2, where W_p plot shows a downward curvature ($\frac{d^2W_p}{dt^2} < 0$).
- Region 3, where W_p plot shows a straight line ($\frac{d^2W_p}{dt^2} \approx 0$).

Region 1 is observed in wells MU_{L3} and MU_{R1} . Region 1 dominates during the early time of the flowback operation.

Region 2 is observed in five wells (MU_{L1} , MU_{L2} , MU_{L3} , MU_{R2} and MU_{R3}). In wells MU_{L1} and MU_{L3} , Region 2 occurs at the late time scale. In well MU_{R3} , Region 2 occurs at the intermediate time scale. In wells MU_{L2} and MU_{R2} , Region 2 dominates during the whole flowback operation.

Region 3 is observed in wells MU_{L1} , MU_{R1} and MU_{R3} . In well MU_{L1} it occurs at the early time, while in well MU_{R1} it occurs at the late time scale. In well MU_{R3} , Region 3 occurs at the early and late time scales.

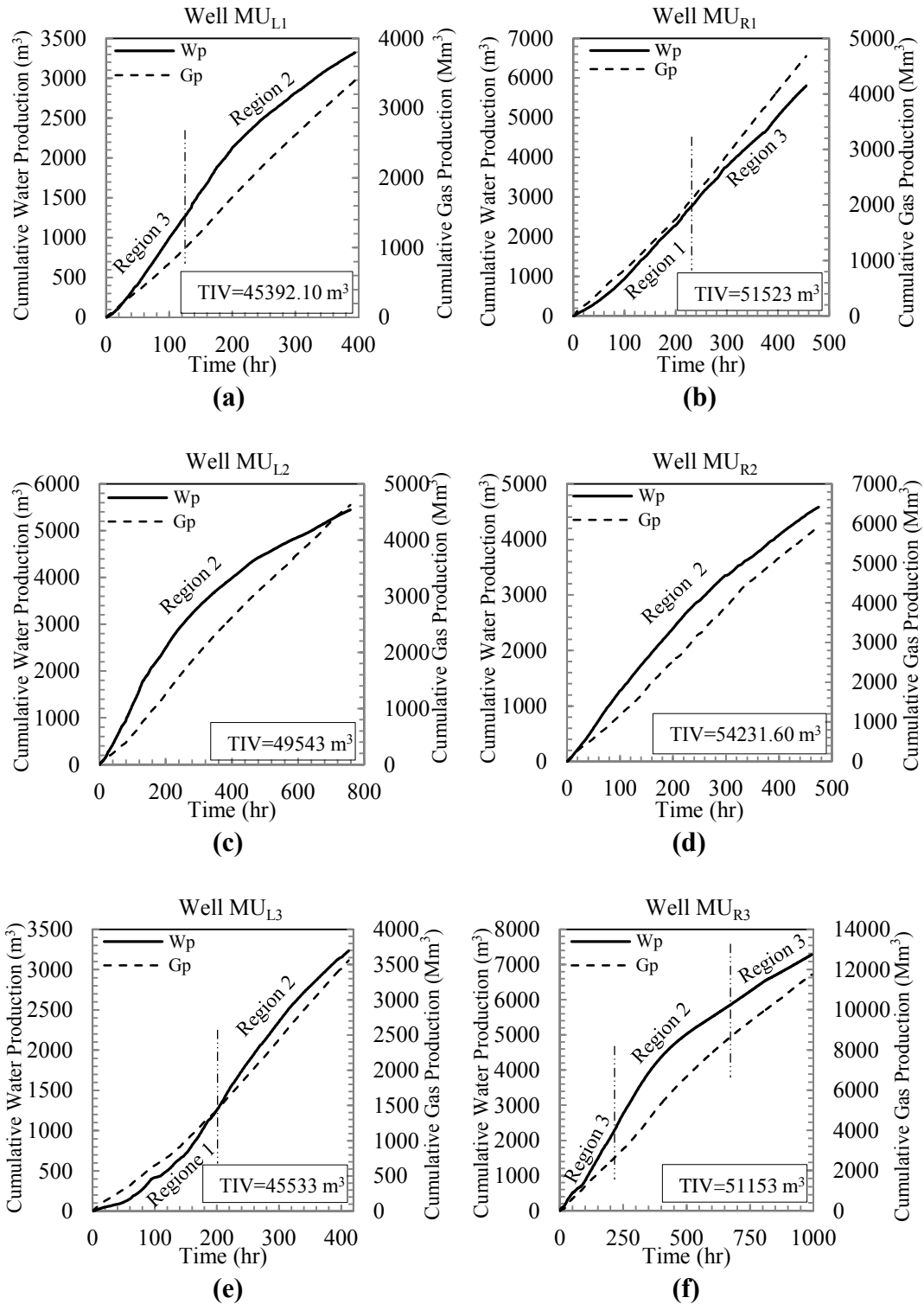


Fig. 4.6. Comparison of cumulative water and gas production (W_p and G_p) versus cumulative time of the six wells drilled in the Muskwa formation. Total injected volume (TIV) for the six wells is given in each graph.

Figure 4.7 shows the cumulative water and gas production (W_P and G_P) versus cumulative time. Plots (b, d, and f for wells OP_{R1} , OP_{R2} , and OP_{R3} , respectively) on the right hand side of Figure 4.7 show W_P and G_P versus cumulative time of the three wells drilled and completed on the right side of the pad. Plots (a, c, and e for wells OP_{L1} , OP_{L2} , and OP_{L3} , respectively) on the left hand side of Figure 4.7 show W_P and G_P versus cumulative time of the three wells drilled and completed on the left side of the pad in the Otter Park formation. The total injected volume (TIV) for each well is also given in Figure 4.7.

Similar to the wells in the Muskwa formation here in the OtterPark formation, the G_P plots show an immediate gas breakthrough. In general, three dominant Regions (Regions 1, 2 and 3) are observed based on the shape of the W_P plots as defined above for the wells completed in the Muskwa formation.

Region 1 is observed in wells OP_{L1} and OP_{R1} . Region 1 dominates during the early time of the flowback operation.

Region 2 is observed in wells OP_{L3} and OP_{R3} . In well OP_{L3} , Region 2 dominates during the whole flowback operation. In OP_{R3} , it occurs at the intermediate time scale.

Region 3 is observed in five wells (OP_{L1} , OP_{L2} , OP_{R1} , OP_{R2} and OP_{R3}). In wells OP_{L1} and OP_{R1} , Region 3 occurs at the late time scale. In wells OP_{L2} and OP_{R2} , it occurs during the whole flowback operation. Interestingly, in well OP_{R3} Region 3 occurs at the early and late time scales.

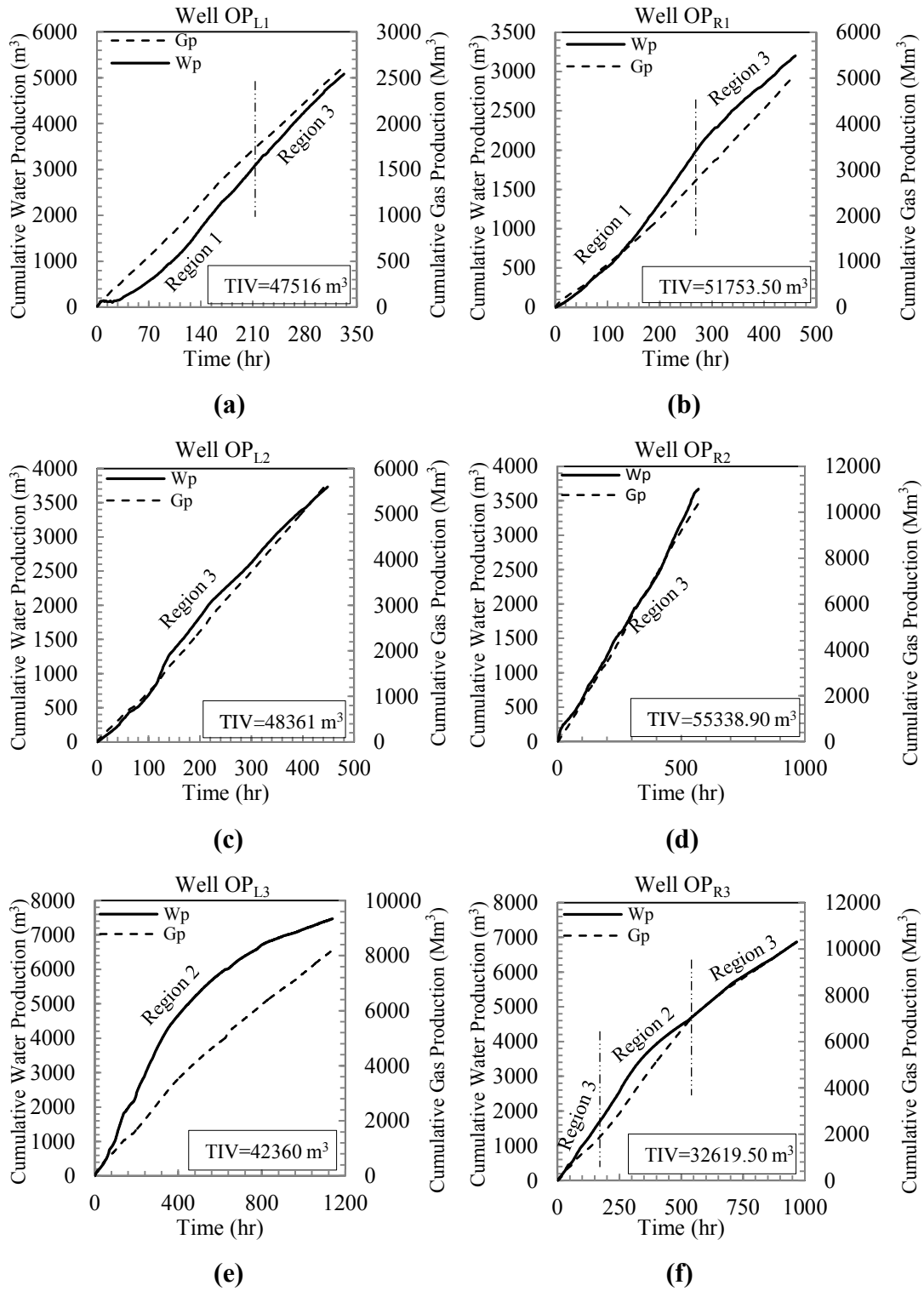


Fig. 4.7. Comparison of cumulative water and gas production (W_p and G_p) versus cumulative time of the six wells drilled in the Otter Park formation. Total injected volume (TIV) for six wells is mentioned in each graph.

Figure 4.8 compares the cumulative water and gas production (W_P and G_P) versus cumulative time of six wells drilled in the Evie formation. Plots (b, d, and f for wells EV_{R1} , EV_{R2} , and EV_{R3} , respectively) on the right hand side of Figure 4.8 show W_P and G_P versus cumulative time of the three wells drilled and completed on the right side of the pad. Plots (a, c, and e for wells EV_{L1} , EV_{L2} , and EV_{L3} , respectively) on the left hand side of Figure 4.8 show W_P and G_P versus cumulative time of the three wells drilled and completed on the left side of the pad in the Evie formation. Figure 4.7 also shows the total injected volume (TIV) in each well.

In general, three dominant Regions (Regions 1, 2 and 3) are observed based on the shape of the W_P plots as defined above for the wells completed in the Muskwa and the Otter Park formations.

Region 1 is observed only in well EV_{L3} and it occurs during the early time of the flowback operation.

Region 2 is identified in four wells (EV_{L2} , EV_{R1} , EV_{R2} and EV_{R3}). In wells EV_{L2} , EV_{R1} and EV_{R2} , Region 2 dominates the whole flowback operation. In well EV_{R3} , Region 2 occurs at the intermediate time scale.

Region 3 is observed in three wells (EV_{L1} , EV_{L3} , and EV_{R3}). In EV_{L1} , Region 3 dominates during the complete flowback operation. In well EV_{L3} , it occurs at the late time scale. In EV_{R3} , Region 3 is observed at the early and late time scales.

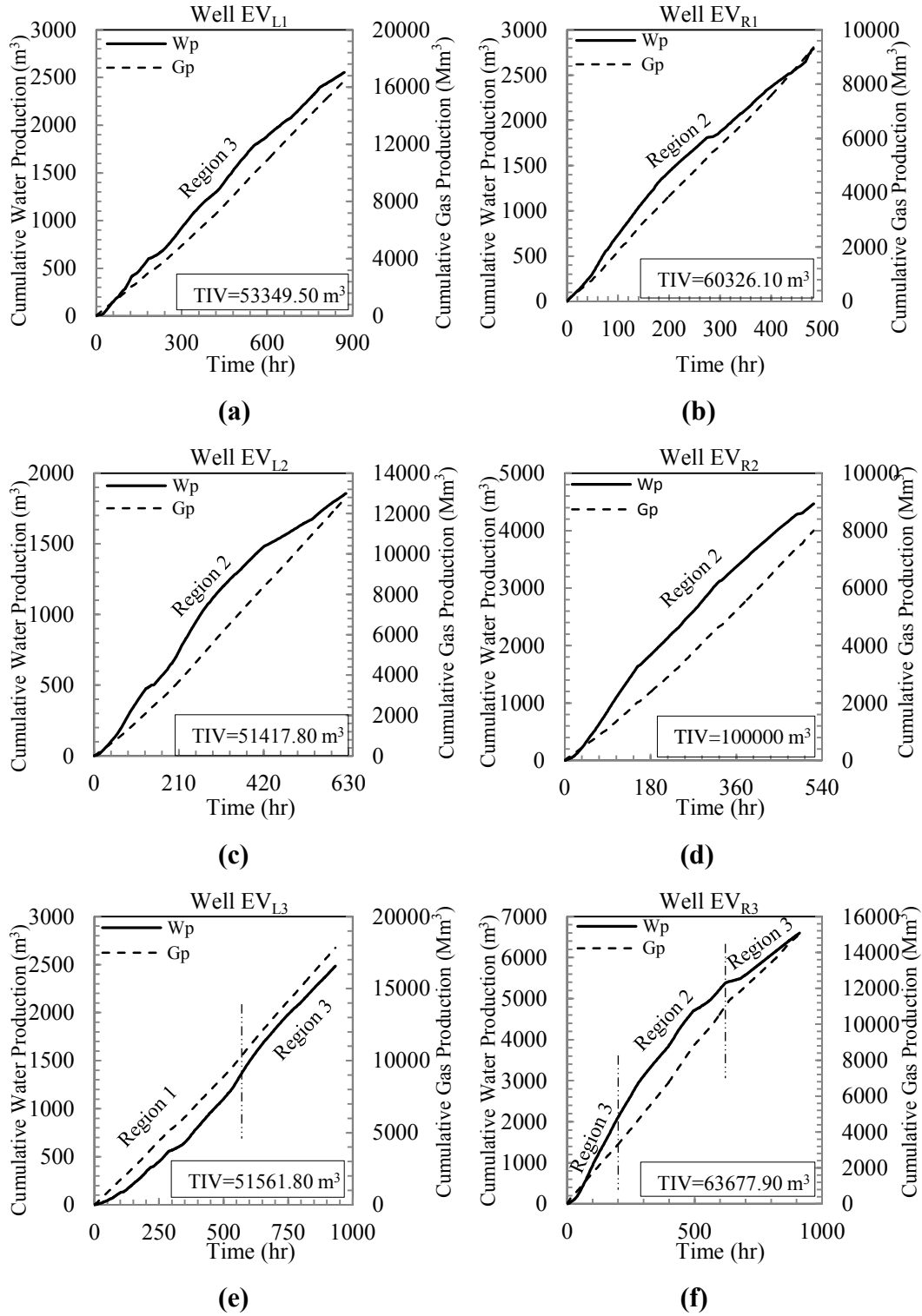


Fig. 4.8. Comparison of cumulative water and gas production (W_p and G_p) versus cumulative time of the six wells drilled in the Evie formation. Total injected volume (TIV) for the six wells is given in each graph.

4.3.1. Interpretation of Cumulative Production Plots

In general, the cumulative water production plots of the eighteen wells show three dominant Regions:

1. Region 1, where W_p plot shows an upward curvature ($\frac{d^2W_p}{dt^2} > 0$).
2. Region 2, where W_p plot shows a downward curvature ($\frac{d^2W_p}{dt^2} < 0$).
3. Region 3, where W_p plot shows a straight line ($\frac{d^2W_p}{dt^2} \approx 0$).

In Region 1, the W_p plot shows an upward curvature. The slope of the W_p curve can be interpreted as a water production rate. In the part of the W_p plots where the curvature is upward, the second derivative of the cumulative water production with respect to time is positive ($\frac{d^2W_p}{dt^2} > 0$), which means that the water flow rate increases with time.

During Region 2, W_p plot shows a downward curvature. In the part of the W_p plots where the curvature is downward, the second derivative of the cumulative water production with respect to time is negative ($\frac{d^2W_p}{dt^2} < 0$), which shows that the water flow rate decreases with time. Region 2 can also be explained in terms of relative change in the volumes of water and gas in fractures. Decrease in water flow rate with time in fractures can be explained by: 1) decrease in water saturation and relative permeability with time as gas is introduced from the matrix into the fractures.

In Region 3, W_P plot shows a straight line. During Region 3 the second derivative of the cumulative water production with respect to time is ($\frac{d^2 W_P}{dt^2} \approx 0$), which means that the water flow rate remains constant with time.

4.4. Flowback Rate History

The frequency and accuracy of flow rate measurement in any transient analysis is very important for meaningful analysis. However, flow rate measurement is challenging due to the device limitations. The measured flow rate in wells in the Horn River basin is noisy. Therefore, the water flow rate plots are classified based on the general trend observed in the water flow rate plots. The gas flow rate plots of eighteen wells show an immediate gas breakthrough. This immediate gas breakthrough was not observed in the gas wells discussed in chapter III.

Figure 4.9 shows the water and gas flow rate measured at the surface during the flowback of the six wells drilled in the Muskwa formation. Plots (b, d, and f for wells MU_{R1} , MU_{R2} , and MU_{R3} , respectively) on the right hand side of Figure 4.9 show water and gas flow rate of the three wells drilled and completed on the right side of the pad. Plots (a, c, and e for wells MU_{L1} , MU_{L2} , and MU_{L3} , respectively) on the left hand side of Figure 4.9 show the water and gas flow rate of the three wells drilled and completed on the left side of the pad in the Muskwa formation.

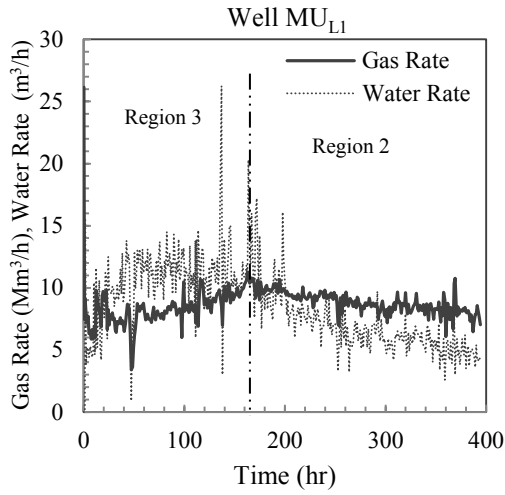
In general, the flow rate plots of the six wells in the Muskwa formation show three distinct Regions:

1. Region 1, where water flow rate increases with time.
2. Region 2, where water flow rate decreases with time.
3. Region 3, where water flow rate remains constant.

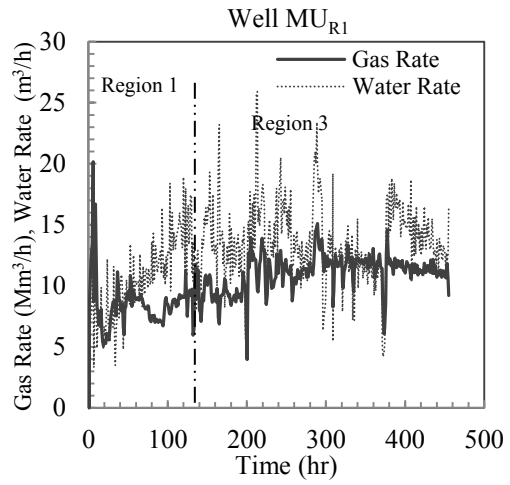
Region 1 is observed in wells MU_{L3} and MU_{R1} . Region 1 in rate plots correspond to Region 1 in the cumulative water production plots (see Figures 4.6, 4.7 and 4.8). Region 1 dominates during the early time of the flowback operation (flow rate plots of both the wells are consistent with the W_p plots). Region 1 is also observed in well MU_{L2} , where flow rate plot is not consistent with W_p plot in Figure 4.6 (c).

Region 2 is observed in wells MU_{L1} , MU_{L2} , MU_{L3} , MU_{R2} and MU_{R3} . Region 2 in rate plots correspond to Region 2 in the cumulative water production plots (see Figures 4.6, 4.7 and 4.8). In wells MU_{L1} and MU_{L3} , Region 2 occurs at late time scale. In well MU_{R3} , Region 2 occurs at intermediate time scale. In well MU_{R2} Region 2 dominates the whole flowback operation (flow rate plots of all the wells are consistent with the W_p plots except well MU_{L2} (see Figure 4.6 (c)).

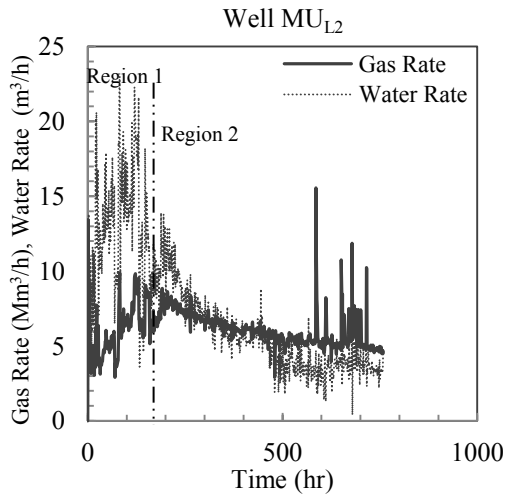
Region 3 is observed in wells MU_{L1} , MU_{R1} and MU_{R3} . Region 3 in rate plots correspond to Region 3 in the cumulative water production plots (see Figures 4.6, 4.7 and 4.8). In well MU_{L1} , Region 3 occurs at the early time scale, in well MU_{R1} , it occurs at the late time scale. In well MU_{R3} , Region 3 occurs at the early and late time scale (flow rate plots of all wells are consistent with the W_p plots).



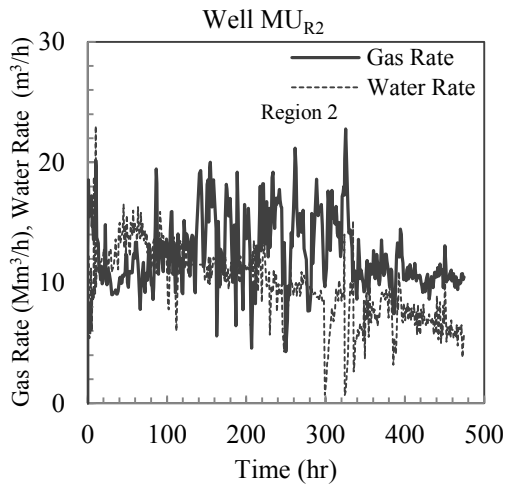
(a)



(b)



(c)



(d)

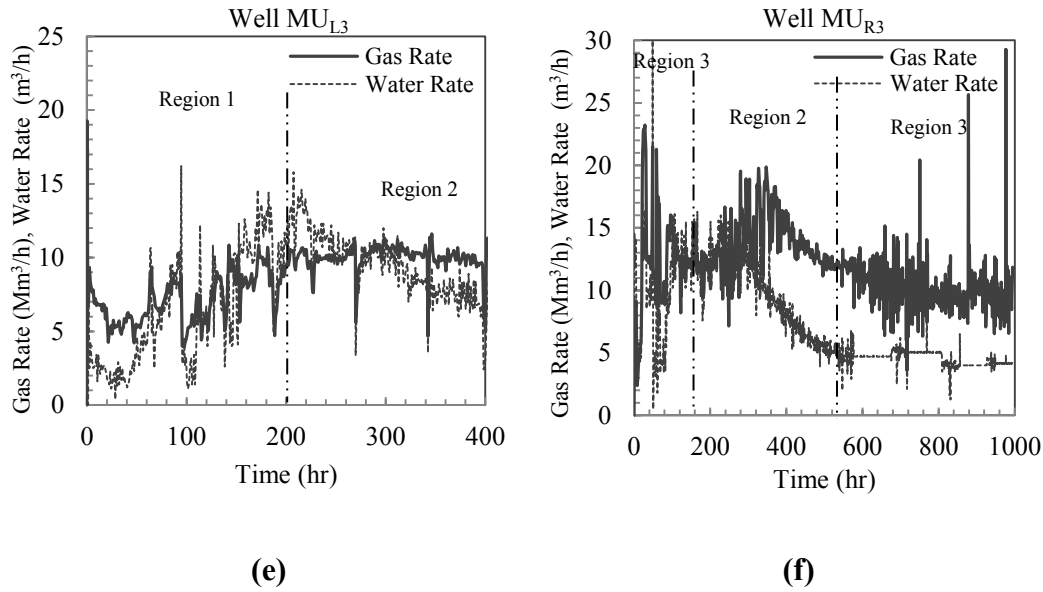


Fig. 4.9. Water and gas flow rate history measured during the flowback operation of six wells in the Muskwa formation.

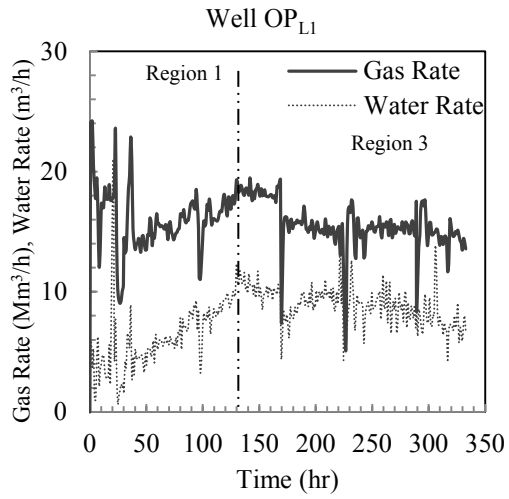
Figure 4.10 shows the water and gas flow rate of the six wells drilled in the Otter Park formation. Plots (b, d, and f for wells OP_{R1}, OP_{R2}, and OP_{R3}, respectively) on the right hand side of Figure 4.10 show the water and gas flow rate of the three wells drilled and completed on the right side of the pad. Plots (a, c, and e for wells OP_{L1}, OP_{L2}, and OP_{L3}, respectively) on the left hand side of Figure 4.10 show the water and gas flow rate of the three wells drilled and completed on the left side of the pad in the Otter Park formation.

Similar to wells in the Muskwa formation, here in the Otter Park formation three Regions are identified in the rate plots of the six wells. In Region 1, water flow rate increases with time. In Region 2, water flow rate decreases with time. In Region 3, water flow rate remains constant with time.

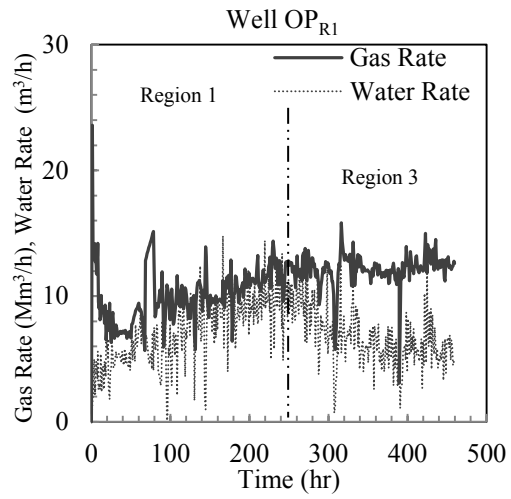
Region 1 is identified in wells OP_{L1} and OP_{R1} . Region 1 in the rate plots correspond to the Region 1 in the cumulative water production plots (see Figures 4.6, 4.7 and 4.8). Region 1 dominates during the early time of the flowback operation (flow rate plots of the both wells are consistent with the W_p plots). Region 1 is also observed in wells OP_{L2} and OP_{L3} , where flow rate plots are not consistent with W_p plots in Figure 4.7 (c and e).

Region 2 is observed in wells OP_{L3} and OP_{R3} . Region 2 in the rate plots correspond to the Region 2 in the cumulative water production plots (see Figures 4.6, 4.7 and 4.8). In well OP_{L3} , Region 2 dominates during the whole flowback operation, and in OP_{R3} it occurs at the intermediate time scale (see Figure 4.7 (e and f)).

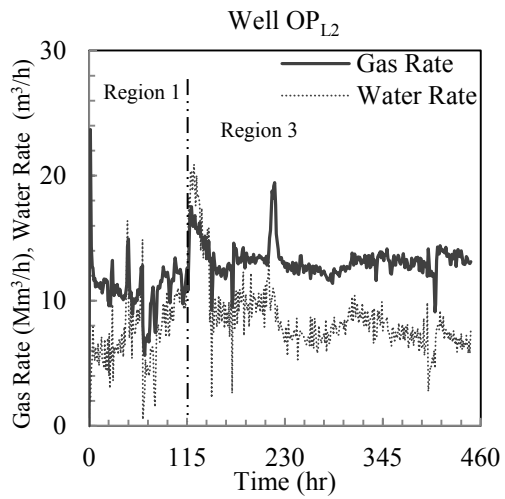
Region 3 is observed in wells OP_{L1} , OP_{L2} , OP_{R1} , OP_{R2} and OP_{R3} . Region 3 in the rate plots correspond to the Region 3 in the cumulative water production plots (see Figures 4.6, 4.7 and 4.8). In wells OP_{L1} and OP_{R1} Region 3 occurs at the late time scale. In wells OP_{L2} and OP_{R2} it occurs during the whole flowback operation. In well OP_{R3} , Region 3 occurs at the early and late time scales (flow rate plots of all the wells are consistent with the wells in the W_p plots).



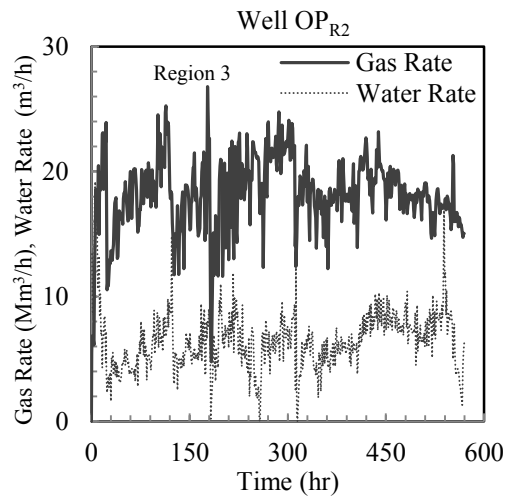
(a)



(b)



(c)



(d)

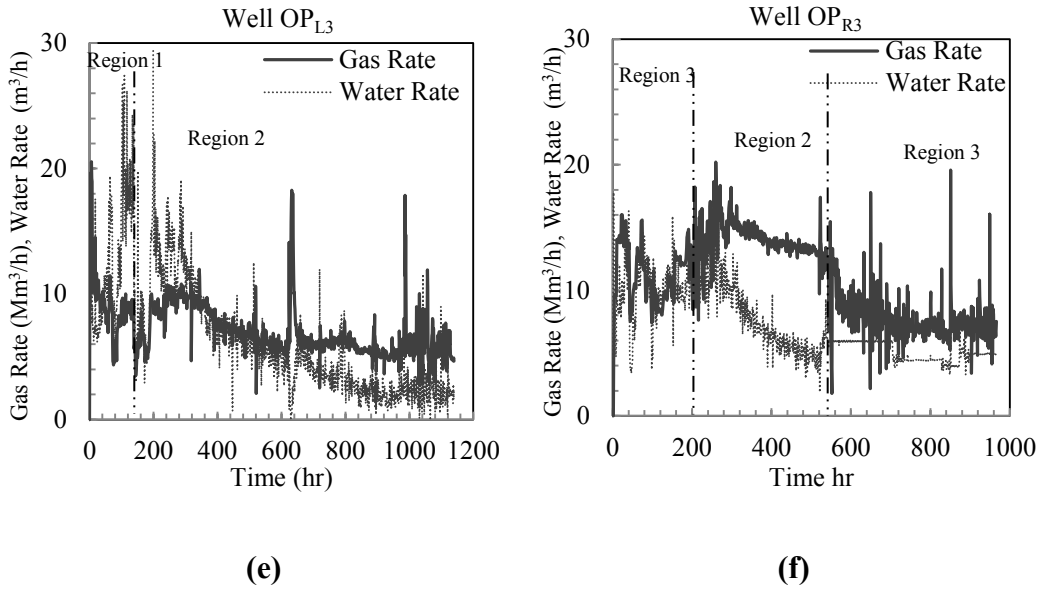


Fig. 4.10. Water and gas flow rate history measured during the flowback operation of six wells in the Otter Park formation.

Figure 4.11 shows the water and gas flow rate of the six wells drilled in the Evie formation. Plots (b, d, and f for wells EV_{R1}, EV_{R2}, and EV_{R3}, respectively) on the right hand side of Figure 4.11 show the water and gas flow rate of the three wells drilled and completed on the right side of the pad. Plots (a, c, and e for wells EV_{L1}, EV_{L2}, and EV_{L3}, respectively) on the left hand side of Figure 4.11 show the water and gas flow rate of the three wells drilled and completed on the left side of the pad in the Evie formation.

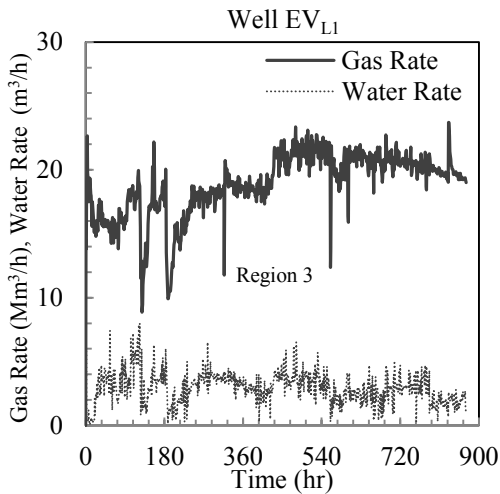
The rate plots in the Evie formation again show three distinct Regions (Regions 1, 2 and 3) which are consistent with the three Regions (Regions 1, 2 and 3) in the cumulative water production plots (see Figures 4.6, 4.7 and 4.8).

Region 1 is observed in wells EV_{L2}, EV_{L3}, EV_{R1}, EV_{R2} and EV_{R3}. Region 1 in the flow rate plots correspond to Region 1 in the cumulative production plots. It

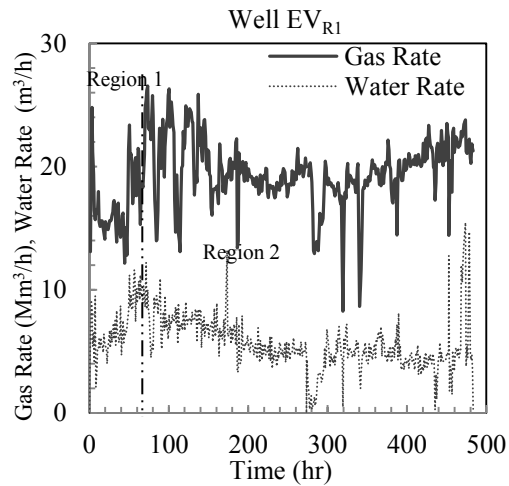
occurs during the early time of the flowback operation in five wells. Only the water flow rate plot of well EV_{L3} is consistent with cumulative water production plot in Figure 4.8 (e).

Region 2 is identified in four wells (EV_{L2} , EV_{R1} , EV_{R2} and EV_{R3}). Region 2 here in rate plots correspond to Region 2 in the cumulative water production plots (see Figures 4.6, 4.7 and 4.8).

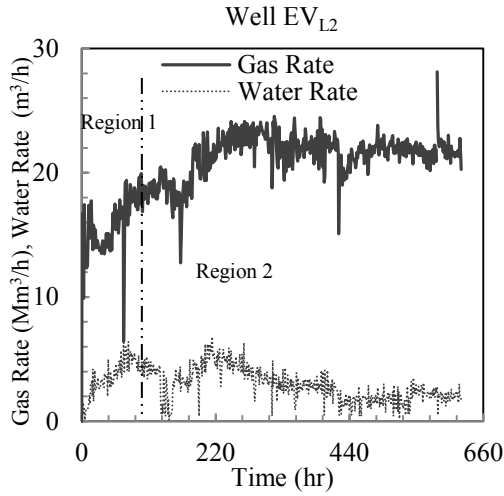
Region 3 is observed in wells EV_{L1} , EV_{L3} , and EV_{R3} (see Regions 1, 2 and 3 in Figures 4.6, 4.7 and 4.8, respectively). In EV_{L1} , Region 3 dominates during the complete flowback operation. In wells EV_{L3} and EV_{R3} , it occurs at late time scale.



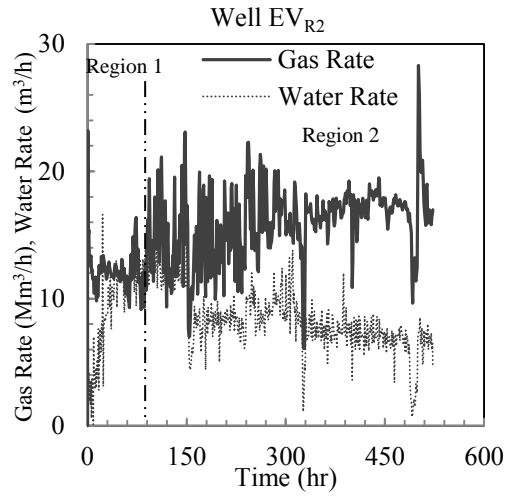
(a)



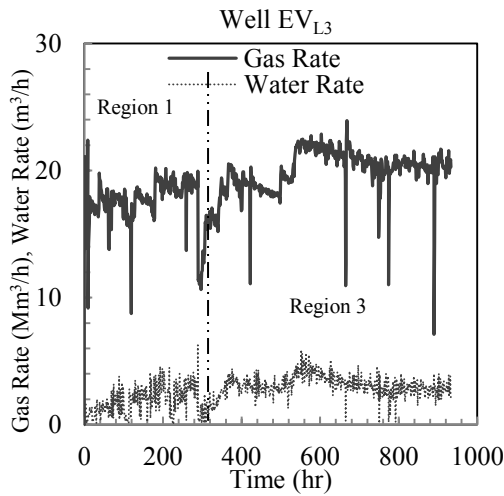
(b)



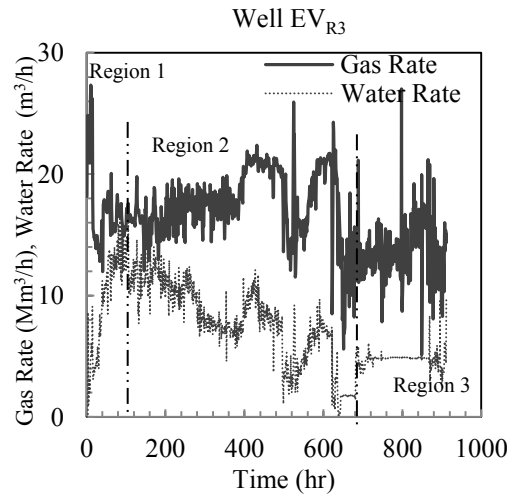
(c)



(d)



(e)



(f)

Fig. 4.11. Water and gas flow rate history measured during the flowback operation of six wells in the Evie formation.

4.4.1. Interpretation of Rate Plots

Unlike the rate plots of the three field cases discussed in chapter 3, here in the rate plots single phase region is missing. An immediate gas breakthrough is observed in all the eighteen wells during the early time of the flowback operation (see Figures 4.9, 4.10 and 4.11).

Although the rate plots are noisy but the general trend for some wells is in agreement with the slope of the cumulative water production plots discussed in previous section. The water flow rate plots of the Muskwa, the Otter Park and the Evie formations (see Figures 4.9, 4.10 and 4.11) of the eighteen multifractured horizontal wells are categorized into three Regions:

- i) Region 1, where water flow rate increases with time.
- ii) Region 2, where water flow rate decreases with time.
- iii) Region 3, where water flow rate remains constant with time.

During region 1, water flow rate increases with time. This observation is backed with an upward curvature in cumulative water production plots. Where, ($\frac{d^2W_p}{dt^2} > 0$) justifies the increase in water flow rate with time. In Region 2, water flow rate decreases with time. The downward curvature ($\frac{d^2W_p}{dt^2} < 0$) in cumulative water production plots show the decrease in water flow rate. In Region 3, where water flow rate remains constant is also backed by cumulative water production plots ($\frac{d^2W_p}{dt^2} \approx 0$). One should note that correlating increasing, decreasing and constant water flow rate trends with cumulative production plots are always not

true. This is because in some wells increasing, decreasing and constant trends in water flow rate plots is not consistent with cumulative water production plots. This inconsistency is due to the noisiness in flow rate measurements.

The possible reasons of rate changes in the three Regions are similar to those discussed in section 4.3.1 (interpretation of cumulative production plots). In addition, the change in drawdown and choke size can affect the flow rate plots.

4.5. Gas Water Flow Rate Ratio Plots

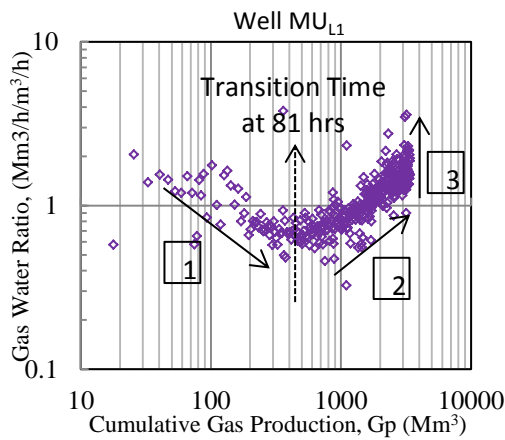
Classification of flow regimes based on the individual rate plots is challenging due to the limitation in flow rate measurements and also the effect of choke size and pressure drawdown variations. Therefore the normalized parameter of gas water flow rate ratio might be more representative for flow regime classification.

Figure 4.12 shows the log-log plots of the gas water flow rate ratio (GWR) versus cumulative gas production (G_p) of the six wells drilled in the Muskwa formation. Plots (b, d, and f for wells MU_{R1} , MU_{R2} and MU_{R3} , respectively) on the right hand side of Figure 4.12 show GWR versus G_p of the three wells drilled and completed on the right side of the pad. Plots (a, c, and e for wells MU_{L1} , MU_{L2} and MU_{L3} , respectively) on the left hand side of Figure 4.12 show GWR versus G_p of the three wells drilled and completed on the left side of the pad in the Muskwa formation. In general, five dominant Regions are observed in the GWR plots of six wells. The dotted arrow in Figure 4.12 (a, b, c, d, e and f) show the

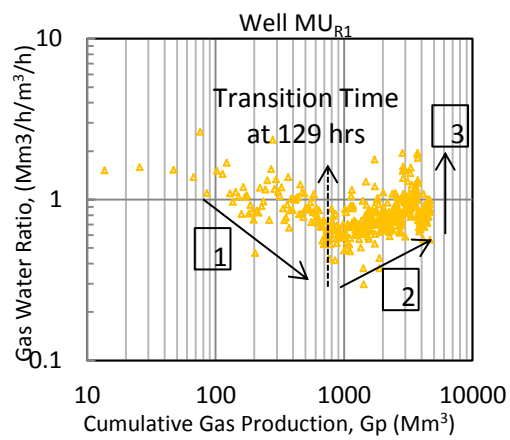
transition time where the free gas depletion occur for each well. Transition time is the time when free gas in fractures is depleted.

- Region 0: GWR increases with time.
- Region 1: GWR decreases with time.
- Region 2: GWR increases with time.
- Region 3: GWR sharply increases with time.
- Region 4: GWR sharply decreases with time.

Region 0 is only observed in well MU_{R3}. Regions 1 and 2 are observed in wells MU_{L1}, MU_{L2}, MU_{L3}, MU_{R1}, MU_{R2} and MU_{R3}. Region 3 is observed in wells MU_{L1}, MU_{L2}, MU_{L3}, MU_{R1} and MU_{R2}. Region 4 is only observed in well MU_{R3}.



(a)



(b)

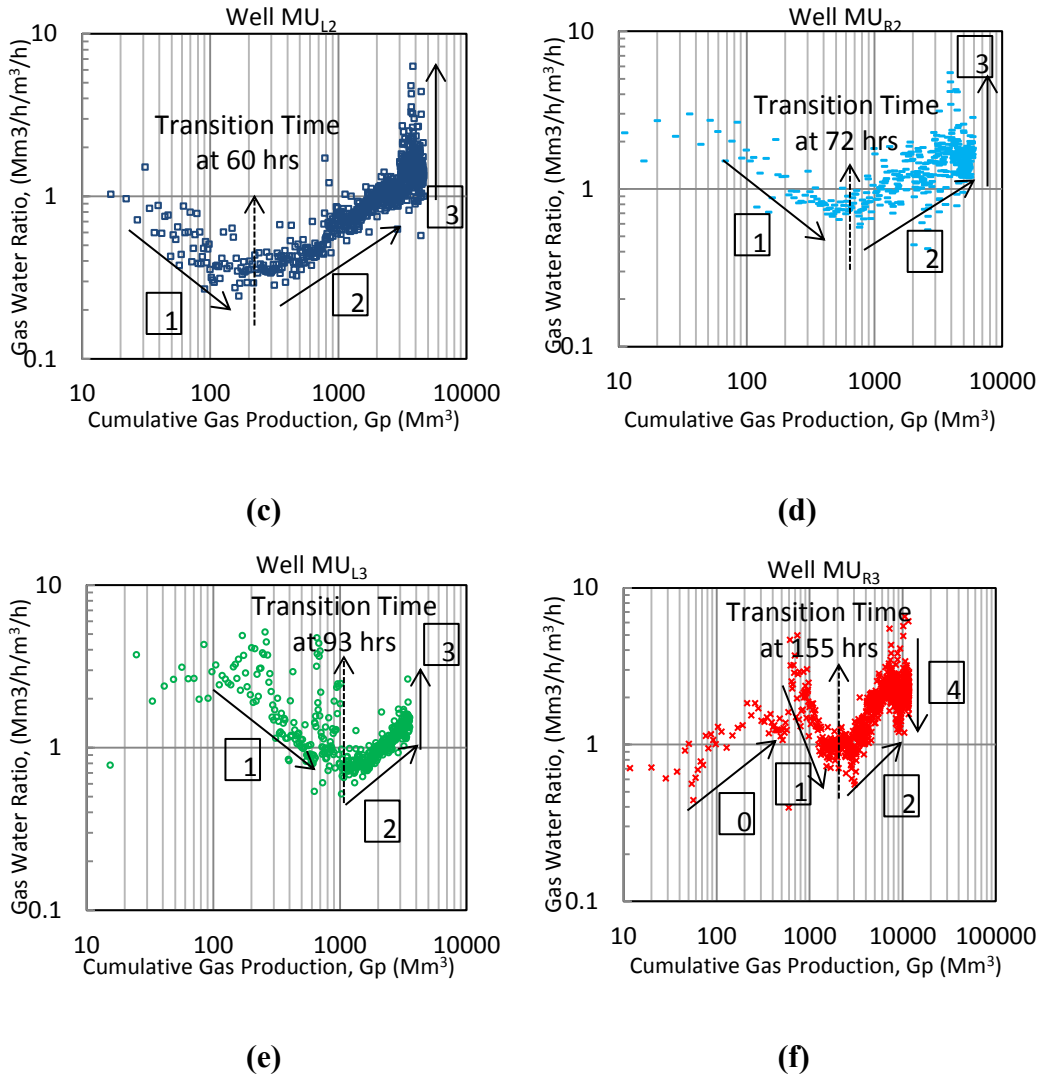


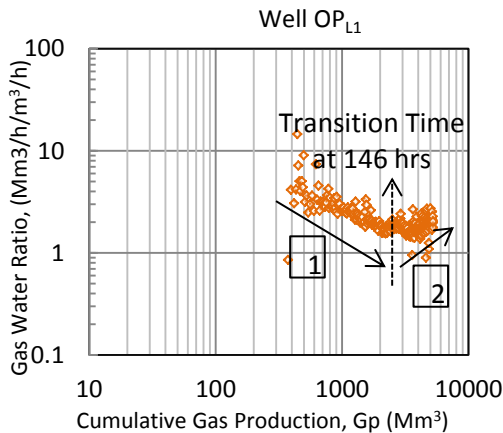
Fig. 4.12. Gas water flow rate ratio (GWR) versus cumulative gas production (G_p) of the six wells drilled in the Muskwa formation. The dotted arrow shows the transition time in fractures.

Figure 4.13 shows the log-log plots of the gas water flow rate ratio (GWR) versus cumulative gas production (G_p) of the six wells drilled in the Otter Park formation. Plots (b, d, and f for wells OP_{R1} , OP_{R2} and OP_{R3} , respectively) on the right hand side of Figure 4.13 show GWR versus G_p of the three wells drilled and completed on the right side of the pad. Plots (a, c, and e for wells OP_{L1} , OP_{L2} and OP_{L3} , respectively) on the left hand side of Figure 4.13 show the GWR versus G_p

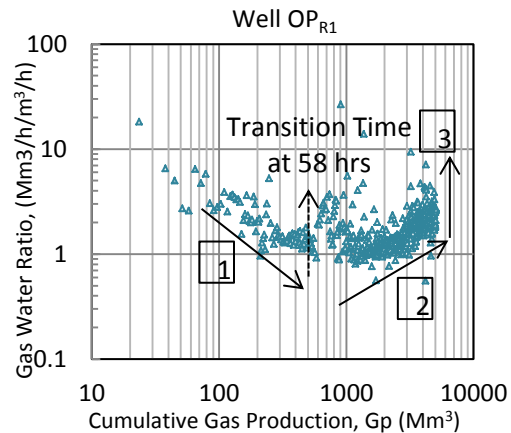
of the three wells drilled and completed on the left side of the pad in the Otter Park formation. The dotted arrow in Figure 4.13 (a, b, c, d, and e) show the transition time where the free gas depletion occur for each well. Transition time is the time when free gas in fractures is depleted.

The GWR plots of the six wells completed in the Otter park formation are also classified into five dominant Regions (Regions 0, 1, 2, 3 and 4).

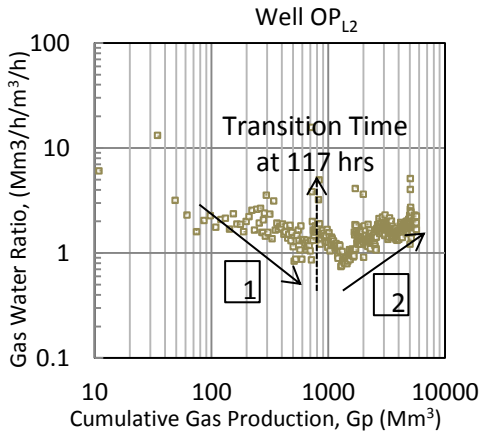
Region 0 is observed in wells OP_{R2} and OP_{R3} . Region 0 in OP_{R2} is similar to that in well MU_{R3} , but it is different from that in well OP_{R3} . Region 1 is observed in wells OP_{L1} , OP_{L2} , OP_{L3} , OP_{R1} , OP_{R2} and OP_{R3} . Region 2 is observed in all wells except well OP_{R2} . Region 3 is observed in wells OP_{L3} , OP_{R1} and OP_{R2} . Region 4 is observed only in well OP_{R3} .



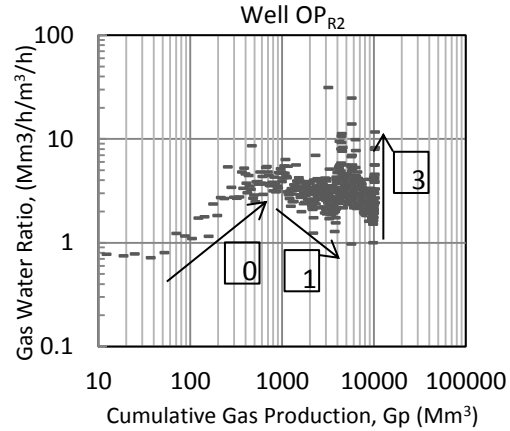
(a)



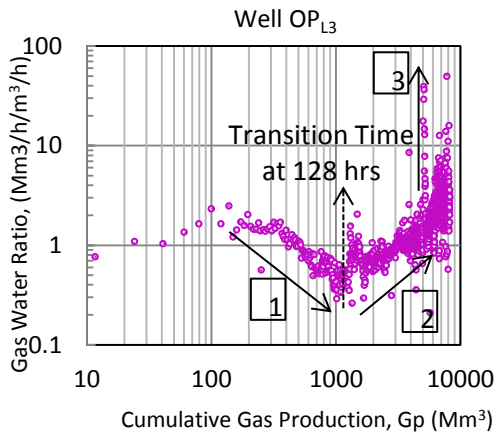
(b)



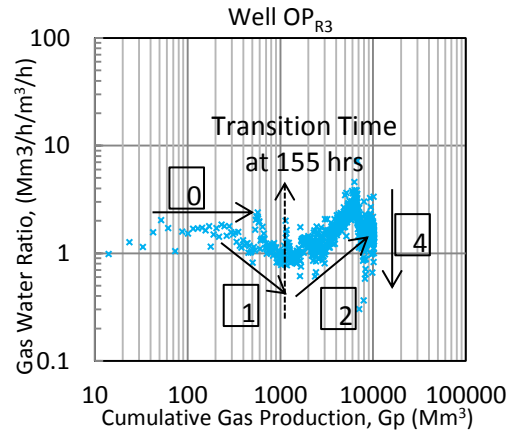
(c)



(d)



(e)



(f)

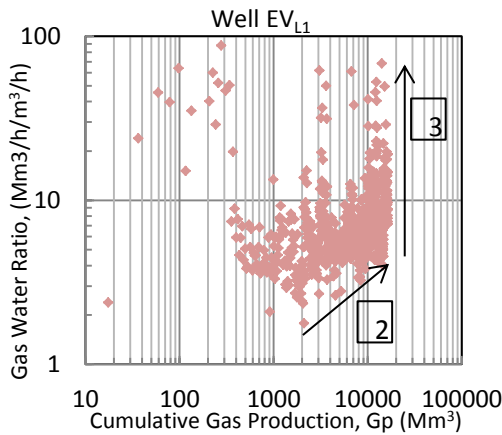
Fig. 4.13. Gas water flow rate ratio (GWR) versus cumulative gas production (G_p) of the six wells drilled in the Otter Park formation. The dotted arrow shows the transition time in fractures.

Figure 4.14 shows the log-log plots of the gas water flow rate ratio (GWR) versus cumulative gas production (G_p) of the six wells drilled in the Evie formation. Plots (b, d, and f for wells EV_{R1} , EV_{R2} and EV_{R3} , respectively) on the right hand side of Figure 4.14 show GWR versus G_p of the three wells drilled and

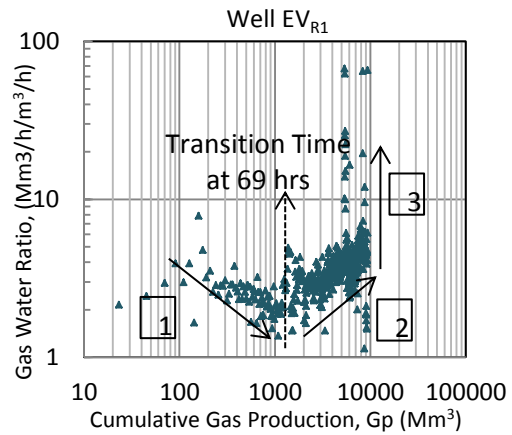
completed on the right side of the pad. Plots (a, c, and e for wells EV_{L1} , EV_{L2} and EV_{L3} , respectively) on the left hand side of Figure 4.14 show the GWR versus G_p of the three wells drilled and completed on the left side of the pad in the Evie formation. The dotted arrow in Figure 4.14 (b, c, d, and f) show the transition time where the free gas depletion occur for each well. Transition time is the time when free gas in fractures is depleted.

The GWR plots of six wells in the Evie formation are classified into four dominant Regions (Regions 0, 1, 2 and 3).

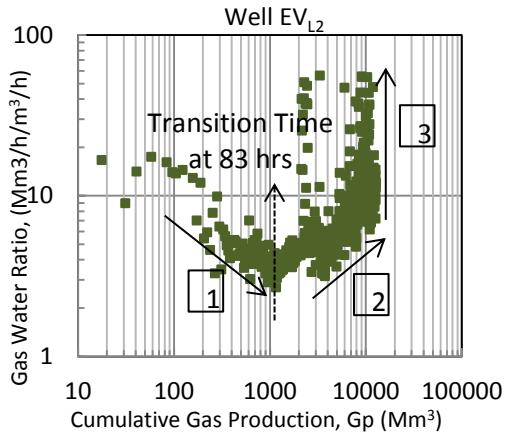
Region 0 is observed only in well EV_{R2} , which is similar to that observed in well OP_{R3} in the Otter Park formation. Regions 1, 2 and 3 are observed in wells EV_{L1} , EV_{L2} , EV_{L3} , EV_{R1} , EV_{R2} and EV_{R3} .



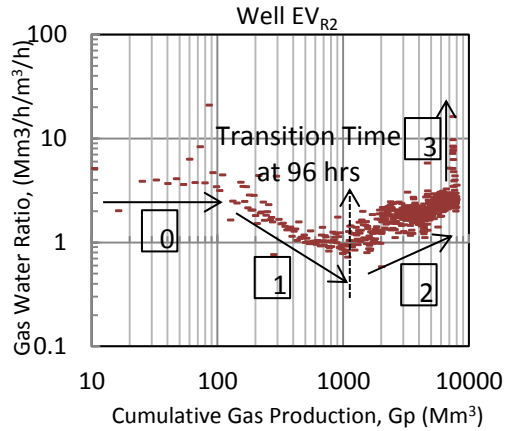
(a)



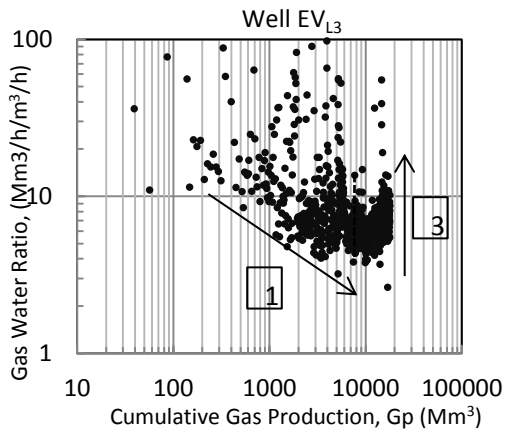
(b)



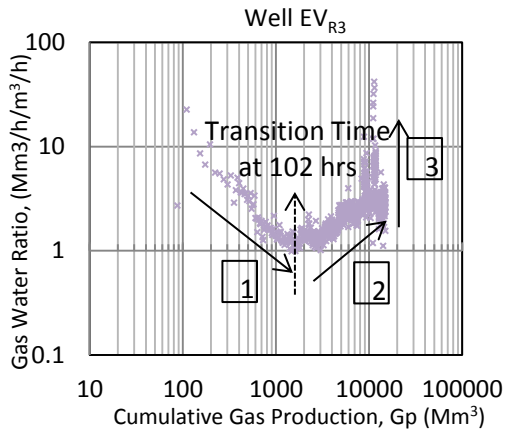
(c)



(d)



(e)



(f)

Fig. 4.14. Gas water flow rate ratio (GWR) versus cumulative gas production (G_p) of the six wells drilled in the Evie formation. The dotted arrow shows the transition time in fractures.

4.5.1. Interpretation of Gas Water Flow Rate Ratio Plots

In general, the GWR plots of the eighteen wells in the three shale formations show five dominant Regions:

- Region 0, where GWR increases/remains constant with cumulative gas production.
- Region 1, where GWR decreases with time.
- Region 2, where GWR increases with time.
- Region 3, where GWR sharply increases with time.
- Region 4, where GWR sharply decreases with time.

Region 1 is the only trend that is occurred in all the eighteen wells. During Region 1, GWR decreases with time. In other words the ratio between gas and water flow rates decreases with time. The decrease in GWR is probably because the ratio between gas and water saturations, and that between gas and water relative permeabilities in fractures decreases with time.

Region 2 is observed in all the wells except well OP_{R2} . Region 2 corresponds to the intermediate time scale. In Region 2 GWR increases with time. During this Region the ratio between gas and water saturations, and that between gas and water relative permeabilities in fractures increases with time. Region 2 in GWR plots behave similar to Region 2 in the cumulative production plots and therefore can be an indication of water depletion in hydraulic fractures (a half slope trend) as discussed by Ilk et al., (2010).

Region 3 is identified in fourteen wells (except wells OP_{L1} , and OP_{L2}). Region 3 corresponds to the response at the late time scale. Region 3 is observed immediately after Region 2. In this Region GWR increases sharply with time which indicates that water rate decreases to very low values and gas rate increases

(see Figures 4.9, 4.10 and 4.11). Sharp increase in GWR can be explained by water depletion in primary fractures (as observed in Region 2) which in turn increases the gas saturation and thus increases the relative permeability to gas in fractures.

Region 0 is observed in one well (MU_{R3}) of the Muskwa, two wells (OP_{R2} and OP_{R3}) of the Otter Park and one well (EV_{R2}) of the Evie formations. For wells MU_{R3} and OP_{R2} , GWR increases with cumulative gas production (which represents time). For wells OP_{R3} and EV_{R2} , GWR remains constant with time. Constant GWR can be because of one reason: 1) both water and gas flow rates are changing with same rate or with a constant ratio. In case of constant GWR for wells OP_{R3} and EV_{R2} , both water and gas flow rates are constant as observed in rate plots (see Figures 4.10(f) and 4.11(d)). The constant GWR ratio can be because of the presence of highly conductive hydraulic fractures that allow water and gas to flow at constant rate for very short time just after the well is put on flowback.

Region 4 is observed in wells MU_{R3} and OP_{R3} . In Region 4 GWR decreases sharply which means that water flow rate increases and gas flow rate decreases. This observation is surprising, since water in primary fractures is almost depleted, a sudden increase in water flow rate could be an indication of the communication between wells in the same formation or wells in other members of shale formation.

4.6. Flowback Pressure History

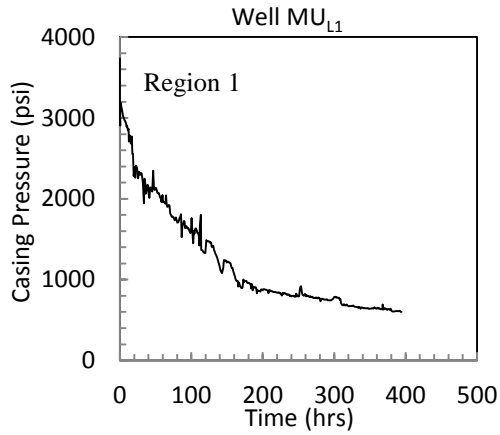
In Figure 4.15, we present the plot of casing pressure (p_c) versus cumulative time. Plots (b, d, and f for wells MU_{R1} , MU_{R2} , and MU_{R3} , respectively) on the right hand side of Figure 4.15 show p_c versus cumulative time of the three wells drilled and completed on the right side of the pad. Plots (a, c, and e for wells MU_{L1} , MU_{L2} , and MU_{L3} , respectively) on the left hand side of Figure 4.15 show p_c versus cumulative time of the three wells drilled and completed on the left side of the pad in the Muskwa formation.

The casing pressure plots of the six wells show two distinct Regions:

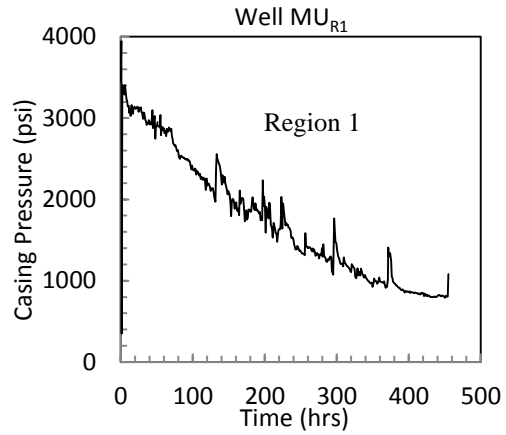
- In Region 1, casing pressure decreases with time.
- In Region 2, casing pressure remains constant with time.

Region 1 is observed in all the six wells. In wells MU_{L2} and MU_{R3} , Region 1 only occurs at the early time scale. In the remaining four wells Region 1 occurs during the whole flowback operation.

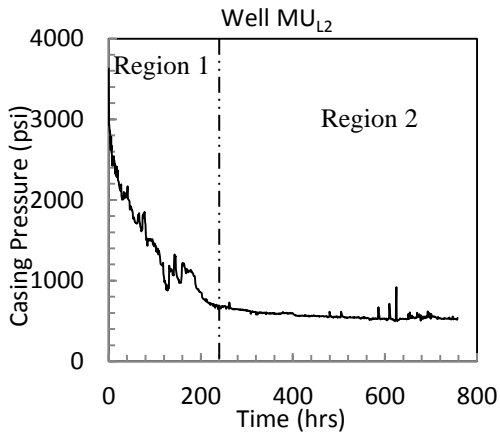
Region 2 is observed only in two wells (MU_{L2} and MU_{L3}) and it occurs at the late time scale.



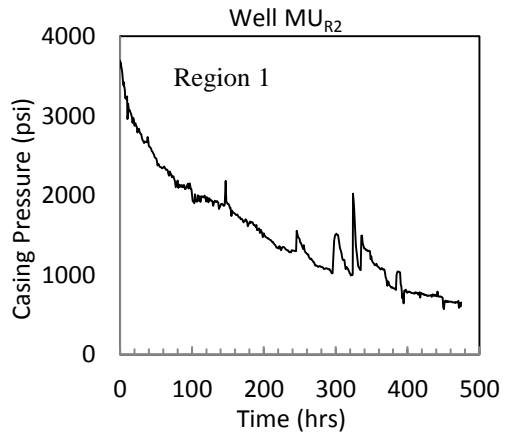
(a)



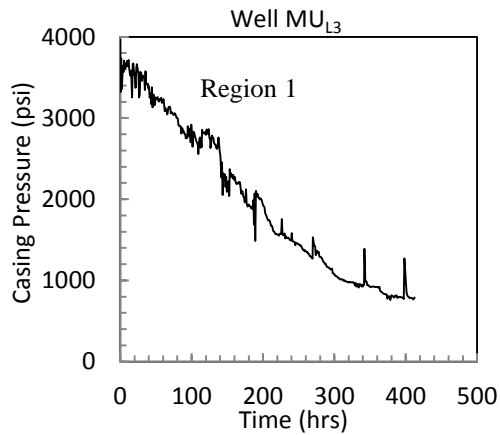
(b)



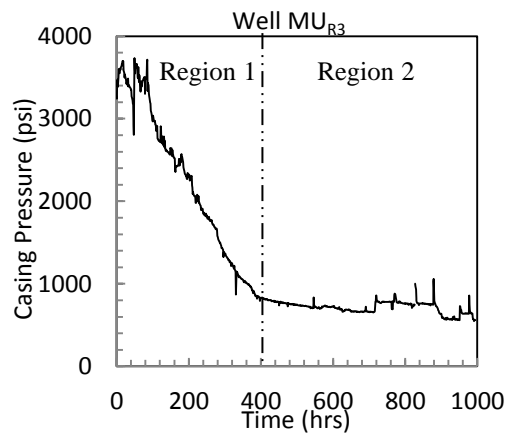
(c)



(d)



(e)



(f)

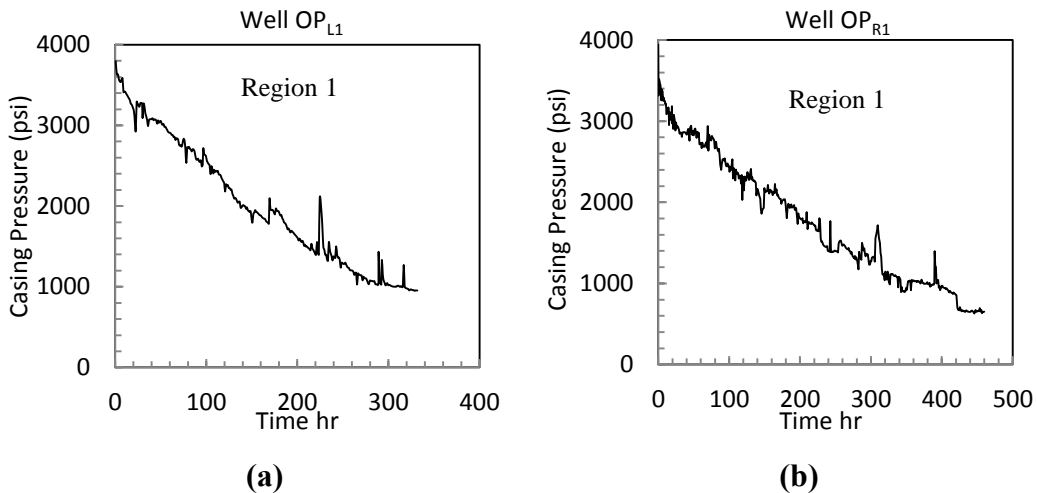
Fig. 4.15. Casing pressure measured at surface during the flowback of the six wells in the Muskwa formation.

Figure 4.16 shows the casing pressure (p_c) of the six wells measured at the surface during the flowback operation in the Otter Park formation. Plots (b, d, and f for wells OP_{R1} , OP_{R2} , and OP_{R3} , respectively) on the right hand side of Figure 4.16 show the casing pressure of the three wells drilled and completed on the right side of the pad. Plots (a, c, and e for wells OP_{L1} , OP_{L2} , and OP_{L3} , respectively) on the left hand side of Figure 4.16 show the casing pressure of the three wells drilled and completed on the left side of the pad in the Otter Park formation.

Similar to the wells in the Muskwa formation, here in Otter Park formation (p_c) plots show two Regions (Regions 1 and 2). In Region 1, casing pressure decreases with time. In Region 2, casing pressure remains constant with time.

Region 1 is observed in all the six wells. In wells OP_{L3} and OP_{R3} , Region 1 occurs at the early time scale. In the remaining four wells, Region 1 occurs during the whole flowback operation.

Region 2 is observed in wells OP_{L3} and OP_{R3} and it occurs at the late time scale.



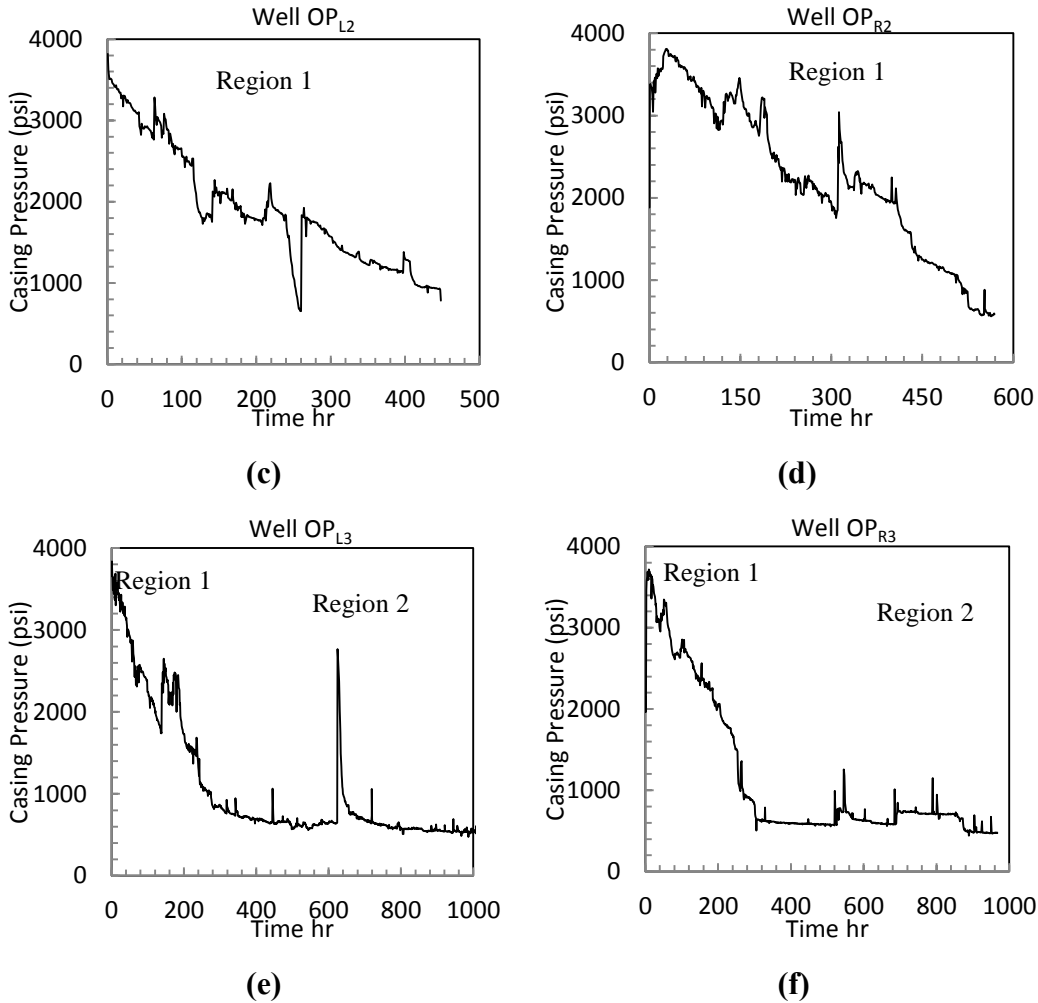
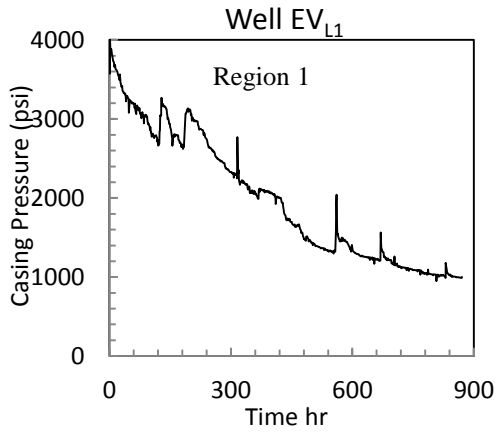


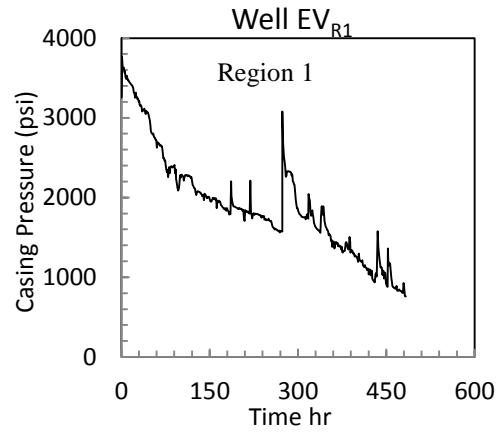
Fig. 4.16. Casing pressure measured at surface during the flowback of the six wells in the Otter Park formation.

Figure 4.17 shows the casing pressure versus cumulative time of the six wells drilled in the Evie formation. Plots (b, d, and f for wells EV_{R1} , EV_{R2} , and EV_{R3} , respectively) on the right hand side of Figure 4.17 show the casing pressure of the three wells drilled and completed on the right side of the pad. Plots (a, c, and e for wells EV_{L1} , EV_{L2} , and EV_{L3} , respectively) on the left hand side of Figure 4.17 show the casing pressure of the three wells drilled and completed on the left side of the pad in the Evie formation.

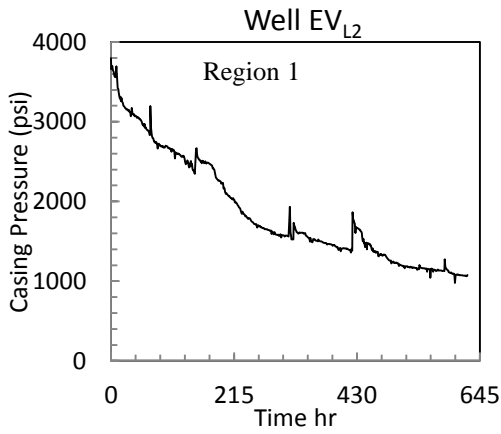
The casing pressure plots in the Evie formation show only Region 1, where casing pressure decreases with time. Region 1 occurs during the complete flowback operation.



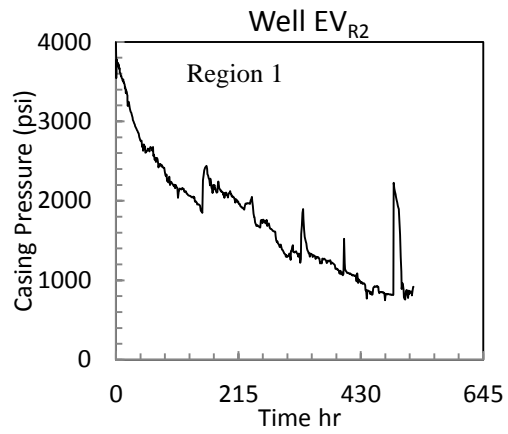
(a)



(b)



(c)



(d)

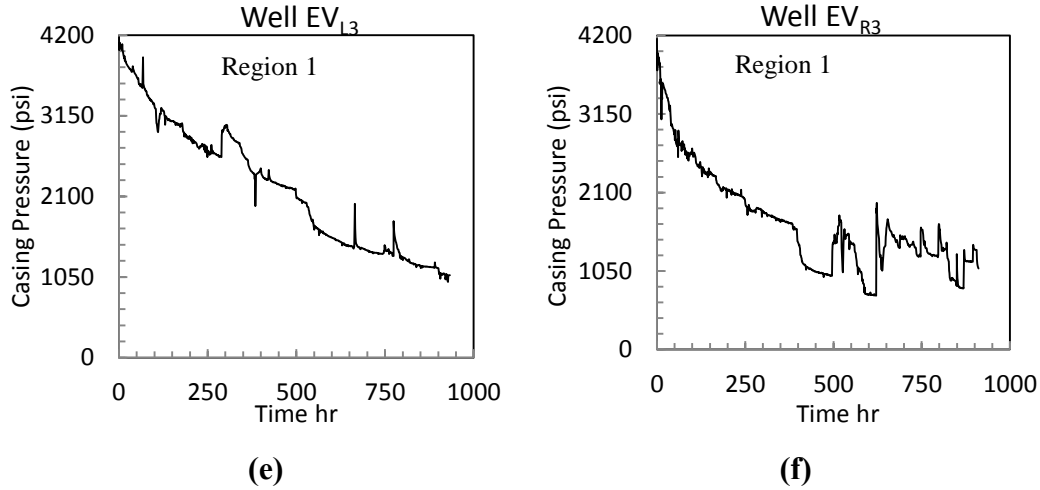


Fig. 4.17. Casing pressure measured at surface during the flowback of the six wells in the Evie formation.

4.7. Water Normalized Productivity Index Plots

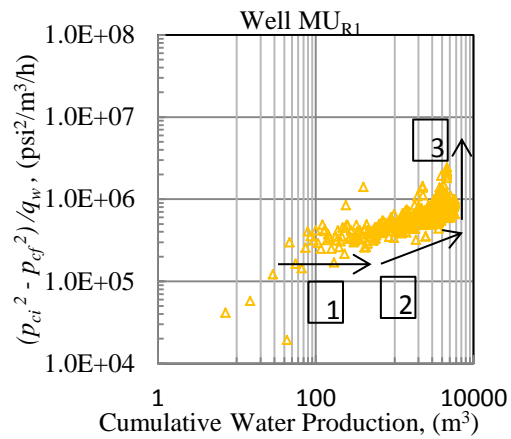
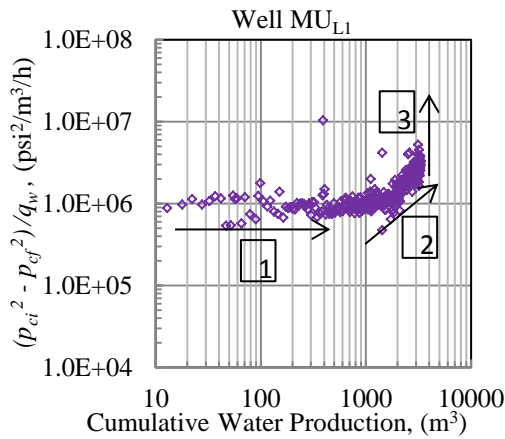
By definition, water normalized productivity index (WNPI) is the ratio of the difference between initial casing pressure squared and final casing pressure squared over water flow rate at surface.

$$WNPI = \frac{(p_{ci}^2 - p_{cf}^2)}{q_w}$$

Figure 4.18 shows the log-log plots of water normalized productivity index $(p_{ci}^2 - p_{cf}^2/q_w)$ versus cumulative water production (W_P) of the six wells drilled in the Muskwa formation. Plots (b, d, and f for wells MU_{R1}, MU_{R2} and MU_{R3}, respectively) on the right hand side of Figure 4.18 show $(p_{ci}^2 - p_{cf}^2/q_w)$ versus W_P of the three wells drilled and completed on the right side of the pad. Plots (a, c, and e for wells MU_{L1}, MU_{L2} and MU_{L3}, respectively) on the left hand side of Figure 4.18 show $(p_{ci}^2 - p_{cf}^2/q_w)$ versus W_P of the three wells drilled and

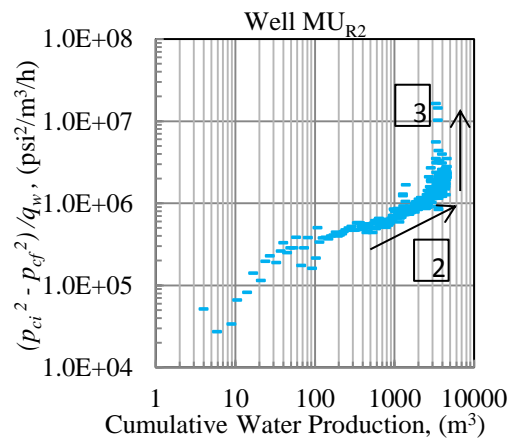
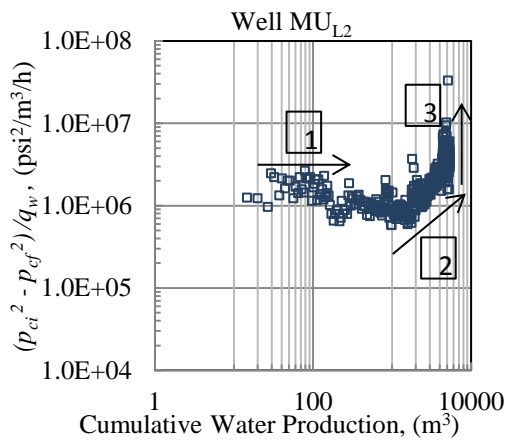
completed on the left side of the pad in the Muskwa formation. In general, three dominant Regions are observed in the water normalized productivity index plots.

- Region 1, where $(p_{ci}^2 - p_{cf}^2)/q_w$ remains constant with time. This Region is observed in wells MU_{L1}, MU_{L2} and MU_{R1}.
- Region 2, where $(p_{ci}^2 - p_{cf}^2)/q_w$ increases with time. Region 2 is observed in all the six wells.
- Region 3, where $(p_{ci}^2 - p_{cf}^2)/q_w$ sharply increases with time. Region 3 is observed in wells MU_{L1}, MU_{L2}, MU_{R1}, MU_{R2} and MU_{R3}.



(a)

(b)



(c)

(d)

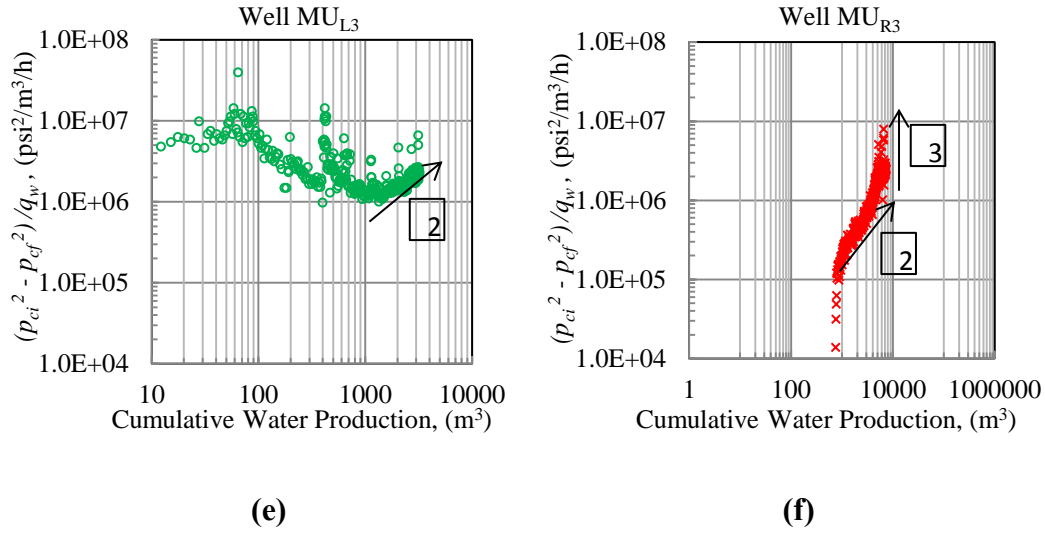


Fig. 4.18. Water normalized productivity index (WNPI) versus cumulative water production (W_p) of the six wells drilled in the Muskwa formation.

Figure 4.19 shows the log-log plots of water normalized productivity index ($p_{ci}^2 - p_{cf}^2/q_w$) versus cumulative water production (W_p) of the six wells drilled in the Otter Park formation. Plots (b, d, and f for wells OP_{R1} , OP_{R2} and OP_{R3} , respectively) on the right hand side of Figure 4.19 show ($p_{ci}^2 - p_{cf}^2/q_w$) versus (W_p) of the three wells drilled and completed on the right side of the pad. Plots (a, c, and e for wells OP_{L1} , OP_{L2} and OP_{L3} , respectively) on the left hand side of Figure 4.19 show the ($p_{ci}^2 - p_{cf}^2/q_w$) versus (W_p) of the three wells drilled and completed on the left side of the pad in the Otter Park formation.

The WNPI plots of the six wells in the Otter Park formation are also classified into three Regions (Regions 1, 2 and 3). Region 1 is observed in wells OP_{L1} , OP_{L2} , OP_{L3} and OP_{R1} . Region 2 is observed in all the six wells of the OtterPark formation. Region 3 is observed in just two wells (OP_{L3} and OP_{R1}).

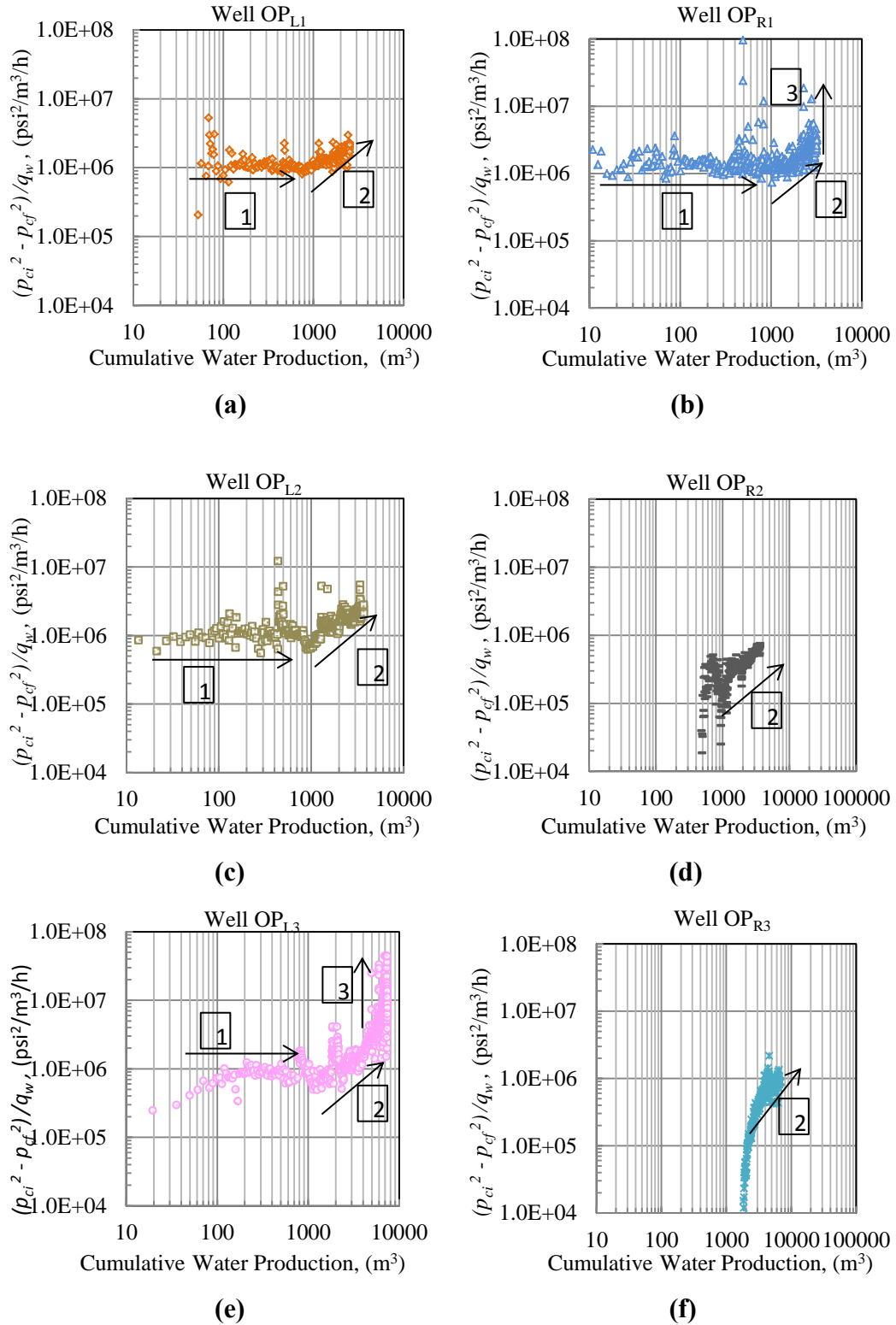
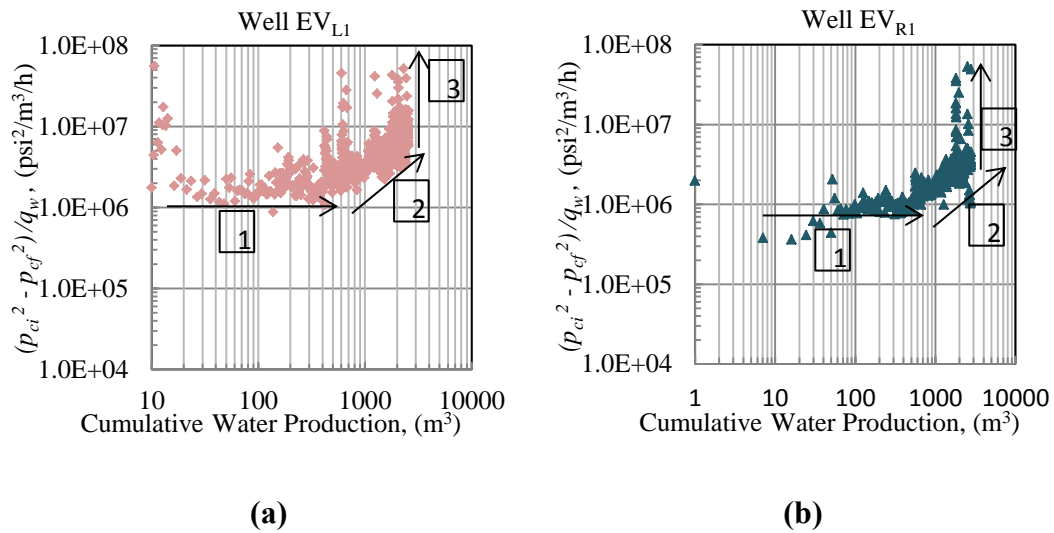


Fig. 4.19. Water normalized productivity index (WNPI) versus cumulative water production (W_p) of the six wells drilled in the Otter Park formation.

Figure 4.20 shows the log-log plots of the water normalized productivity index $(p_{ci}^2 - p_{cf}^2/q_w)$ versus cumulative water production (W_P) of the six wells drilled in the Evie formation. Plots (b, d, and f for wells EV_{R1} , EV_{R2} and EV_{R3} , respectively) on the right hand side of Figure 4.20 show $(p_{ci}^2 - p_{cf}^2/q_w)$ versus W_P of the three wells drilled and completed on the right side of the pad. Plots (a, c, and e for wells EV_{L1} , EV_{L2} and EV_{L3} , respectively) on the left hand side of Figure 4.20 show the $(p_{ci}^2 - p_{cf}^2/q_w)$ versus W_P of the three wells drilled and completed on the left side of the pad in the Evie formation.

The WNPI plots of the six wells in the Evie formation show three dominant Regions (Regions 1, 2 and 3). Three Regions 1, 2 and 3 are observed in all the six wells of the Evie formation.



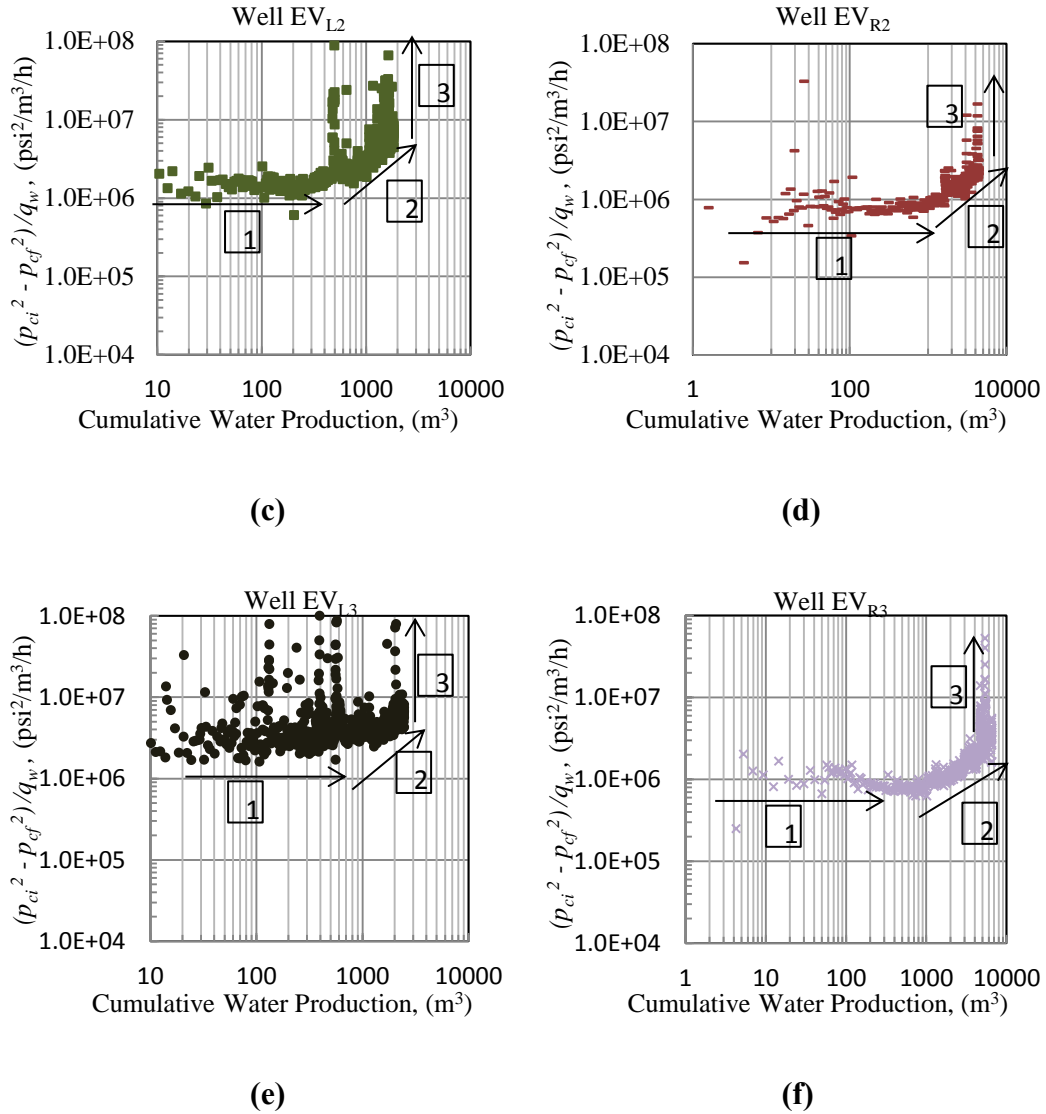


Fig. 4.20. Water normalized productivity index (WNPI) versus cumulative water production (W_p) of the six wells drilled in the Evie formation.

4.7.1. Interpretation of Water Normalized Productivity Index Plots

In general, water normalized productivity index plots $(p_{ci}^2 - p_{cf}^2)/q_w$ of the eighteen wells in the three shale formations consistently show three dominant Regions:

- Region 1, where $(p_{ci}^2 - p_{cf}^2/q_w)$ remains constant with time.
- Region 2, where $(p_{ci}^2 - p_{cf}^2/q_w)$ increases with time.
- Region 3, where $(p_{ci}^2 - p_{cf}^2/q_w)$ sharply increases with time.

During Region 1 water normalized productivity index remains constant with time. This is probably because the pressure drawdown increases with a decrease in casing pressure with time. During this Region water flow rate also increases with time that's why this region can be correlated with Region 1 observed in cumulative water production, flow rate and gas water flow rate ratio plots discussed above.

In region 2, water normalized productivity index increases with time. During this Region water flow rate decreases with an increase in pressure drawdown with time. This Region is consistent with Region 2 observed in W_P , q_g and GWR plots and thus indicate transient water depletion in hydraulic fractures (Ilk et al. 2010).

Region 3 corresponds to the late time response which occurs after the water depletion in hydraulic fractures (Region 2). In Region 3, $(p_{ci}^2 - p_{cf}^2/q_w)$ sharply increases which indicates that water flow rate decreases and pressure drawdown is very high. Region 3 here is consistent with the Region 3 in the GWR plots (see Figures 4.12, 4.13 and 4.14).

4.8. Unique Feature of the Horn River Wells

In this section, we compare the GWR plots of the three wells completed in tight reservoirs discussed in chapter III, to that of the wells completed in the Horn

River basin (shale reservoir). Figures 4.21, 4.22 and 4.23 show the gas water flow rate ratio (GWR) or oil water flow rate ratio (OWR) versus cumulative gas production (G_p) or cumulative oil production (N_p) of wells 1, 2 and 3 respectively. Figure 4.24 show the GWR versus G_p of well EV_{R3} (randomly selected for comparison purpose) in shale reservoir.

The comparative study of GWR plots of 21 wells (3 wells in tight reservoirs and 18 wells in shale reservoir in the Horn River basin) suggests that the wells drilled in tight reservoirs behave differently than the wells drilled in the Horn River basin.

We observe a unique feature (Region 1) in wells in the Horn River basin, which is absent in wells drilled in the tight oil and tight gas reservoirs. Region 1 in GWR plots in the Horn River basin suggests presence of free gas in hydraulic fractures before putting the well on flowback. Free gas presence in hydraulic fractures can be due to the counter-current imbibition during the shut-in period of a well pad. This argument can be supported by the experimental study performed on the shale samples of the Horn River basin conducted by Makhanov, K.K., (2013). Makhanov, K.K., (2013) found that during the shut-in period after the hydraulic fracturing operation, spontaneous imbibition may cause water loss and gas release in the Horn River basin.

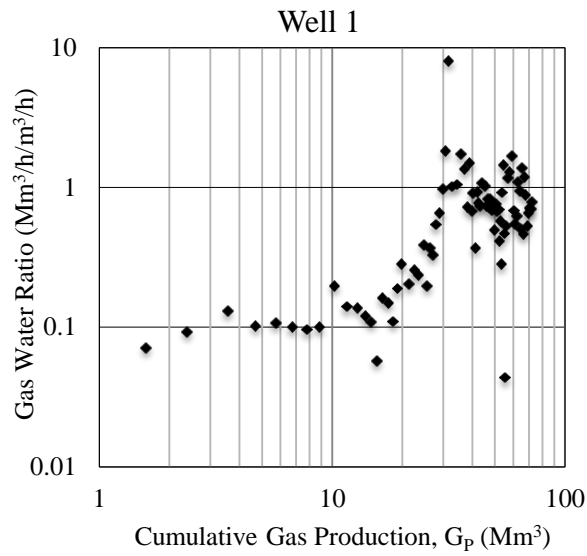


Fig. 4.21. Gas water flow rate ratio (GWR) versus cumulative gas production (G_p) of Well 1 in a tight gas reservoir.

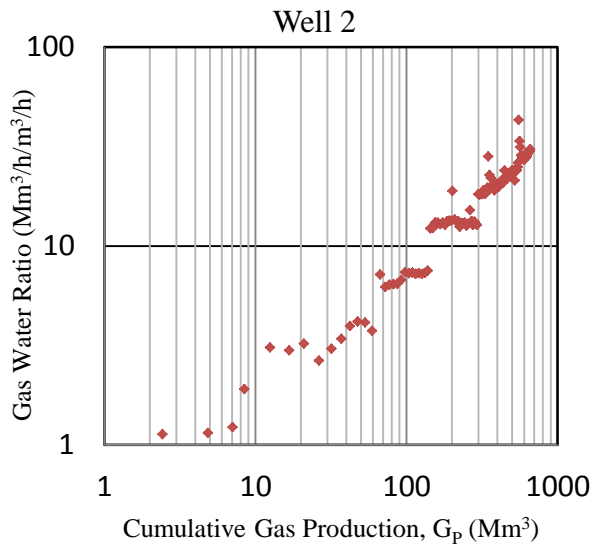


Fig. 4.22. Gas water flow rate ratio (GWR) versus cumulative gas production (G_p) of Well 2 in a tight gas reservoir.

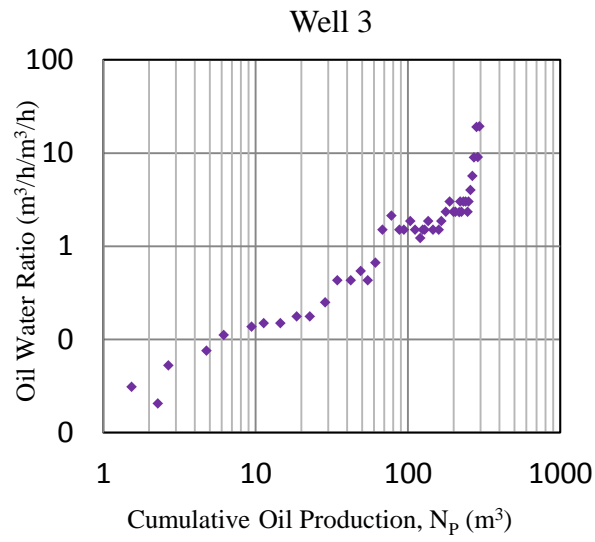


Fig. 4.23. Oil water flow rate ratio (OWR) versus cumulative oil production (N_p) of Well 3 in a tight oil reservoir.

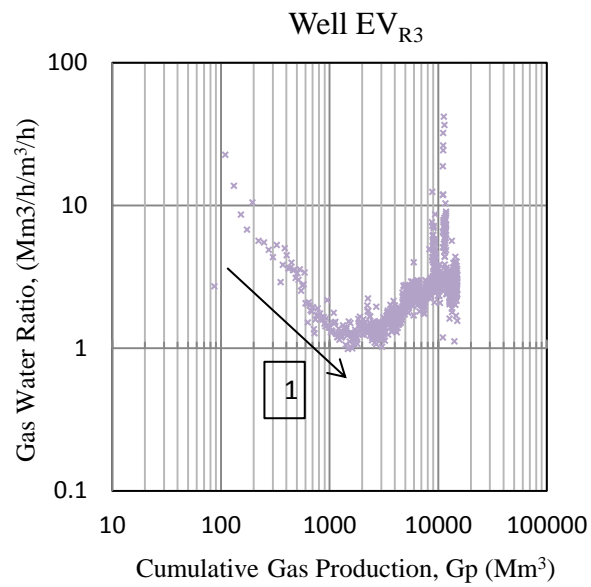


Fig. 4.24. Gas water flow rate ratio (GWR) versus cumulative gas production (G_p) of Well EV_{R3} in the Horn River basin.

4.9. Comparative Interpretation of Cumulative Production, Flow Rate, GWR and WNPI Plots

In this section, an attempt is made to compare the response of cumulative production, flow rate, gas water flow rate ratio and water normalized productivity index plots of 18 wells drilled and completed in the Horn River basin.

In order to compare the four plot types (cumulative production, flow rate, GWR and WNPI plots) of the 18 wells in the Horn River basin, we select wells MU_{L1} and MU_{L3}, which have the most pronounced responses (Regions 1 and 2). We then compare the observed behaviours of 1) cumulative water production versus cumulative time plot, 2) water flow rate versus time plot, 3) log-log plot of gas water flow rate ratio versus cumulative gas production and 4) log-log plot of water normalized productivity index versus cumulative water production of the four wells.

Figures 4.25, 4.26, 4.27 and 4.28 show the W_p vs t , q_w and q_g vs t , log-log plot of GWR vs G_p and log-log plot of WNPI vs W_p of four wells respectively. Region 1 in four plot types is correlated to one another and thus is an evidence of initial free gas in hydraulic fractures. The second region (Region 2) is also correlated in W_p vs t , q_w and q_g vs t , log-log plot of GWR vs G_p and log-log plot of WNPI vs W_p and therefore is an evidence of water depletion in hydraulic fractures.

Table 4.2 and 4.3, summarizes the observed behaviour of four plot types in the Horn River basin.

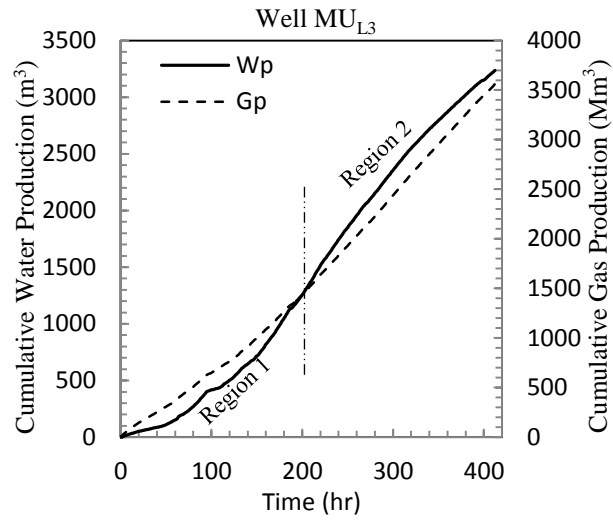


Fig. 4.25. Cumulative water and gas production plot of Well MU_{L3} with most pronounced Regions 1 and 2 used for the comparison study.

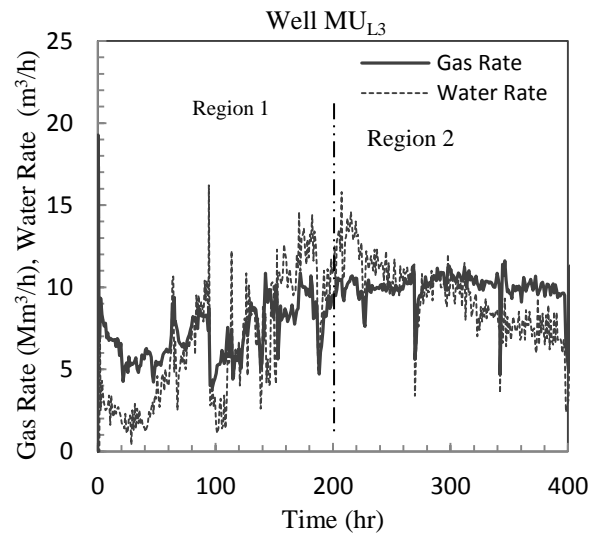


Fig. 4.26. Water and gas flow rate plot of Well MU_{L3} with most pronounced Regions 1 and 2 used for the comparison study.

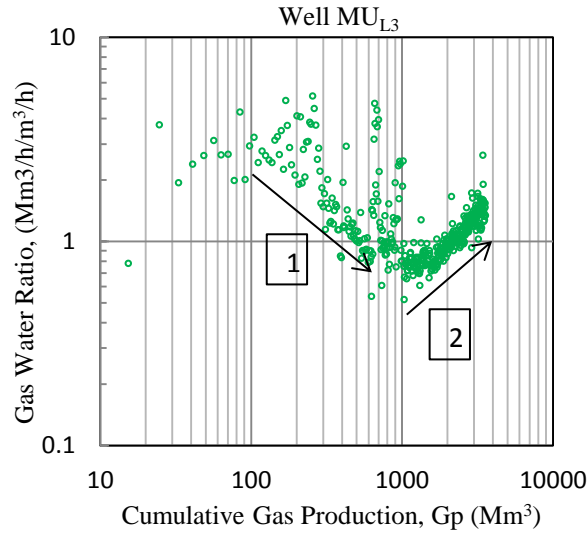


Fig. 4.27. Gas water flow rate ratio versus cumulative gas production plot of Well MU_{L3} with most pronounced Regions 1 and 2 used for the comparison study.

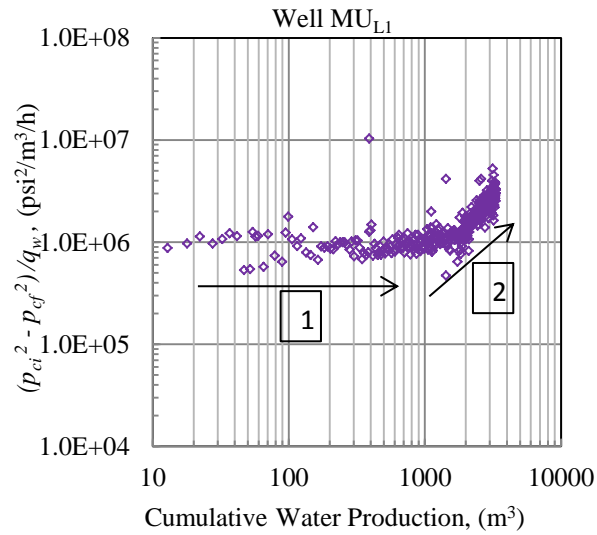


Fig. 4.28. Water normalized productivity index versus cumulative water production plot of Well MU_{L1} with most pronounced Regions 1 and 2 used for the comparison study.

Table 4.2. Observed behaviour (Region 1) of the four plot types in the Horn River basin.

Plot Type	Observed Behavior	Description	Fracture Response
W_p vs. t	Region 1	W_p with an upward curvature ($\frac{d^2W_p}{dt^2} > 0$)	Free Gas Depletion in Fractures
q_w vs. t	Region 1	Water flow rate increases with time	
log-log GWR vs. G_p	Region 1	GWR decreases with time	
log-log WNPI vs. G_p	Region 1	WNPI remains constant with time	

Table 4.3. Observed behaviour (Region 2) of the four plot types in the Horn River basin.

Plot Type	Observed Behavior	Description	Fracture Response
W_p vs. t	Region 2	W_p with a downward curvature ($\frac{d^2W_p}{dt^2} < 0$)	Water Depletion in Fractures
q_w vs. t	Region 2	Water flow rate decreases with time	
Log-log GWR vs. G_p	Region 2	GWR increases with time	
log-log WNPI vs. G_p	Region 2	WNPI increases with time	

4.10. Flowback Analysis of Shale Gas Wells

Sections 4.1 to 4.9 discussed in this chapter and recent work of Ghanbari et al. (2013) on flowback data of several multi-fractured horizontal wells completed in the Horn River basin, demonstrate two dominant differences between the flowback behaviour of the shale gas and tight gas (oil) wells:

1) An immediate gas breakthrough is observed in shale gas wells, while in tight oil and tight gas wells, there is an initial period of single phase water flow.

2) The plot of gas-water flow rate ratio (GWR) versus cumulative gas production (G_p), for shale gas wells, shows two distinct regions. In the first region, GWR decreases with G_p , and in the second region it increases with G_p . However, the GWR plot of tight gas wells or OWR (oil-water ratio) of tight oil wells does not show the first region.

These two observations suggest that the fracture network of shale gas wells, before the flowback operation, is partly saturated with some initial free gas. This initial free gas is possibly released during the shut-in period due to counter-current imbibition phenomenon (Dehghanpour et al, 2012; Dehghanpour et al, 2013; Makhanov, 2013) and/or redistribution of the gas initially existing in the natural fracture network (Ghanbari et al., 2013). To further justify the different behaviours of the tight oil/gas and shale gas wells, Ezulike et al. (2013) compared the relative permeability versus time and relative permeability versus cumulative gas/oil production plots of the similar well groups. Consistently, they observed different relative permeability profiles for tight oil/gas and shale gas wells.

Chapter V

Conclusions and Recommendation

5.1. Conclusions

We compared the flowback behaviour of three multi-fractured horizontal wells completed in tight reservoirs by conducting volumetric and pressure/rate transient analysis. We also performed the diagnostic analysis on flowback data of 18 multi-fractured horizontal wells completed in shale gas reservoir by developing four plot types.

5.1.1. Volumetric Analysis

In general a consistent behaviour is observed when plotting the cumulative production of water and gas/oil measured during the three flowback operations. The cumulative production plots of the three cases demonstrate two dominant regions. Initially water production linearly increases with time, and the main part of recovered water is produced during this period. After gas/oil breakthrough the cumulative curve deviates from the linear behaviour, and for the oil case it reaches to a plateau. The flowback efficiency (total load recovery divided by total injected volume) of the oil case is more than two times of the gas cases. This can be explained by 1) unfavourable mobility ratio and gravity effects for the displacement of water by gas (Parmar et al., 2012; Parmar et al., 2013), and 2) forced and spontaneous imbibition of water into the gas-saturated rock matrix (Dehghanpour et al., 2012; Dehghanpour et al., 2013; Makhanov, 2013). The first

explanation is backed by a much earlier breakthrough of gas compared with that of oil observed here.

5.1.2. Transient Analysis

The rate plots of the three wells consistently show three regions. In Region 1, water phase production dominates, while in Region 3, gas/oil production dominates. Region 2 is the transition period when water rate decreases quickly and gas/oil rate increases. The length of Region 1 for the oil well is significantly longer than that for the gas wells due to quick gas breakthrough as discussed above. The simple analytical model presented in this paper that can be considered as an extension of previous models (Crafton (1996), Crafton (1997), Crafton (1998)) can be used for the analysis of Region 1 data. The main results of this model are the total storage coefficient and dimensionless fracture parameter that can be interpreted to obtain the fracture half-length. However, it should be noted that application of the proposed model, and similar that of the previous single-phase models, require high frequency pressure and rate data measured at the beginning of flowback operation. We used the proposed model to describe the flowback transient behavior of the three wells studied here. Although, the measured data do not have the sufficient frequency, the estimated values of total storage coefficient and dimensionless fracture parameter are in agreement with the results of the volumetric analysis.

5.1.3. Diagnostic Analysis

We study the flowback behaviour of 18 multifractured horizontal wells completed in the Horn River basin. In this study we developed four plot types (cumulative water and gas production versus time, water and gas flow rate versus time, gas-water flow rate ratio versus cumulative gas production and water normalized productivity index versus cumulative water production). In general two dominant regions are observed. The cumulative production and flow rate plots show an immediate gas breakthrough. This immediate gas breakthrough does not occur in tight oil and gas wells. The gas-water flow rate ratio plots show two dominant regions. In region 1, GWR decreases with time. This region is absent in tight oil and gas wells. Region 1 in GWR plots suggests the presence of initial free gas in hydraulic fractures before putting the well on flowback. The presence of initial free gas is possibly due to the counter current imbibition phenomena occurred during the shut-in period (Dehghanpour et al, 2012, 2013; Makhanov, 2013), and/or redistribution of the gas initially existing in the natural fracture network (Ghanbari et al., 2013). Whereas, in region 2 GWR increases with time and is an evidence of water depletion in hydraulic fractures as also confirmed by Ilk et al. (2010).

5.2. Recommendations and Future Work

The frequent and accurate measurements of rate and pressure data are important for analyzing the early time of flowback data. It is recommended to

record rate and pressure on minute basis. The high frequency data measurement can be a first step for better understanding of flowback physics.

Analysis of Regions 2 and 3 by analytical or semi-analytical methods is challenging since it requires simultaneous solution of

- 1) Transient multi-phase flow in the wellbore,
- 2) Fracture/reservoir water saturation change in time and space,
- 3) Bottom-hole multi-phase pressure and rate.

However, there has been recent attempts to solve this problem by simulation and stochastic techniques (Clarkson (2012); Williams-Kovacs and Clarkson (2013)).

Application of the proposed model (discussed in chapter III), on multi-fractured horizontal wells completed in shales, remains the subject of a future study.

REFERENCES

1. Abdelaziz, K., Hani, Q., and Naiem, B. 2011. Tight Gas Sands Development is Critical to Future World Resources. Paper SPE 142049 presented at the SPE Middle East Unconventional Gas Conference and Exhibition, Muscat, Oman, 31st January-2nd February.
2. Agarwal, R.G., Gardner, D.C., Kleinstieber, S.W., and Fussell, D.D. 1999. Analyzing Well Production Data Using Combined-Type-Curve and Decline-Curve Concepts. SPE Reservoir Evaluation & Engineering 2 (5): 478-486. SPE-57916-PA. DOI: 10.2118/57916-PA.
3. Asadi, M., Woodroof, R.W., Malone, S., W., and Shaw, D. R. 2002. Monitoring Fracturing Fluid Flowback with Chemical Tracers: A Field Case Study. Paper SPE 77750 presented at the SPE Annual Technical Conference and Exhibition, San Antonio, Texas, 29TH September-2 October.
4. Asadi, M., Woodroof, R.A., and Himes, R. E., 2008. Comparative study of flowback analysis using polymer concentrations and fracturing-fluid tracer methods: A field study. SPE Production and Operations, 23(2):147–157, May 2008.
5. Athichanagorn, S, Horne, R.N., and Kikani, J. 2002. Processing and Interpretation of Long-Term Data Acquired From Permanent Pressure Gauges. SPE Reservoir Evaluation & Engineering 5 (5): 384-391. SPE-80287-PA. DOI: 10.2118/80287-PA.

6. Bello, R.O., 2009. Rate Transient Analysis in Shale Gas Reservoirs with Transient Linear Behavior. Ph.D thesis, Texas A & M University, Texas.
7. Clarkson, C. R. 2012. Modeling 2-Phase Flowback of Multi-Fractured Horizontal Wells Completed in Shale. Paper SPE 162593 presented at the SPE Canadian Unconventional Resources Conference, Calgary, Alberta, Canada, 30th October-1st November.
8. Clarkson, C.R., Jordan, C.L., Seidle, J.P, and Gierhart, R.R. 2008. Production Data Analysis of Coalbed-Methane Wells. SPE Reservoir Evaluation & Engineering 11 (2): 311-325. SPE-107705-PA. DOI: 10.2118/107705-PA.
9. Crafton, J.W., 1996. The Reciprocal Productivity Index Method, A Graphical Well Performance Simulator. Paper presented at the 43th Southwestern Petroleum Short Course, Lubbock, Texas, USA, 16 April.
10. Crafton, J.W., 1997. Oil and Gas Well Evaluation Using the Reciprocal Productivity Index Method. Paper SPE 37409 presented at the SPE Production Operations Symposium, Oklahoma City, Oklahoma, 9-11 March.
11. Crafton, J.W., 1998. Well Evaluation Using Early Time Post-Stimulation Flowback Data. Paper SPE 49223 presented at the SPE Annual Technical Conference and Exhibition, New Orleans, Louisiana, 27-30 September.
12. Crafton, J. W., and Gunderson, D. (2006). Use of Extremely High Time Resolution Production Data to Characterize Hydraulic Fracture Properties; Paper SPE-103591, presented at the SPE Annual Technical Conference

- and Exhibition, San Antonio, Texas, USA, 24-27 September.
13. Crafton, J. W., and Gunderson, D. (2007). Stimulation Flowback Management: Keeping a Good Completion Good; Paper SPE-110851, presented at the SPE Annual Technical Conference and Exhibition, Anaheim, California, USA, 11-14 November.
 14. Crafton, J. W. (2008). Modeling Flowback Behaviour or Flowback Equals “Slowback”; Paper SPE-119894, presented at the SPE Shale Gas Production Conference, Fort Worth, Texas, USA, 16-18 November.
 15. Crafton, J. W. (2010). Flowback Performance in Intensely Naturally Fractured Shale Gas Reservoirs; Paper SPE-131785 presented at the SPE Unconventional Gas Conference, Pittsburgh, PA, USA, 23-25 February.
 16. Craig, D.P., 2006. Analytical Modeling of a Fracture-Injection/Fall off Sequence and the Development of a Refracture Candidate Diagnostic Test. Ph.D thesis, Texas A & M University, Texas.
 17. Dehghanpour, H., Zubair, H.A., Chhabra, A., and Ullah, A. 2012. Liquid Intake of Organic Shales. [dx.doi.org/10.1021/ef300979447](https://doi.org/10.1021/ef300979447), Energy Fuels 2012, 26, 5750-5758.
 18. Dehghanpour, H., Lan, Q., Saeed, Y., Fei, H., and Qi, Z. 2013. Spontaneous Imbibition of Brine and Oil in Gas Shales: Effect of Water Adsorption and Resulting Microfractures. [dx.doi.org/10.1021/ef4002814](https://doi.org/10.1021/ef4002814), Energy Fuels 2013, 27, 3039-3049.
 19. Ebrahim, G., Abbasi, M.A., Dehghanpour, H., and Bearinger, D., 2013. Flowback Volumetric and Chemical Analysis for Evaluating Load

Recovery and its Impact on Early-Time Production. Paper SPE 167163-MS presented at the SPE Canadian Unconventional Resources Conference, Calgary, Alberta, Canada. <http://dx.doi.org/10.2118/167165-MS>.

20. Ezulike, D.O., Dehghanpour, H., and Hawkes, R.V., 2013. Understanding Flowback as a Transient 2-Phase Displacement Process: An Extension of the Linear Dual Porosity Model. Paper SPE 167164-MS presented at the SPE Canadian Unconventional Resources Conference, Calgary, Alberta, Canada.
21. El-Banbi, A.H., 1998. Analysis of Tight Gas Well Performance. Ph.D thesis, Texas A & M University, Texas.
22. Fan, L., Thompson, J.W., and Robinson, J.R. 2010. Understanding Gas Production Mechanism and Effectiveness of Well Stimulated in the Haynesville Shale through Reservoir Simulation. Paper CSUG/SPE 136696 presented at the SPE Unconventional Resources & International Petroleum Conference, Calgary, 19-21 October.
23. Gdanski, R., Weaver, J., and Slabaugh, B., 2007. A new model for matching fracturing fluid flowback composition. Paper SPE 106040 presented at SPE Hydraulic Fracturing Technology Conference, College Station, Texas, USA, 29-31 January.
24. Gdanski, R.D., Fulton, D.D., and Johnson, B.J., 2010. Returns Matching Reveals New Tools for Fracture/Reservoir Evaluation. Paper SPE 133806

presented at SPE Tight Gas Completions Conference, San Antonio, Texas, USA, 2-3 November.

25. Gdanski, R.D., and Gary P. Funkhouser 2011. Surfactant Modeling for Insight into Load Recovery Enhancement for Fracturing Treatment. Paper SPE 141296 presented at SPE International Symposium on Oilfield Chemistry, The Woodlands, Texas, USA, 11-13 April.
26. Gdanski, R.D., and Janson Bryant 2012. Modeling Gel Filter Cake Recovery by Flow and Dilution Mechanism. Paper SPE 151225 presented at SPE Hydraulic Fracturing Technology Conference, The Woodlands, Texas, USA, 6-8 February.
27. Hayatdavoudi, A. 1996. Application of a new technique in acid flowback analysis. Paper SPE 31078 presented at the SPE Formation Damage Control Symposium, Lafayette, Louisiana, 14-15 February.
28. Hurtado, A. L., Asadi, M., Woodroof, R. A., Casas, D.D., Morales, R., and O'Jeito S.A. de C.V. 2005. Production Enhancement for a Northern Mexico Field Well Resulting from Flowback Evaluations Using Chemical Tracers: A Case History. Paper SPE 95064 presented at the SPE Latin American and Caribbean Petroleum Engineering Conference, Rio de Janeiro, Brazil, 20-23 June.
29. Ilk, D., Anderson, D. M., Stotts, G.W.J., Mattar, L., and Blasingame, T. A. 2010. Production-Data Analysis, Pitfalls, Diagnostics. SPE Reservoir Evaluation & Engineering, 13(3): 538-552. DOI: 10.2118/102048-PA.

30. Ilk, D., Currie, S. M., Symmons, D., Rushing, J. A., Broussard, N. J., and Blasingame, T. A. 2010. A Comprehensive Workflow for Early Analysis and Interpretation of Flowback Data from wells in Tight Gas/Shale Reservoir Systems. Paper SPE 135607 presented at the SPE Annual Technical Conference and Exhibition, Florence, Italy, 19-22 September.
31. Kikani, J., and He, M. 1998. Multiresolution Analysis of Long-Term Pressure Transient Data Using Wavelet Methods. Paper SPE 48966 presented at the SPE Annual Technical Conference and Exhibition, New Orleans, 27-30 September.
32. King, G.E., 2010. Thirty Years of Gas Shale Fracturing: What Have We Learned?. Paper SPE 133456 presented at the SPE Annual Technical Conference and Exhibition, Florence, Italy, 19-22 September.
33. Lee, J; Rollins, J.B; and Spivey, J.P; 2003. Pressure Transient Testing. SPE Textbook Series Volume 9.
34. Makhanov, K.K., 2013. An Experimental study of Spontaneous Imbibition in Horn River Shales. MSc thesis, University of Alberta, Canada.
35. Mattar, L., and Anderson, D.M. 2003. A Systematic and Comprehensive Methodology for Advanced Analysis of Production Data. Paper SPE 84472 presented at the SPE Annual Technical Conference and Exhibition, Denver, 5-8 October.
36. Mattar, L., and Anderson, D.M. 2005. Dynamic Material Balance (Oil or Gas-in-Place without Shut-ins). Paper 2005-113, presented at the

Canadian International Petroleum Conference (Annual Technical Meeting), Calgary, 7-9 June.

37. Mayerhofer, M.J., Ehlig-Economides, C.A., and Economides, M.J., 1995. Pressure Transient Analysis of Fracture Calibration Tests. *Journal of Petroleum Technology*, 47(3): 229-234.
38. Medeiros, F., Ozkan, E, and Kazemi, H. 2008. Productivity and Drainage Area of Fractured Horizontal Wells in Tight Gas Reservoirs. *SPE Reservoir Evaluation & Engineering*, 11(5): 902-911. SPE-108110-PA. DOI: 10.2118/108110-PA.
39. Medeiros, F., Kurtoglu, B., and Ozkan, E., and Kazemi, H. 2010. Analysis of Production Data From Hydraulically Fractured Wells in Shale Reservoirs. *SPE Reservoir Evaluation & Engineering*. 13(3): 559-568. SPE-110848-PA. DOI: 10.2118/110848-PA.
40. Ouyang, L.B., and Kikani, J. 2002. Improving Permanent Downhole Gauges (PDG) Data Processing via Wavelet Analysis. Paper SPE 78290 presented at the European Petroleum Conference, Aberdeen, 29-31 October.
41. Ozkan, E., Raghavan, R. and Apaydin, O.G., 2010. Modeling of fluid transfer from shale matrix to fracture network, Paper SPE 134830 presented at the SPE Annual Technical Conference and Exhibition, Florence, Italy.
42. Palacio, J.C. and Blasingame, T.A. 1993. Decline Curve Analysis Using Type Curves-Analysis of Gas Well Production Data. Paper SPE 25909

presented at Joint Rocky Mountain Regional and Low Permeability Reservoirs Symposium, 26-28 April.

43. Parmar, J.S., Dehghanpour, H. and Kuru, E. 2012. Unstable Displacement: A Missing Factor in Fracturing Fluid Recovery. Paper SPE 162649 presented at the SPE Canadian Unconventional Resources Conference, Calgary, Alberta, Canada, 30th october-1st november.
44. Parmar, J.S., Dehghanpour, H. and Kuru, E. 2013. Drainage Against Gravity: Factors Impacting the Load Recovery in Fractures. Paper SPE 164530 presented at the Unconventional Resources Conference, The Woodlands, Texas, USA, 10-12 April.
45. Peres, A.M.M., Onur, M., and Reynolds, A.C. 1993. A new general pressure analysis procedure for slug tests. SPE Formation Evaluation, 8(4):292-298, December.
46. Reynolds, M.M., Munn, D.L. 2010. Development Update for an Emerging Shale Gas Giant Field-Horn River Basin, British Columbia, Canada. Paper SPE 130103 presented at the SPE Unconventional Gas Conference, Pittsburgh, Pennsylvania, USA, 23-25 February.
47. Song, B., Economides, M.J., and Ehlig-Economides, C. 2011(a). Design of Multiple Transverse Fracture Horizontal Wells in Shale Gas Reservoirs. Paper SPE 140555 presented at the SPE Hydraulic Fracturing Technology Conference, The Woodlands, Texas, USA, 24-26 January.
48. Song, B., Ehlig-Economides, C. 2011(b). Rate-Normalized Pressure Analysis for Determination of Shale Gas Well Performance. Paper SPE

144031 presented at the SPE North American Unconventional Gas Conference and Exhibition, The Woodlands, Texas, USA, 14-16 June.

49. Williams-Kovacs, J.D., and Clarkson, C. R. 2013. Stochastic Modeling of Two-Phase Flowback of Multi-Fractured Horizontal Wells to Estimate Hydraulic Fracture Properties and Forecast Production. Paper SPE 164550 presented at the SPE Unconventional Resources Conference, USA, The Woodlands, Texas, 10-12 April.
50. Zahid, S., Bhatti, A.A., Khan, H.H., and Ahmad, T. 2007. Development of Unconventional Gas Resources: Stimulation Perspective. Paper SPE 107053 presented at the SPE Production and Operations Symposium, USA, Oklahoma City, Oklahoma, 31st March-3rd April.

APPENDIX A

DEVELOPMENT OF FLOWING MATERIAL BALANCE

EQUATION (RADIAL FLOW)

In this section, we develop a relationship for fracture pressure in time and space. We use the well-known diffusivity equation which describes the radial flow of fluid in porous media (Lee et al., 2003). The diffusivity equation for radial flow of fracturing fluid through the hydraulic fractures towards the horizontal well is given by

$$\frac{1}{r} \frac{\partial}{\partial r} \left(r \frac{\partial P_f}{\partial r} \right) = \frac{\phi_f C_t \mu}{K_f} \frac{\partial P_f}{\partial t}. \quad (\text{A.1})$$

Substituting Eq. (8) into Eq. (A.1) gives

$$\frac{1}{r} \frac{\partial}{\partial r} \left(r \frac{\partial P_f}{\partial r} \right) = \frac{\phi_f C_t \mu (-q_s) B_s}{K_f C_{st}}. \quad (\text{A.2})$$

Integrating with respect to r gives

$$\left(r \frac{\partial P_f}{\partial r} \right) = - \frac{\phi_f C_t \mu q_s B_s}{K_f C_{st}} \frac{r^2}{2} + C_1. \quad (\text{A.3})$$

We assume $\frac{\partial P}{\partial r} = 0$ at $r = r_e$ to determine C_1 :

$$C_1 = \left(\frac{\phi_f C_t \mu q_s B_s}{K_f C_{st}} r_e^2 \right). \quad (\text{A.4})$$

Substituting C_1 in Eq. (A.3) gives

$$\frac{\partial P_f}{\partial r} = \frac{\phi_f C_t \mu q_s B_s}{K_f C_{st}} \left(-r + \frac{r_e^2}{r} \right). \quad (\text{A.5})$$

Integrating with respect to r gives

$$P_f(r, t) = \frac{\phi_f C_{t\mu} q_s B_s}{K_f 2C_{st}} r_e^2 \left[-\frac{r^2}{2r_e^2} + \ln(r) \right] + C_2 \quad (\text{A.6})$$

We consider the boundary condition $P = P_{wf}$ at $r = r_w$ and assume $\frac{r_w^2}{r_e^2} \approx 0$ to calculate C_2 :

$$C_2 = P_{wf} - \frac{\phi_f C_{t\mu} q_s B_s}{K_f 2C_{st}} r_e^2 \ln(r_w). \quad (\text{A.7})$$

Substituting C_2 in Eq. (A.6) gives fracture pressure in time and space:

$$P_f(r, t) = P_{wf} - \frac{\phi_f C_{t\mu} q_s B_s}{K_f 2C_{st}} r_e^2 \left[\ln\left(\frac{r_w}{r}\right) + \frac{r^2}{2r_e^2} \right] \quad (\text{A.8})$$

Now we develop the relationship between average reservoir pressure and bottomhole flowing pressure. Starting with the average reservoir pressure equation

$$\bar{P}(t) = \frac{\int_{r_w}^{r_e} P_f dV_f}{\int_{r_w}^{r_e} dV_f}. \quad (\text{A.9})$$

We assume cylindrical geometry

$$V_f = \pi r^2 h_f \phi_f.$$

$$dV_f = \pi h_f \phi_f 2r dr.$$

Substitute above equations in Eq. (A.9) gives

$$\bar{P} = \frac{\int_{r_w}^{r_e} (P_f \pi h_f \phi_f 2r) dr}{\int_{r_w}^{r_e} (\pi h_f \phi_f 2r) dr}.$$

$$\bar{P} = \frac{2\pi h_f \phi_f \int_{r_w}^{r_e} (P_f r) dr}{2\pi h_f \phi_f \int_{r_w}^{r_e} (r) dr}.$$

Here, $P_f(r, t) = P_{wf} - \frac{\phi_f C_t \mu q_s B_s}{K_f 2C_{st}} r_e^2 \left[\ln \left(\frac{r_w}{r} \right) + \frac{r^2}{2r_e^2} \right]$.

Substituting P_f in average pressure equation and solving gives

$$\bar{P} = \frac{1}{\left(\frac{r_e^2 - r_w^2}{2} \right)} \left\{ \int_{r_w}^{r_e} \left[P_{wf} - \frac{\phi_f C_t \mu q_s B_s}{K_f 2C_{st}} r_e^2 \left[\ln \left(\frac{r_w}{r} \right) - \frac{r^2}{2r_e^2} \right] \right] r dr \right\}. \quad (\text{A.10})$$

Solving each part separately

$$P_{wf} \int_{r_w}^{r_e} r dr = P_{wf} \frac{r_e^2 - r_w^2}{2}.$$

Now solving the second part

$$\int_{r_w}^{r_e} r \ln \left(\frac{r_w}{r} \right) dr.$$

Solving through integration by parts

$$\int u \cdot v' = u \cdot v - \int v \cdot u'.$$

Therefore, the second part will become

$$-\frac{\phi_f C_t \mu (q_s) B_s}{K_f 2C_{st}} r_e^2 \int_{r_w}^{r_e} r \ln \left(\frac{r}{r_w} \right) dr = -\frac{\phi_f C_t \mu q_s B_s}{K_f 2C_{st}} r_e^2 \left[\frac{r_e^2}{2} \ln \left(\frac{r_w}{r_e} \right) + \frac{1}{4} (r_e^2 - r_w^2) \right].$$

Solving the third part

$$\int_{r_w}^{r_e} \frac{r^3}{2r_e^2} dr = \frac{1}{2r_e^2} \left(\frac{r_e^4}{4} - \frac{r_w^4}{4} \right).$$

The final form of Eq. (A.9) becomes

$$\bar{P} = P_{wf} - \frac{\phi_f C_t \mu q_s B_s}{K_f 2C_{st}} r_e^2 \left[\ln \left(\frac{r_w}{r_e} \right) \left(\frac{r_e^2}{r_e^2 - r_w^2} \right) + \left(\frac{1}{2} \right) + \frac{1}{4} \left(\frac{r_e^2 + r_w^2}{r_e^2} \right) \right].$$

Assuming that $\left(\frac{r_e^2}{r_e^2 - r_w^2} \right) \approx 1$ and $\left(\frac{r_e^2 + r_w^2}{r_e^2} \right) \approx 1$

$$\bar{P} = P_{wf} - \frac{\phi_f C_t \mu q_s B_s}{K_f 2C_{st}} r_e^2 \left[\ln \left(\frac{r_w}{r_e} \right) + \left(\frac{1}{2} \right) + \frac{1}{4} \right].$$

$$\bar{P} = P_{wf} - \frac{\phi_f C_t \mu q_s B_s}{K_f 2C_{st}} r_e^2 \left[\ln \left(\frac{r_w}{r_e} \right) + \frac{3}{4} \right]. \quad (\text{A.11})$$

Solving for various Drainage shapes

$$\ln \left(\frac{r_w}{r_e} \right) + \frac{3}{4}$$

$$\ln \left(\frac{r_e}{r_w} \right) - \frac{3}{4} = \ln \left(\frac{r_e}{r_w} \right) + \ln e^{-3/4}.$$

$$\ln \left(\frac{r_e}{r_w} \right) - \frac{3}{4} = \ln \left(\frac{r_e}{r_w \cdot e^{3/4}} \right).$$

After solving Eq. (A.11) for various drainage shapes gives

$$\bar{P}(t) = P_{wf} + \frac{\phi_f C_t \mu q_s B_s}{K_f 2C_{st}} r_e^2 \left[\frac{1}{2} \ln \left(\frac{4A}{C_A \gamma r_w^2} \right) \right] \quad (\text{A.12})$$

APPENDIX B

DEVELOPMENT OF FLOWING MATERIAL BALANCE

EQUATION (LINEAR FLOW)

In this section, we develop a relationship for fracture pressure in time and space for the linear case. The diffusivity equation for linear flow of fracturing fluid through the hydraulic fractures towards the horizontal well is given by

$$\frac{\partial^2 P_f}{\partial x^2} = \frac{\phi_f C_{t\mu}}{K_f} \frac{\partial P_f}{\partial t}. \quad (\text{B.1})$$

Substituting Eq. (8) into Eq. (B.1) gives

$$\frac{\partial^2 P_f}{\partial x^2} = \frac{\phi_f C_{t\mu}}{K_f} \frac{(-q_s) B_s}{C_{st}}. \quad (\text{B.2})$$

Integrating with respect to x gives

$$\left(\frac{\partial P_f}{\partial x} \right) = - \frac{\phi_f C_{t\mu} q_s B_s}{K_f C_{st}} x + C_1. \quad (\text{B.3})$$

We assume $\frac{\partial P}{\partial r} = 0$ at $x = y_e$ to determine C_1 :

$$C_1 = \left(\frac{\phi_f C_{t\mu} q_s B_s}{K_f C_{st}} y_e \right). \quad (\text{B.4})$$

Substituting C_1 in Eq. (B.3) gives

$$\frac{\partial P_f}{\partial x} = \frac{\phi_f C_{t\mu} q_s B_s}{K_f C_{st}} (-x + y_e). \quad (\text{B.5})$$

Integrating with respect to x gives

$$P_f(x, t) = \frac{\phi_f C_{t\mu} q_s B_s}{K_f C_{st}} \left[-\frac{x^2}{2} + y_e x \right] + C_2 \quad (\text{B.6})$$

We consider the boundary condition $P = P_{wf}$ at $x = 0$ to calculate C_2 :

$$C_2 = P_{wf} \quad (B.7)$$

Substituting C_2 in Eq. (B.6) gives fracture pressure in time and space:

$$P_f(x, t) = P_{wf} - \frac{\phi_f C_{t\mu} q_s B_s}{K_f C_{st}} r_e^2 \left[\frac{x^2}{2} - y_e x \right] \quad (B.8)$$

Now we develop the relationship between average reservoir pressure and bottomhole flowing pressure. Starting with the average reservoir pressure equation.

$$\bar{P}(t) = \frac{\int_0^{y_e} P_f dV_f}{\int_0^{y_e} dV_f} \quad (B.9)$$

We assume cuboid geometry

$$V = whx$$

$$V_f = w_f h_f \phi_f x.$$

$$dV_f = w_f h_f \phi_f dx.$$

Substitute above equations in Eq. (B.9)

$$\bar{P} = \frac{\int_0^{y_e} (P_f w_f h_f \phi_f) dx}{\int_0^{y_e} w_f h_f \phi_f dx}.$$

$$\text{Here, } P_f(x, t) = P_{wf} - \frac{\phi_f C_{t\mu} q_s B_s}{K_f C_{st}} \left[\frac{x^2}{2} - y_e x \right]$$

Substituting P_f and solving

$$\bar{P} = \frac{1}{y_e} \left\{ \int_0^{y_e} \left[P_{wf} - \frac{\phi_f C_{t\mu} q_s B_s}{K_f C_{st}} \left[\frac{x^2}{2} - y_e x \right] \right] dx \right\} \quad (B.10)$$

Solving for the average pressure drop, the final form of Eq. (B.9) becomes

$$\bar{P} = P_{wf} + \frac{\phi_f C_{t\mu} q_s B_s}{K_f 3C_{st}} y_e^2. \quad (\text{B.11})$$

Relationship between RNP and MBT

As we assume that at the very early time, matrix influx is zero ($q_m = 0$), the production mechanism is fluid expansion and fracture closure:

$$N_p B_s = -C_{st}(\bar{P} - P_i). \quad (\text{B.12})$$

Where, N_p is the cumulative production of the fracturing fluid. Rearranging Eq. (B.12) gives the average fracture pressure as

$$\bar{P}(t) = P_i - \frac{N_p B_s}{C_{st}}. \quad (\text{B.13})$$

Substituting Eq. (B.13) into Eq. (B.11) gives

$$P_i - P_{wf} = \frac{N_p B_s}{C_{st}} + \frac{\phi_f C_{t\mu} q_s B_s}{K_f 3C_{st}} y_e^2. \quad (\text{B.14})$$

Dividing both sides of Eq. (B.14) by $q_s B_s$ gives

$$\frac{P_i - P_{wf}}{q_s} = \frac{N_p B_s}{q_s C_{st}} + \frac{\phi_f C_{t\mu} q_s B_s}{K_f 3C_{st}} y_e^2. \quad (\text{B.15})$$

The terms $\frac{P_i - P_{wf}}{q_s}$ and $\frac{N_p}{q_s}$ are referred to as rate normalized pressure (RNP) and material balance time (MBT).

$$RNP = \frac{B_s}{C_{st}} MBT + \frac{\phi_f C_{t\mu} B_s}{3C_{st} K_f} y_e^2. \quad (\text{B.16})$$